Thermo-Responsive Nanogels as Versatile Platform for Smart Drug Delivery Systems and Multi-Functional Photothermal Agents

Inaugural-Dissertation

to obtain the academic degree

Doctor rerum naturalium (Dr. rer. nat.)

submitted to the Department of Biology, Chemistry and Pharmacy

of Freie Universität Berlin

by

LORYN ELISABETH THEUNE

(NÉE FECHNER)

Berlin

DECLARATION

The following doctoral thesis was carried out from October 2015 until April 2020 in the research group of Prof. Dr. Calderón at the department of Biology, Chemistry and Pharmacy of Freie Universität Berlin.

I hereby declare that the submitted thesis is my own work and was prepared autonomously without the aid of other sources than the ones cited and acknowledged. The work was not submitted to any other prior doctoral procedure.

Berlin, den 01.04.2019

Loryn Theune

1st Reviewer: Prof. Dr. Marcelo Calderón

2nd Reviewer: Prof. Dr. Rainer Haag

Date of thesis defense: 13.06.2019

ACKNOWLEDGEMENTS

First and foremost, my gratitude goes to **Marcelo Calderón** as my supervisor for giving me the opportunity to perform this thesis within his research group, for his trust in my ideas and my work, and his support throughout the whole time.

A warm thanks goes to **Rainer Haag** as second referee of this work.

A thanks to all collaboration partners for the fruitful work. In particular, I want to thank **Sarah Hedtrich** and **Rawan Charbaji** for the discussions and cooperative way of working together, I've learned a lot and your view and suggestions broadened my horizon. A warm thanks also goes to **Jens Buchmann**, who was open for a quite spontaneous collaboration. A Thanks also to **Jan Laufer** and **Fabian Schuhmacher**.

A special thanks to **Stefanie, Gregor** und **Franz** for proof reading this thesis.

Thanks to all members and former members of the AG Calderón for the atmosphere and good times in the lab and office! Thanks to **Joy**, for your support and encouragement to continue even in stressful and frustrating times and your steady interest in my development. Thanks **Gregor** for always having an open ear for my concerns and your constructive feedback. A huge thanks also to **Stefanie**, for your honest feedback and your supervision. I have learned so much. Thanks for your patience with all my questions and openness to my ideas. A thanks also goes to **Emanuel**, for his honest and humorous, and **Ernesto** for his cordial nature. I appreciated the vivid discussion I had with you, **Julián**, and your advice for all kind of problems in the lab. **Michael**, thanks for always bringing a smile to my face. A warm thanks also to **Jeannett Holzknecht** for her optimism and positive radiance. My thanks also goes to **Ana Sonzogni** for spreading her good mood.

For the good talks, the laughs and for the fruitful discussions I want to thank all people sharing the office with me including **Emanuel, Laura, Julian and Gregor**. For the constructive feedback and the ideas, I want to thank all members of the 'soft-materials subgroup' including **Joy, Enrico, Michael, Stefanie, Alexis, Anna, Lucila and Gregor**. My gratitude goes to **Sebastian**,

who supported me a lot in the lab work in the end phase of this thesis (in particular with the homogenizer). In addition, I want to thank **Katrin, Cata, Lydia, Smriti, Sandra and Anna Puigalli** for the good times in the lab. I want to thank **Nicolas Guillaume** for his contributions to this thesis through his work during his 4-month internship.

Thanks to all coffee group members for the funny, interesting, cheery, motivational and wonderful odd talks. Thanks to **Felix, Mathias, Ann-Cathrin and Emanuel** who in particular in the final stage of writing always brought some minutes of relaxation to me.

Warm thanks also goes to **Svenja** for her friendship, the pleasant lunch breaks and her open ear and support in all kind of areas. A thank also goes to the first-semester-crew **Lisa** and **Ben**, without you I wouldn't have managed these studies so well. I also want to thank **Ulli** who became a close friend and was always reachable and supportive. Thanks also to **Paula**, for sharing so many important moments throughout the last 23 years. A huge thanks to the whole ‚Spieleabend'-crew: **Franz, Lari, Mo, Johanna, Georg, Maria and Oussama**. For your support, your belief in me and all these convivial hours of fun. A special thanks also to the Martin-Luther-WG **Mo, Lisa, Vanessa** and **Eric**.

A huge thanks also to my whole family, **Marlis, Otto, Renée, Jorris, Sandrine, Heiko and Theresa** for always finding supportive words and your implicitness in your belief in me. Thanks also for respecting when I didn't want to talk about the work and putting my mind on something else.

And finally, I want to thank **Joseph** for his love, his endless patience with me, for cheering me up when needed, for celebrating the good and sharing the bad moments and so many wonderful hours. Thank you!

ABSTRACT

Nano-sized smart drug delivery agents such as responsive nanogels evolved as promising carrier systems for therapeutic actives. With a targeted delivery of their cargos, they improve pharmacokinetic profiles of the drugs and thus provide the potential to overcome dose limits, and reduce the occurrence of toxic side effects. However, the complexity of the occurring diseases and the huge variability of possible therapeutic actives, ranging from small molecules to therapeutic proteins, make it essential to adjust the carriers to the specific requirements. This work addresses that need by identification of key parameters to control the properties and structure of responsive nanogels and develop adaption concepts to broaden the range of cargo therapeutics and extend the field of applications.

In a comprehensive investigation of reaction kinetics and nanogel formation under various conditions, key parameters to control the properties of thermo-responsive nanogels could be elucidated. Using this knowledge, the network density, size, and swelling ability of the nanogels could be adjusted for efficient encapsulation of proteins. The use of the thermo-responsive polymer poly-N-isopropyl methacrylamide (PNIPMAM) beside poly-N-isopropyl acrylamide (PNIPAM) allowed a precise tuning of the volume phase transition temperature (VPTT) of the resulting nanogels in the range between 34 – 47 °C. For all nanogels, a temperature triggered release of the encapsulated proteins was demonstrated *in vitro.* The delivery of the proteins into viable skin layers could be confirmed using *ex vivo* skin. The tuning of the temperature-response of the nanogels allowed the use of external heat sources to trigger dermal protein delivery in high efficiency and under temporal and local control.

Next, the adjustment of the assessed nanogels for mucosal delivery of anti-inflammatory drugs was targeted. Therefore, the crosslinker was modified incorporating disulfides which should endow the nanogels to interact with mucus and thus overcome its clearance mechanisms. Using the reductive cleavage of the disulfides into thiols, studies of the degradation profiles of resulting nanogels could be used as a proof for the successful incorporation of disulfides in PNIPMAM based nanogels. In contrast, the use of PNIPAM alone or as a copolymer with

PNIPMAM resulted in no or only partly degradation of the resulting nanogels indicating a premature cleavage of the disulfides during nanogel formation. Studies on the interaction with mucus and the penetration into freshly excised porcine jejunum punches revealed that the presence of disulfides in the nanogels enabled the nanogels to overcome mucosal clearance mechanisms. The i*n vitro* assay of the encapsulation of hydrophobic small molecular weight drug Budesonide (BUD) and hydrophilic protein Etanercept (ETN) demonstrates the nanogels' potential for submucosal delivery of both anti-inflammatory actives.

Finally, semi-interpenetration method was employed as a tool to adapt the thermo-responsive nanogels for systemic application in combination cancer therapy. The introduction of the near infrared (NIR)-transducing polymer polypyrrole (PPY) through physical entanglement of linear PPY chains into the nanogel network was found beneficial by complementing of properties of both without affecting each other. As a result, the semi-interpenetrated nanogels still exhibited the same VPTT as their thermo-responsive non-interpenetrated analogues but acted as excellent photothermal transducer with high photostability. This enabled the use of the generated heat by the PPY chains under NIR exposure for photothermal ablation of cancerous tissue as well as to trigger the thermo-responsive network and the release of an encapsulated drug. In addition, the photothermal transducing abilities could be used for the determination of *ex vivo* biodistribution profiles and time dependent tumor accumulation. The transducing property also translate the nanogels into contrast agents in photoacoustic (PA) imaging. Increased therapeutic outcomes against tumors could be demonstrated *in vitro* and *in vivo* induced by combination effects of the chemotherapeutic drug Methotrexate (MTX) delivered by the nanogels, and photothermal treatment with NIR light.

Altogether, this thesis demonstrates that thermo-responsive nanogels are an excellent and variable platform for the delivery of a range of therapeutic actives. For the adjustment of the nanogels and the addition of useful functionalities, cross-linker modification and semi-interpenetration were proven to be efficient tools to broaden the range of applications from dermal to mucosal and systemic administration.

KURZFASSUNG

Responsive Nanogele haben sich als vielversprechende so genannte „smarte“ Wirkstoff-transportsysteme in nanometer Größe herausgestellt. Mit einer gezielten Freisetzung ihrer Cargos haben sie das Potential die pharmakokinetischen Profile der Medikamente zu verbessern und so Dosisgrenzen zu überwinden und das Auftreten unerwünschter Nebenwirkungen zu reduzieren.

Die Komplexität der auftretenden Krankheiten und die große Variabilität der möglichen therapeutischen Wirkstoffe, die vom kleinen Molekülen bis zu therapeutischen Protein reichen, machen es jedoch notwendig, die Carrier an die spezifischen Anforderungen anzupassen. Die vorliegende Arbeit befasst sich mit dieser Erfordernis mit dem Ziel durch die Identifizierung von Schlüsselparametern die Kontrolle über die Eigenschaften und die Struktur von responsiven Nanogelen zu erhalten. Des Weiteren sollen Anpassungskonzepte für die Nanogele entwickelt werden, um das Spektrum an Wirkstoffen sowie mögliche Anwendungsfelder zu erweitern.

In einer umfassenden Untersuchung der Reaktionskinetik und der Nanogel-Bildung unter verschiedenen Bedingungen konnten die wichtigsten Faktoren zur Steuerung der Eigenschaften von thermo-responsiven Nanogelen identifiziert werden. Mit diesem Wissen konnte die Parameter Netzwerkdichte, Größe und Schwellfähigkeit der Nanogele für eine effiziente Verkapselung von Proteinen angepasst werden. Die Verwendung des thermo-responsiven Polymers Poly-N-Isopropylmethacrylamid (PNIPMAM) neben Poly-N-Isopropylacrylamid (PNIPAM) ermöglichte eine genaue Einstellung der Volumenphasenübergangstemperatur (VPTT) der resultierenden Nanogele im Bereich von 34 - 47 °C. Für alle Nanogele konnte eine temperaturbedingte Freisetzung der verkapselten Proteine *in vitro* und die Abgabe der Proteine in lebensfähige Hautschichten *ex vivo* nachgewiesen werden. Die Feinjustierung der Übergangstemperatur der Nanogele ermöglichte außerdem die Nutzung externer Wärmequellen, um die Freisetzung und Penetration von Proteinen in die Haut mit hoher Effizienz und unter zeitlicher und lokaler Kontrolle auszulösen.

Als nächstes wurde die Anpassung der thermo-responsiven Nanogele für eine Verabreichung von entzündungshemmenden Medikamenten auf Mucus angestrebt. Daher wurde der Vernetzer der Nanogele mit Disulfiden modifiziert, die es den Nanogelen ermöglichen sollen, mit dem Mucus zu interagieren und so die mucus-korrelierten Clearance-Mechanismen zu überwinden. Durch die Spaltung von Disulfiden in Thiole unter reduktiven Bedingungen konnten Studien über die Abbauprofile der Nanogele als Nachweis für die erfolgreiche Integration der Disulfide in PNIPMAM-basierten Nanogele dienen. Im Gegensatz dazu wurde bei der Verwendung von PNIPAM, allein oder als Copolymer mit PNIPMAM, keiner oder nur ein teilweiser Abbau der resultierenden Nanogele beobachtet, was auf eine vorzeitige Spaltung der Disulfide während der Nanogelbildung hindeutet. Studien über die Wechselwirkung mit Mucus und die Penetration in frisch exzidierte Jejunum-Ausschnitte vom Schwein zeigten, dass das Vorhandensein von Disulfiden den Nanogelen ermöglichte, die Schleimschicht zu überwinden und unterliegende Zellschichten zu erreichen. Ein *in vitro*-Assay bezüglich der Eignung der Nanogele zur Verkapselung von hydrophobem, niedermolekularen Budesonid (BUD) und dem hydrophilen Protein Etanercept (ETN) zeigte das Potenzial der Nanogele für die submukosale Lieferung beider entzündungshemmenden Wirkstoffe.

Schließlich wurde semi-Interpenetration als Methode zur Anpassung der thermo-responsiven Nanogele an die systemische Anwendung in der kombinatorischen Krebstherapie untersucht. Die Einführung des nahinfraroten (NIR) umwandelnden Polymers Polypyrrol (PPY) über eine physikalische Verflechtung linearer PPY-Ketten in das Netzwerk der thermo-responsiven Nanogele stellte sich als vorteilhaft heraus, da die Eigenschaften beider Systeme ergänzt wurden ohne sich gegenseitig zu beeinflussen. Die semi-interpenetrierten Nanogele zeigten immer noch die gleiche VPTT wie ihre thermo-responsiven, nicht-interpenetrierten Analoga, fungierten aber als exzellenter photothermischer Umwandler mit hoher Photostabilität. Dies ermöglichte die Nutzung der durch die PPY-Ketten unter NIR-Exposition erzeugten Wärme zur Auslösung des Volumenphasenübergangs des thermo-responsiven Netzwerks, zur Freisetzung eines verkapselten Medikaments, sowie zur photothermischen Ablation von Tumorgewebe. Darüber hinaus konnten die Fähigkeit zur Umwandlung von NIR in Wärme für die Bestimmung von *ex vivo* Biodistributionsprofilen und zeitabhängiger Tumorakkumulation

genutzt werden. Die Eigenschaft der NIR-Umwandlung macht die Nanogele außerdem zu Kontrastmitteln in der photoakustische (PA) Bildgebung. Verbesserte therapeutische Ergebnisse gegen Krebstumore konnten durch Kombinationseffekte des von den Nanogelen freigesetzten Chemotherapeutikums Methotrexat (MTX) und der photothermischen Behandlung mit NIR-Licht *in vitro* und *in vivo* erzeugt werden.

Insgesamt konnte in dieser Arbeit gezeigt werden, dass thermo-responisve Nanogele eine ausgezeichnete und variable Plattform für den Transport und die kontrollierte Freisetzung einer Reihe von therapeutischen Wirkstoffen sind. Für die Anpassung der Nanogele an wirkstoff- und krankheitsbedingte Anforderungen und die Ergänzung nützlicher Funktionen haben sich die Modifikation des Vernetzers und die semi-Interpenetration als effiziente Methoden erwiesen um das Anwendungsspektrum von dermal zu mukosal und systemisch zu erweitern.

TABLE OF CONTENTS

ABBREVIATIONS

The abbreviations are distinguished between chemicals and other abbreviations such as, e.g. methods or properties.

Abbreviation	Chemical
AA	Acrylic acid
ABC	Dendritic acrylamide
Ac-Cl	Acryloyl chloride
APS	Ammonium persulfate
BIS	Bis-acrylamide
BOC anhydride	Di-tert-butyl dicarbonate
BSA	Bovine serum albumin
BSA-FITC	FITC conjugated bovine serum Albumin
BUD	Budesonide
BUD-d8	Deuterated budesonide
Cys	L-cysteine
Cis-platin	Cis-Pt
DCC	N,N'-Dicyclohexylcarbodiimide
DCM	Dichloromethane
DHEA	(1,2,-Dihydroxylethylene)bisacrylamide
DIPEA	N,N-Diisopropylethylamine
DMAP	4-Dimethylaminopyridine
DMF	Dry N,N-dimethylformamide
dPG	Dendritic polyglycerol
EDCI	3-(Ethyliminomethyleneamino)-N,N-dimethylpropan-1-amine
EGF	Epidermal growth factor
ETN	Etanercept
GSH	Reduced glutathione

HCl	Hydrochloric acid
KPS	Potassium persulfate
MeOH	Methanol
MTX	Methotrexate
NaOH	Sodium hydroxide
NIPAM	N-isopropyl acrylamide
NIPMAM	N-isopropyl methacrylamide
P(GME-co-EGE)	Poly(glycidyl methyl ether-co-ethyl glycidyl ether)
PANI	Polyaniline
PBS	Phosphate-buffered saline
PDAEM	*Poly*-(N,N-diethyl acrylamide)
PEDOT:PSS	Poly(3,4-ethylenedioxythiophene) polystyrene sulphate
PEG	Polyethylene glycol
PNIPAM	Poly-N-isopropyl acrylamide
PNIPMAM	Poly-N-isopropyl methacrylamide
POEGMA	Poly-(oligo(ethylene glycol methacrylate)
POx	Poly-(oxazoline)
PPO	Poly-(propylene oxide)
PPY	Polypyrrole
PVA	Polyvinyl alcohol
PVCL	Poly-(vinyl caprolactam)
PVP	Polyvinyl pyrrolidone
RC	Regenerated cellulose
RhodB	Rhodamine B
SDS	Sodium dodecyl sulfate
TEA	Triethylamine
TEMED	N,N,N′,N′-Tetramethyl-ethylenediamine
TFA	Trifluoroacetic acid

Abbreviation	
%ID	Percent of injected dose
CD	Circular dichrosim
DLS	Dynamic light scattering
EE	Encapsulation efficiency
ELISA	Enzyme-linked immunosorbent assay
EPR	Enhanced permeation and retention
eq.	Equivalents
GPC	Gel permeation chromatography
h	Hour(s)
H&E	Hematoxylin and Eosin
i.t.	Intratumorally (i.t.)
i.v.	Intravenous
IR	Infrared
LCST	Lower critical solution temperature
MFI	Mean fluorescence intensity
min	Minute(s)
MIPs	*x-y* Maximum intensity projections
MWCO	Molecular weight cut-off
NIR	Near-infrared
NMR	Nuclear magnetic resonance
O/W	Oil in water
OD	Optical density
PA	Photoacoustic
PDI	Polydispersity index
PDT	Photodynamic therapy
PTT	Photothermal therapy
r.t.	Room temperature
RES	Reticuloendothelial system

R_f	Retardation factor
ROI	Regions of interest
s.c.	Subcutaneous
SC	Stratum corneum
sec	Second(s)
TEM	Transmission electron microscopy
TLC	Thin layer chromatography
TV	Tumor volume (TV)
UCST	Upper critical solution temperature
VE	Viable epidermis
VPTT	Volume phase transition temperature
W/O	Water in oil

1 INTRODUCTION

1.1 NANOMATERIALS FOR MEDICAL APPLICATIONS

Nano-sized materials often show unique optical, mechanical and electronic properties resulting in advantageous functionality in comparison to their macroscale analogues. As a consequence, their field of applications is very broad, ranging from energy storage[1] and electronics[2] to food additives,[3-5] textiles,[6] healthcare,[7-9] and cosmetics.[10] Nanotechnology is a growing field with increasing numbers of products containing synthetic nanoparticles. Beside the beneficial properties of nanomaterials, their widespread use caused scepticm and questions regarding the impact of nanoparticles on health and environment. A prominent example, widely discussed in public, is for instance the use of titanium and zinc oxide nanoparticles in sunscreen products.[11-13] The governmental implantation of faculties specialized on fundamental risk assessments of nanomaterials shows that this topic is taken serious and in the same time underline the seminal significance of nanotechnology.[14, 15]

Particularly in medical applications, a boost in the development of nanomaterials has occurred in the past decades. With the first nomination of the term 'nanomedicine' in the late 1990s, nowadays more and more nano-sized medical devices are in the process of translation into the clinics.[7-9] Thereby, nanomaterials find applications as therapeutics themselves, as part of biomaterials, in imaging and diagnostic tools and, maybe most prominent, as delivery agents for conventional drugs.[7, 16, 17] They provide targeted and site-specific delivery of therapeutic actives and thus overcome main drawbacks of currently available drugs like low solubility, fast elimination and strong side effects.[16] Fuelled by these prospects, the development of new, functional nanoparticles stays is in the special focus of researchers.

Some of the first employed nano-sized delivery agents were liposomes. Consisting of a lipid bilayer, liposomes carry an aqueous void offering the capability to encapsulate both hydrophilic

cargos in their inner part as well as hydrophobic molecules intercalated in the bilayer. As such, the anti-cancer drug Doxorubicin encapsulated in liposomes has found clinical approval as first liposomal therapeutic (DOXIL®) after a long process of optimization.[8] Besides liposomes, metallic nanoparticles, carbon-based materials like carbon nano-tubes and all kinds of polymeric carriers are being investigated for efficient delivery of drugs.[16, 18, 19]

1.2 POLYMERIC DRUG DELIVERY AGENTS

The use of polymers or macromolecules as a basis for nano-sized carriers is widespread due to their huge variety in physicochemical properties, structures and sizes. A well-considered carrier design and choice of the used materials thus allow the control of the carrier properties. Polymeric nanocarriers fill the whole nanoscale range from several nanometres like linear or dendritic polymers (1–15 nm), polymer-drug or polymer-protein-conjugates (5–20 nm), to larger structures like polyplexes (40–60 nm), polymeric micelles (20–100 nm), polymersomes (40–800 nm), nano- and microgels (50 nm–1 μm) and polymeric nano- and microparticles (40 nm–1 μm).[19, 20] In relation to the size of conventional small molecular weight drugs, like above-mentioned anti-cancer drug Doxorubicin, all carriers are at least a magnitude larger, with the bigger carriers like polymeric micelles, polymersomes and nanogels having comparable sizes to naturally occurring transporter structures like viruses and bacteria (Figure 1).

The improvement on the pharmacokinetics of small molecular drugs through combination with polymeric carriers was already postulated by Ringsdorf in 1975.[21] Within the Ringsdorf model, he predicted advances in the biodistribution through conjugation of drugs to polymers. Ringsdorf emphasized the ability to functionalize the polymer with solubilizing or targeting moieties to achieve higher efficiency and reduce side effects.[21] Even though this assessment was long seen with sceptisim,[22] by now many studies and clinical trials prove him right. It is nowadays well known, that for particles with sizes in the nanometer range, the circulation in the blood stream is prolonged due to decreased renal filtration. It was also demonstrated that

surface modifications are able to decrease opsonisation and immune response, and cargos are better solubilized and protected from fast degradation by the carrying polymers.[23-26]

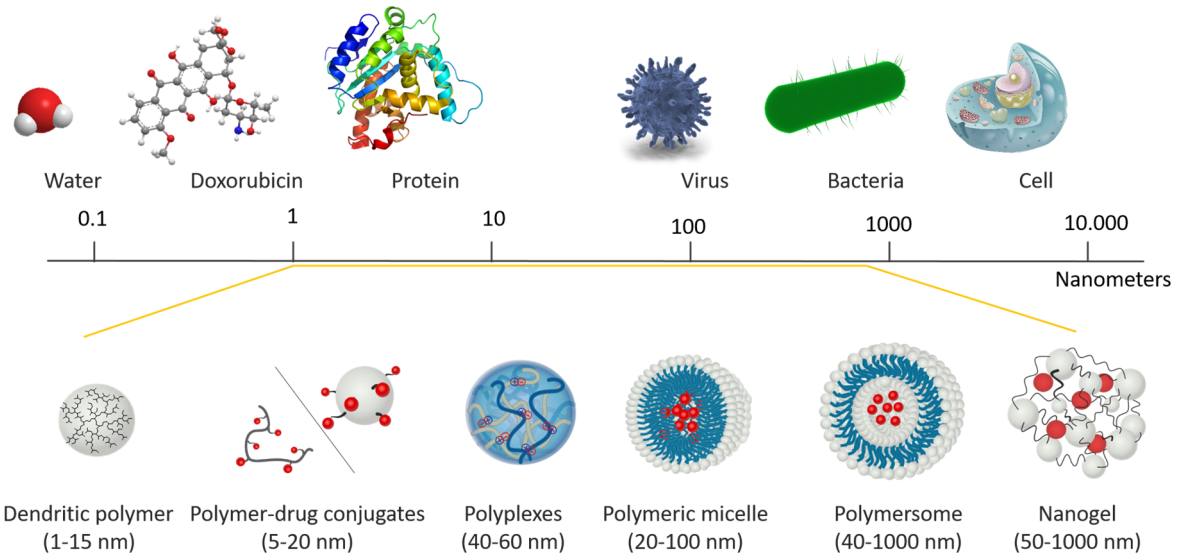

Figure 1. Dimensions of polymeric drug delivery agents set into biological size context: Bigger carriers like polymeric micelles, polymersomes and nanogels having comparable sizes to naturally occurring transporter structures

In particular, the discovery of the solid tumor-related enhanced permeation and retention (EPR) effect in 1986 by Matsumura and Maeda[27] boosted the development of nano-sized carriers for anti-cancer drugs. Due to increased pore sizes between endothelial cells of the tumor vasculature, the penetration of nanoscale structures into the tumor tissue is much more pronounced than in healthy tissue. In combination with poor lymphatic drainage, the clearance of the nanocarriers is reduced leading to a retention of the particles at the tumor site.[28] This so-called 'passive targeting' modality of nanoscale delivery agents is the basis for several already clinically approved therapeutics, e.g. albumin-bound paclitaxel (Abraxane®), and still a motivation for current research.[29] Nevertheless, the huge diversity of tumors, e.g. from different types of cancers or in different stages of development, leads to fluctuations in the occurrence of the EPR effect.[29] Thus, current research focus lies on developing advanced materials able to enhance the EPR effect, on using active targeting modalities, and on responding to microenvironments present at the tumor site.[29]

1.3 STIMULI-RESPONSIVE NANOGELS AS DRUG DELIVERY DEVICES

From the versatile polymeric architectures developed for controlled drug delivery, nanogels emerged as a variable platform to encapsulate a variety of guest molecules.[30-33] Nanogels are soft, polymeric gel particles in nanoscale size capable of holding large amounts of water within their cross-linked network.[30-33] Nanogels have applications in diverse fields of nanomedicine ranging from biosensors,[34-36] diagnostic and imaging agents[37-39] to drug delivery systems.[31, 40, 41]

In particular, stimuli-responsive "smart" nanogels have been studied extensively for drug delivery purposes: here, the release of an encapsulated cargo can be triggered and controlled by internal or external stimuli.[19, 43] 'Internal stimuli' are natural occurring variations, for example in pH, redox potential and temperature of the environment, or the presence of specific enzymes or proteins. In contrast, 'external stimuli' refer to the application of electromagnetic radiation including external heating, light, ultrasound, or magnetic fields. As a response to the stimuli, the nanogels' physico-chemical properties change. In the majority of existing nanogels, this results either in a swelling, shrinking, or degradation of the carrier. All three approaches can be used to release an encapsulated cargo (Figure 2).[42]

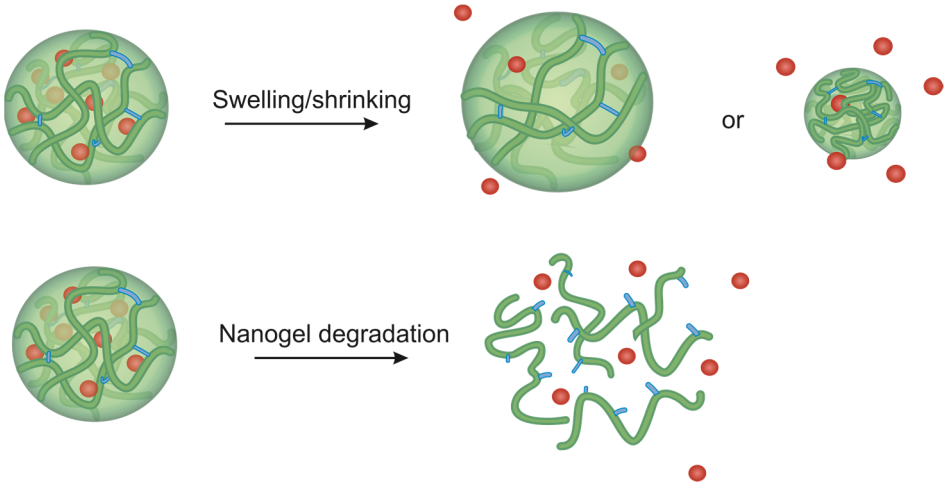

Figure 2. Triggered release of encapsulated cargos (red spheres) from nanogels either by size change or by degradation. Figure modified from reference [42] with permission from Royal Society of Chemistry. Copyright 2018.

1.3.1 pH-RESPONSIVE NANOGELS[§1]

Among the natural triggers used for responsive systems, a change in the pH is one of the most commonly employed.[31, 43, 44] The main reason for this is that the body has several areas where the pH is lower than the physiological value of 7.4 in blood. Namely, the gastric system is very acidic with pH values around 1 – 2.5 to facilitate the digestion and protect the organism from bacteria taken up with the food. In addition, during endocytosis eukaryotic cells form vesicles like endosomes (pH 5 – 6.5) and lysosomes (pH 4), in which the pH is lower than the physiological one. Especially in cancer treatment, pH-responsive systems are promising, as the extracellular matrix of solid tumor tissue is more acidic (pH 6-7) than healthy tissue. This drop stems from an accumulation of lactic acid and other acidic metabolites. Lactic acid is the product of anaerobic glycolysis of glucose caused by the hypoxic conditions present in the tumor tissue.[45, 46] Therefore, pH responsive nanomaterials like nanogels that accumulate in tumor tissues by the EPR effect (cf. sec. 1.2) are attractive candidates for controlled anti-cancer drug delivery systems for. Different approaches for pH responsivity have been explored so far. In general, one can distinguish between two different modes of action: either acid-labile bonds are broken or the ionization degree of the polymer is altered resulting in a changed hydrophilicity and/or a disruption or formation of ionic interactions.

The most common mechanism is a triggered swelling or deswelling behaviour, which can be achieved by incorporating ionizable groups in the nanogel network. Typically, this is realized by co-polymerization of carboxylic and/or amino group containing monomers with the polymer of choice. Subsequently, with differences in the environmental pH, the degree of ionization in the nanogels changes due to abstraction or release of protons by the acidic or basic groups. This results in higher or lower osmotic pressure within the nanogels network and therefore leads to

[§1] This chapter is based on the book chapter "Responsive Nanogels for Anti-cancer Therapy", which has been partially modified. The link to the published form is given in Appendix 7.1. Author contributions: The subchapter of pH-responsive nanogels for the book chapter was written by me. All authors contributed to the final version.

swelling or deswelling of the nanogels.[47] For drug delivery purposes, this pH-dependent ionization can additionally be used to enhance the encapsulation and release behaviour of any charged drug by forming or disrupting ionic bonds between the drug and the polymer scaffold.

pH-induced degradation of responsive nanogels can be achieved either by using ionic bonds to cross-link polymer chains or by the introduction of pH-labile bonds. Ionic-cross-linked systems are highly responsive to the pH because changes in the protonation stage interrupts the electrostatic interactions leading to a degradation of the nanogels.[48] Labile linkers can be introduced to nanogels either in the polymer backbone or in the cross-linker, which both lead to a degradation of the nanogel structure upon a pH trigger. In addition, pH sensitive linkers can be used to covalently bind drugs, which are then released by pH stimulus.

1.3.2 THERMO-RESPONSIVE NANOGELS

Another important class of responsive carriers are thermo-responsive nanogels. Their physico-chemical properties and stimuli-responsive behaviour depend on the polymeric characteristics of the materials used for their synthesis. As a basis, thermo-responsive polymers, which change their solvation state upon a thermal trigger, are used. When exceeding the critical solution temperature of these polymers, the phase transition of the linear polymer chains induces a contraction (or swelling) of the three-dimensional cross-linked nanogel network.[43] For drug delivery applications, precise control of the temperature trigger point (in most cases near body temperature) is required along with a sharp transition profile. A careful selection of used polymers is therefore indispensable. In this section, the basic principle behind the temperature-response, commonly used polymers and their features are discussed.

1.3.2.1 THERMO-RESPONSIVE POLYMERS

Thermo-responsive polymers are a class of "smart" materials that drastically change their physical properties in response to changes in temperatue.[49] This feature renders them into useful materials in a wide range of applications and thus sparked considerable scientific interest.[50]

The most common response to the temperature trigger is a sudden change in their solvation state based on the so-called 'coil-to-globule' transition.

Thermo-responsive polymers can be divided into two classes depending on whether their solubility is decreased or increased above a certain temperature. Most polymers exhibit a lower critical solution temperature (LCST) meaning that they precipitate at higher temperatures but are highly dispersible at low temperatures. Polymers with the opposite behaviour responding to an upper critical solution temperature (UCST) are relatively rare, in particular, with UCSTs in the range of temperatures relevant for biomedical applications.[51, 52] LCST and UCST behaviour is not restricted to aqueous environments, but other (organic) solvents are not suitable for drug delivery applications and will therefore not be discussed here.

The physical foundation for thermo-responsive behaviour lies in a shift of the balance between entropic and enthalpic shares in the dissolution process of the polymer. Thermodynamically, the dissolution of the polymer is feasible when the free Gibbs energy (ΔG, equation (1)) is negative. In the case of LCST polymers, at temperatures below the transition temperature the polymeric chains are surrounded by water molecules forming an orderly hydrogen bond-stabilized hydration shell. This arrangement of water molecules decreases the entropy (ΔS) yielding a small value for ΔS, while the hydration process yields a negative enthalpy contribution. This results in an overall negative Gibbs energy and good dissolution of the polymer.

$$\Delta G = \Delta H - T \cdot \Delta S \qquad (1)$$

Crossing the transition temperature, the entropic term $-T \cdot \Delta S$ outrivals the enthalpy gained by dispersion resulting in a positive ΔG. As a result, the hydrogen bonds between water and polymer chains break and intra-polymer interactions become predominant. This leads to a collapse of the polymer and the formation of polymeric globuli.[51, 53-55]

In many cases, this transition is stated as a change in the thermo-responsive polymers' hydrophilicity which is not perfectly accurate. But it exemplifies the release of water molecules previously bound to polymer chains and the formation of relatively hydrophobic polymer aggregates.[56] Anyway, the hydrophilic-hydrophobic balance is an important factor for the transition temperature. It is generally shifted to higher temperatures when the polymer is more hydrophilic. Here, the hydrated state is energetically favoured (more negative ΔH) and the entropy term can outbalance the enthalpy only at higher temperatures.

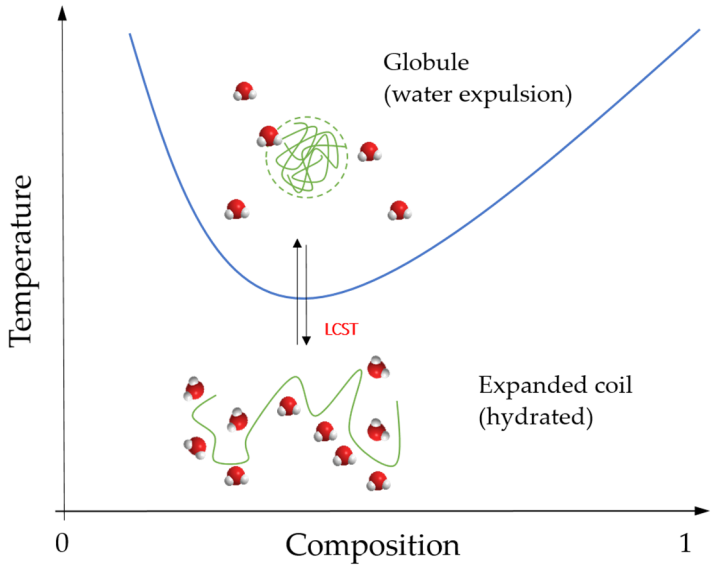

Figure 3. Typical phase diagram of a LCST polymer.

Besides the temperature, other factors such as concentration, molar mass of the polymer chains and presence of salts or additives have an impact on the solubility of a polymer as well. This is typically depicted in phase diagrams, as exemplarily shown in Figure 3. The influence of the molar mass, for example, groups thermo-responsive polymers into three classes.[57] For polymers of type I, a decrease in the LCST is found for increasing molar mass following a typical 'Flory-Huggins' behaviour.[57] Type II describes polymers whose responsiveness is hardly affected by the molar mass, while the dependency on the molar mass for type III polymers is only found at low concentrations.

A selection of biomedically relevant thermo-responsive polymers, their structure and the corresponding range of transition temperature is given in Figure 4.[51, 52, 58]

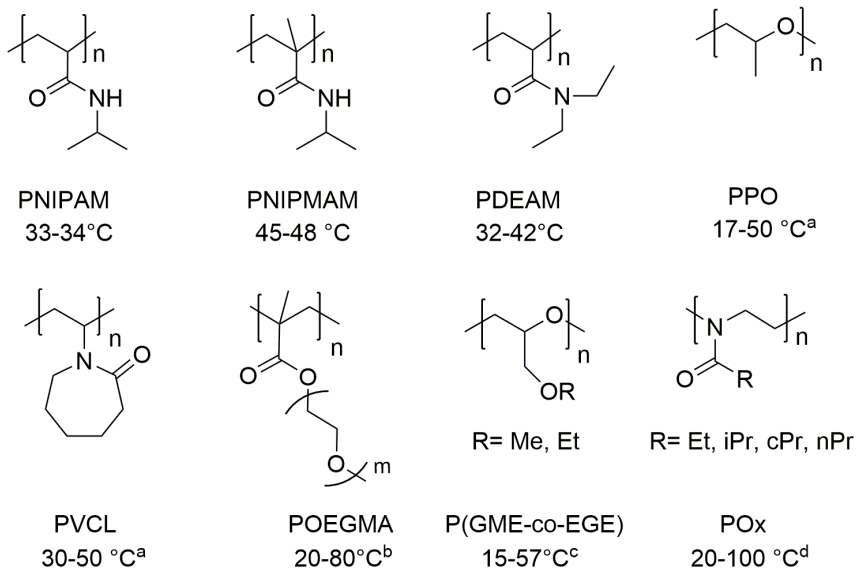

Figure 4. Selection of thermo-responsive LCST polymers and range of transition temperature: *poly*-(N-isopropyl acrylamide) (PNIPAM), *poly*-(N-isopropyl methacrylamide) (PNIPMAM), *poly*-(N,N-diethyl acrylamide) (PDEAM), *poly*-(propylene oxide) (PPO), *poly*-(vinyl caprolactam) (PVCL), *poly*-(oligo(ethylene glycol methacrylate) (POEGMA), p*oly(glycidyl methyl ether-co-ethyl glycidyl ether)* (P(GME-co-EGE), and *poly*-(oxazoline) (POx). [a]Highly dependent on concentration and molar mass,[51, 58] [b]dependent on number of side chain OEG units,[58, 59] [c]dependent on side chain substituent ratio,[60] [d]dependent on side chain substituent and molar mass.[58]

1.3.2.2 Application of Thermo-responsive Nanogels for Drug Delivery

For drug delivery purposes, *poly*-(N-isopropyl acrylamide) (PNIPAM),[61-63] *poly*-oligo(ethylene glycol) methacrylate (POEGMA),[59, 64] and *poly*-vinyl caprolactam (PVCL)[65, 66] are the most frequently used polymers for the formation of nanogels due to their biocompatibility and transition temperatures close to body temperature. Thereby, the thermo-responsive polymers are cross-linked to form a three-dimensional network and their temperature-triggered transition induces a volume change of the resulting nanogel network visible as shrinkage (for LCST polymers) or swelling (for UCST polymers). The temperature at which the nanogel undergo

phase change is referred to as volume phase transition temperature (VPTT). It is usually similar to the transition temperature of the thermo-responsive polymer used, but might be altered by copolymerization, combination with other polymers/materials, and the cross-linker' properties.

For controlled drug delivery, the conformational change of the nanogels can be used to induce the release of encapsulated cargos, e.g. along with the collapse and the expulsion of water. Therefore, control over the VPTT as well as the range of temperature in which the transition of the nanogels occurs are essential factors to prevent premature leakage of the encapsulated cargo.[47] Depending on the specific features and requirements of the respective bioactive that is to be delivered, tuning of the containing polymeric network is needed. In particular, the overall size and cross-linking density must be optimized to achieve both, an effective retention of the bioactive within the nanogels below the VPTT, and a temperature dependent release above the VPTT. In most cases, this bioactive is a small molecular weight drug, even though therapeutic proteins or other macromolecular actives are more frequently in clinical trial and thus gaining popularity by researchers.

The desired VPTT of the nanogels depends on the intended application. One can distinguish between systemic and topical applications of biocactives. A systemic application is defined as the route of administration for medications or other substances into the circulatory and/or lymphatic system of the body. The uptake thereby can be achieved either by absorption through the gastrointestinal tract (oral administration) or by parenteral administration including injection, infusion, or implantation. In contrast, topical administration refers to an application of drugs to body surfaces such as the skin or mucous membranes.

In systemic applications, the delivery system is permanently exposed to 37 °C body temperature after administration and therefore nanogels with VPTTs between 38 – 42 °C are desirable. Higher transition temperatures should be avoided to be able to apply the temperature trigger without damaging the surrounding tissue. On the other hand, in topical application on the skin, the carrier will face a natural temperature gradient ranging from 32 °C on the skin surface up to

37 °C in deeper skin layers.[67, 68] Here, nanogels with VPTTs within this range are of interest, as the temperature trigger will apply itself with increasing penetration depth of the drug carrier.[63, 69-73] As the control over the VPTT of the nanogels is thus a key parameter for temperature-triggered delivery, it is discussed in detail for both applications in the next two paragraphs.

Systemic Application

For systemic applications, the nanogels are exposed to 37 °C body temperature immediately after administration, which imposes a lower boundary on the VPTT. A natural temperature elevation, useful to trigger the transition of the nanogels, can appear, for example, due to an inflammation or infection.[74] However, in most cases, an external hyperthermic stimulus is needed.[47] For longer exposition times at temperatures above 42 °C, protein denaturation and disruption of anatomic structures are pending. Therefore, thermo-responsive nanogels with a VPTT slightly above 37 °C are of interest in order to allow the application of a thermal trigger without affecting surrounding healthy tissue.[42, 43]

PNIPAM and nanogels made from PNIPAM are probably the most investigated systems with numerous reports on their synthesis and detailed mechanistic studies on the phase-separation process.[61, 75-80] However, PNIPAM has a LCST of 32–34 °C which is slightly too low for temperature-triggered delivery of drugs in systemic applications. To overcome this issue, co-polymerization of the thermo-responsive moiety with hydrophilic monomers can be performed, altering the hydrophilic-hydrophobic balance and thus shifting the VPTTs to higher values. The most prominent monomer to incorporate is acrylic acid (AA),[40, 81-83] but other acids like methacrylic,[84] vinylacetic,[85] maleic,[84] fumaric,[84] and allyl-acetic acid[86] have been reported to yield nanogels with higher VPTT as well.

Due to the ionisable character of the carboxyl function, its hydrophilicity is dependent on the pH with high hydrophilicity at basic conditions (bearing a negative charge) and low hydrophilicity in acidic environment due to abstraction of protons. This results in pH-

dependent shifts of the VPTT. For example, Debord and Lyon[83] reported the synthesis of bis-acrylamide (BIS) cross-linked nanogels using random copolymerization of NIPAM, AA and tert-butyl acrylamide and demonstrated strong differences of resulting VPTTs in acidic or basic environments. In addition, the ratio between the used monomers allowed them to fine-tune the VPTT in a broad range (8-48 °C). Yang and co-workers[87] found similar results for PNIPAM-co-AA nanogels with a VPTT of 45 °C at physiological pH of 7.4 and a shift of the transition to lower temperatures (29 °C) in acidic environment. In addition, the authors could demonstrate positive effects for loading the positively charged drug Doxorubicin (as hydrochloride salt) and a pH-dependent release.[87]

Another recent example developed by Calderón et al.[82] is the use of dendritic acrylamide (ABC) bearing three carbocyclic groups along with NIPAM. The formed nanogel exhibited a temperature-induced phase transition upon shifting the pH from physiological (7.4) to lysosomal (pH 5). Furthermore, efficient delivery of the anticancer drug Cis-platin (Cis-Pt) along with the transition (Figure 5) could be shown.

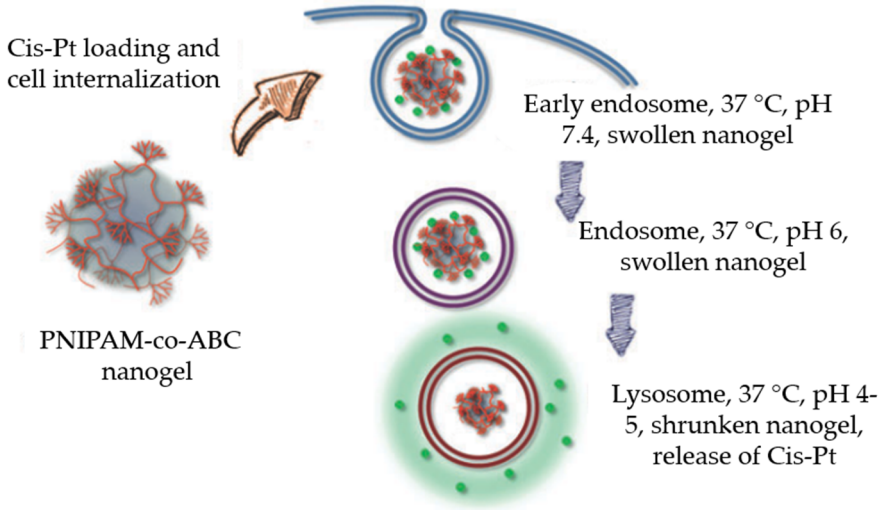

Figure 5. Schematic representation of temperature-induced shrinkage of PNIPAM-co-ABC nanogels and release of encapsulated Cis-Pt upon cell internalization. Adapted from reference [82] with permission from Royal Society of Chemistry. Copyright 2017.

One disadvantage of this strategy is that the inclusion of charges often leads a broader slope of the VPTT. Furthermore, althought the negative charge may be advantageous for positively charged drugs, it can hinder the loading of other drugs. Charges can also negatively affect the nanogels' biological fate, e.g. by enhancing the formation of a protein corona, which can lead to unexpected behaviour *in vivo*.[88, 89]

Another strategy to tune the transition temperature is copolymerization with other thermo-responsive polymers which themselves have a transition at a higher temperature. A requirement for this method is the formation of random copolymers to avoid a two-step transition. An independent transition of the single constituents is typically obtained with core-shell structures[90-92] or with block-copolymers which are not sufficiently interacting and influencing each other.[93]

The structure of poly-N-isopropyl methacrylamide (PNIPMAM) is very close to PNIPAM with the difference that it contains a methyl group in its vinyl backbone (Figure 4). It is proposed that this methyl group induces a steric rigidity to the polymer weakening the intramolecular interactions between the amide groups and favouring hydrogen bonds with surrounding water molecules. This leads to a shift of the transition temperature to higher temperatures (40-45 °C), despite similar hydrophobicity.[76, 94, 95] Studies of phase transition behaviour of linear PNIPAM-PNIPMAM copolymers showed ideal mixing behaviour with a direct dependency of the lower critical solution temperature on the ratio of the two polymers. Djopké and Vogt[95] could demonstrate that the transition temperature of the randomly polymerized linear copolymers can be precisely fine-tuned between 32.5 °C and 47 °C while the transition remains independent on molecular weight and concentration in analogy to the homopolymers. Macro- or nanogels from PNIPAM or PNIPMAM, typically cross-linked with small molecular weight BIS, show similar hydrodynamic radii and spherical shape.[96] Keerl, Pedersen and Richtering[97] synthesized a copolymeric nanogel showing a transition temperature of 39 °C with a sharp transition profile and investigated microscopical structural changes upon the transition. In this regard, the combination of the two monomers is promising to fine-tune the VPTT of thermo-responsive nanogels for the applications as drug delivery devices.

Topical Application

Topical administration of drugs is attractive in particular for the therapy of inflammatory skin diseases and sometimes even inevitable for a targeted and local treatment. However, the skin and especially the outermost layer of the skin, the stratum corneum (SC), is a highly efficient protective barrier, which results in poor absorption of drugs to the underlying viable tissue and thus the need for efficient carrier systems.[98] Nano-sized particles were shown to be an effective tool in overcoming this barrier. The nature of the carrier thereby strongly influences the mechanistic of the penetration pathway. Rigid nanoparticles, for instance, tend to accumulate in the hair follicular openings of the skin while soft particles are able to penetrate through narrow intercellular channels due to their deformability.[99-101]

The variety of possible cargos which can be encapsulated in polymeric nanogels make them attractive carriers, not only for improving skin penetration, but also for an enhanced solubility of small and medium molecular weight drugs of hydrophobic nature. Thermo-responsive nanogels are particular promising candidates, as the skin has a natural temperature gradient from 32 °C on the skin surface to 37 °C in viable skin layers.[67, 68] . As a result, nanogels with a response in between this temperature range can use the occurring gradient to trigger the release of their encapsulated cargos only after reaching a certain penetration depth (Figure 6).

Several polymeric nanogels have been developed for this reason demonstrating the excellent performance of the temperature-triggered delivery.[69-72] For instance, the delivery of the hydrophobic drug Dexamethasone could be enhanced 2.5-fold to the epidermis and even 30-fold to the dermis when delivered by thermo-responsive nanogels as compared to a commercial cream. These nanogels were based on linear P(GME-co-EGE) and dendritic polyglycerol (dPG) and had a VPTT of 32 °C. For improved encapsulation of the hydrophobic drug, the nanogels were decorated with β-cyclodextrin, which itself is also known to promote skin penetration.[71] In addition, similar nanogels without β-cyclodextrin decoration have shown exceptional delivery capabilities for the anti-inflammatory, therapeutic protein Etanercept (ETN).[70] The investigation of the underlying penetration mechanisms indicates that besides the release of the therapeutic

also the simultaneous expulsion of water molecules from the nanogels above their VPTT is crucial for their performance as penetration enhancers. It induces hydration of the skin, which assists the penetration of the therapeutics into deeper skin layers.[69] In another study, PNIPAM was used as a thermo-responsive polymer cross-linked with dPG for the generation of nanogels with a VPTT of 34 °C.[70, 72] Efficient dermal delivery with the help of these nanogels was demonstrated for a range of proteins including model proteins like bovine serum albumin (BSA) and L-aspaginase II, and the therapeutically active proteins such as ETN and transglutaminase-1.

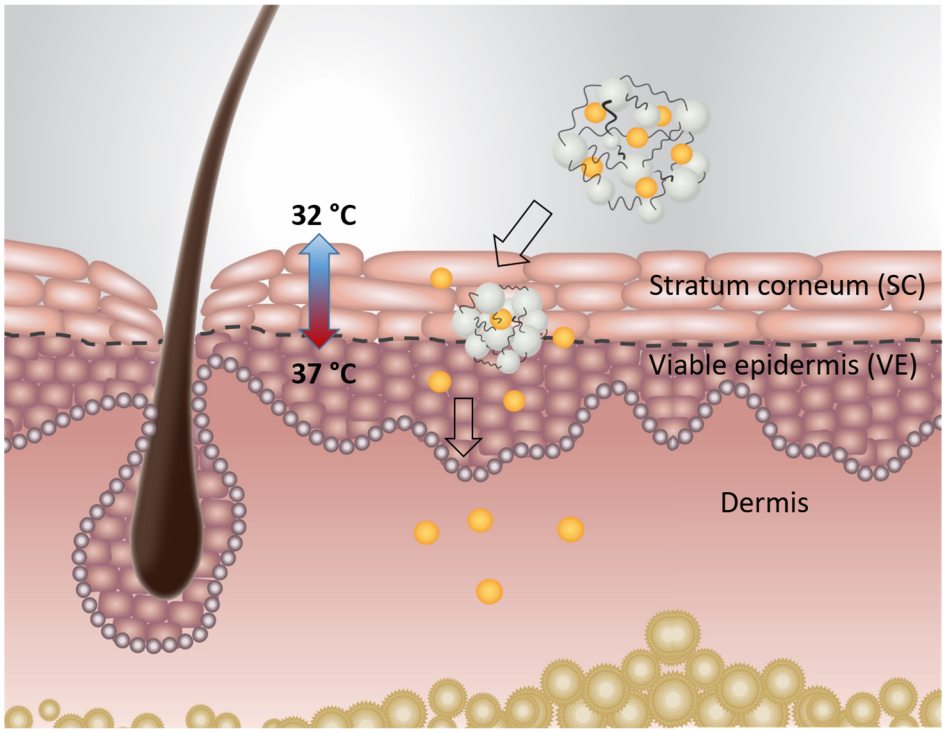

Figure 6. Schematic presentation of dermal delivery triggered by the thermal gradient in the skin.

For the generation of nanogels in the above-mentioned work, dPG was used to crosslink different thermo-responsive polymers. It was chosen due to its hydrophilic and biocompatible character and its multi-functionality, which allows easy modification. In addition, it is known for its ability to stabilize proteins against degradation and denaturation.[20, 102, 103] Indeed, the use of dPG as macromolecular cross-linker of thermo-responsive polymers increased the stability of the nanogels themselves[104] as well as the encapsulated protein, efficiently protecting it and

maintaining its biological function.[70, 72] In addition, all mentioned nanogels were designed to have VPTTs between 32-34 °C in order to take advantage of the natural temperature gradient in the skin as a trigger for the release of their cargo. Nevertheless, nanogels with higher VPTTs could be of interest as well, as they endow the possibility, in combination with an external hyperthermic stimulus, for a temporal and local control of the delivery.

1.3.3 REDOX-DEGRADABLE NANOGELS

The third important class of responsive nanogels are redox-sensitive carriers.[42] Thereby, the redox-response is achieved by incorporation of disulfide bonds within the nanogels' network. The reduction of the disulfides to thiols, results most cases in a degradation of the network. The importance of this class of nanogels relies on the occurrence of increased redox potentials within most intracellular compartments due to the presence of reduced glutathione (GSH) in relatively high concentrations (2-10 mM) in comparison to concentrations in the blood plasma (2-20 μM).[105-107] This makes the use of disulfide bridges particularly interesting in carriers designed to deliver drugs after cellular internalization. The fast cleavage of the disulfides under increased redox potentials will degrade the nanogels resulting in a burst release of the cargo and faster clearance of the polymeric fragments from the body reducing toxicity concerns.[42]

Similar to pH-labile bonds, disulfides can be introduced either in the polymeric backbone or in the cross-linker of the nanogels' network. In most cases, the latter is used as the introduction of disulfides into the cross-linker allows the variation of different monomers for nanogel synthesis without any chemical modifications. For example, Zhong and co-workers developed redox-degradable nanogels using hyaluronic acid cross-linked with disulfide bearing L-cysteine dimethacrylamide.[108] They demonstrated excellent loading abilities for the apoptosis inducing protein cytochrome c, high redox sensitivity and efficient delivery of the drug after internalization in human breast cancer cells. In many cases, redox-responsive moieties are combined with either pH or temperature responsive polymers resulting in dual-sensitive nanogels. Tian, Bian and Yang used for instance POEGMA in combination with N,N'-bis(acryloyl)cystamine for the generation of temperature and redox-sensitive nanogels.

Taking advantage of the temperature-response of POEGMA, they could generate the nanogels using precipitation polymerization technique (Chapter 1.4).[64] Synergistic interplay of the temperature and the redox triggers is reported by Yang and co-workers.[109] They found that the application of elevated temperature enhanced the cell internalization of nanogels loaded with the anticancer drug Doxorubicin. In combination with the degradation of the nanogels in reductive cell environment, yielding a burst release of the drug, increased therapeutic effects were observed for the combination of both triggers.

Apart from the controlled degradation upon a redox-trigger, disulfide-containing particles are interesting candidates for interaction with thiol- and disulfide-rich biological materials, for example mucus. Mucosal layers are found in many regions of the body including the eyes, respiratory tract, gastrointestinal tract and reproductive organs. The gel layer protects underlying epithelial cells from foreign particles, bacteria and viruses by a constant secretion of newly produced gel matrix and shedding of the old. The rate of this mucosal turnover depends on mucus thickness and can range from several minutes, like in the eye or nose, to hours and days in the gastrointestinal and vaginal tract.[110-112] Therefore, drug delivery to underlying epithelial cells requires carriers able to overcome this mucosal clearance. The mucus layer consists of an aqueous gel matrix formed from cross-linked and entangled mucin fibers, filled with sloughed cells, bacteria, proteins and cell debris. Due to the presence of cysteine in the backbone of mucins the mucosal layer contains both, free thiols and disulfides responsible for the cross-linking of mucins.[112, 113] Mucosal drug delivery agents are typically divided into two classes dependent on their interaction with the mucus as mucoadhering or mucopenetrating.

Thereby, penetrating particles are subdivided into actively and passively penetrating. In the passive approach, particles are designed to minimize any interactions with the mucus and thereby "slip" through which is typically achieved by surface functionalization with PEG or copolymers of polyoxyethylene and polyoxypropylene.[110] In the active approach, mucosal disulfides in close proximity to the carrier are locally cleaved by the release of oxidizing agents. The carriers thus clears its ways through the mucosal layer.

Adhering particles stick to the mucosal layer resulting in prolonged residence time of the incorporated drugs. This strategy is mainly used for mucosal layers with a slow turnover rate. Typical carriers consist of poly-AA and adhere through ionic interactions and physical entanglement. Beside poly-AA also alginate, cellulose derivatives, pectins and chitosan-based particles are used. For all of them, thiolation is reported to strongly enhance adhesion properties through interaction with free thiols in the mucins.[114-119] To our knowledge the interaction of disulfide containing particles with mucus have not been investigated so far, but both, mucopenetration though disulfide exchange reactions or mucoadhering properties through the generation of free thiols are conceivable prospects.

1.4 SYNTHESIS STRATEGIES FOR NANOGELS

For the synthesis of polymeric nanogels several techniques have been developed in order to gain control over particle size and prevent the formation of macroscopic gels. For the radical-based synthesis, where the polymeric chains are grown *in situ*, two major strategies evolved, namely, precipitation/dispersion and emulsion polymerization (Figure 7). For the synthesis of gels in the nanometer range, the classical emulsion polymerization method was modified which resulted in the development of the so called mini- and microemulsion polymerization technique (Figure 7).[42]

Thermo-responsive nanogels are typically synthesized using precipitation or dispersion polymerization. The main mechanistic difference between these two is the location of the polymerization process which is determined by the swelling degree of the formed precursor particles.[120] Both processes start initially with a homogenous mixture of initiator, monomer, possibly surfactant, and cross-linker solubilized in a continuous phase. During the polymerization process, after reaching a critical chain length, growing polymer chains are no longer soluble in the continuous phase resulting in the formation of precursor particles. In a precipitation polymerization these particles do not swell in the medium, they precipitate, and form nucleates which grow through coagulation and incorporation of further precipitating polymer chains. In contrast, in dispersion polymerization, precursor particles are slightly swollen in the continuous phase leading to further polymerization mainly within these particles and no coagulation of the precursors (Figure 7).

In dispersion polymerization, the addition of stabilizing surfactants is indispensable to avoid that the coagulation becomes too strong and that larger particles are formed. In contrast, precipitation polymerization can be performed either with or without surfactants. Nevertheless, in both techniques the surfactant concentrations are always below the critical micelle concentration and only stabilize the formed precursor particles but do not form a closed vesicle.

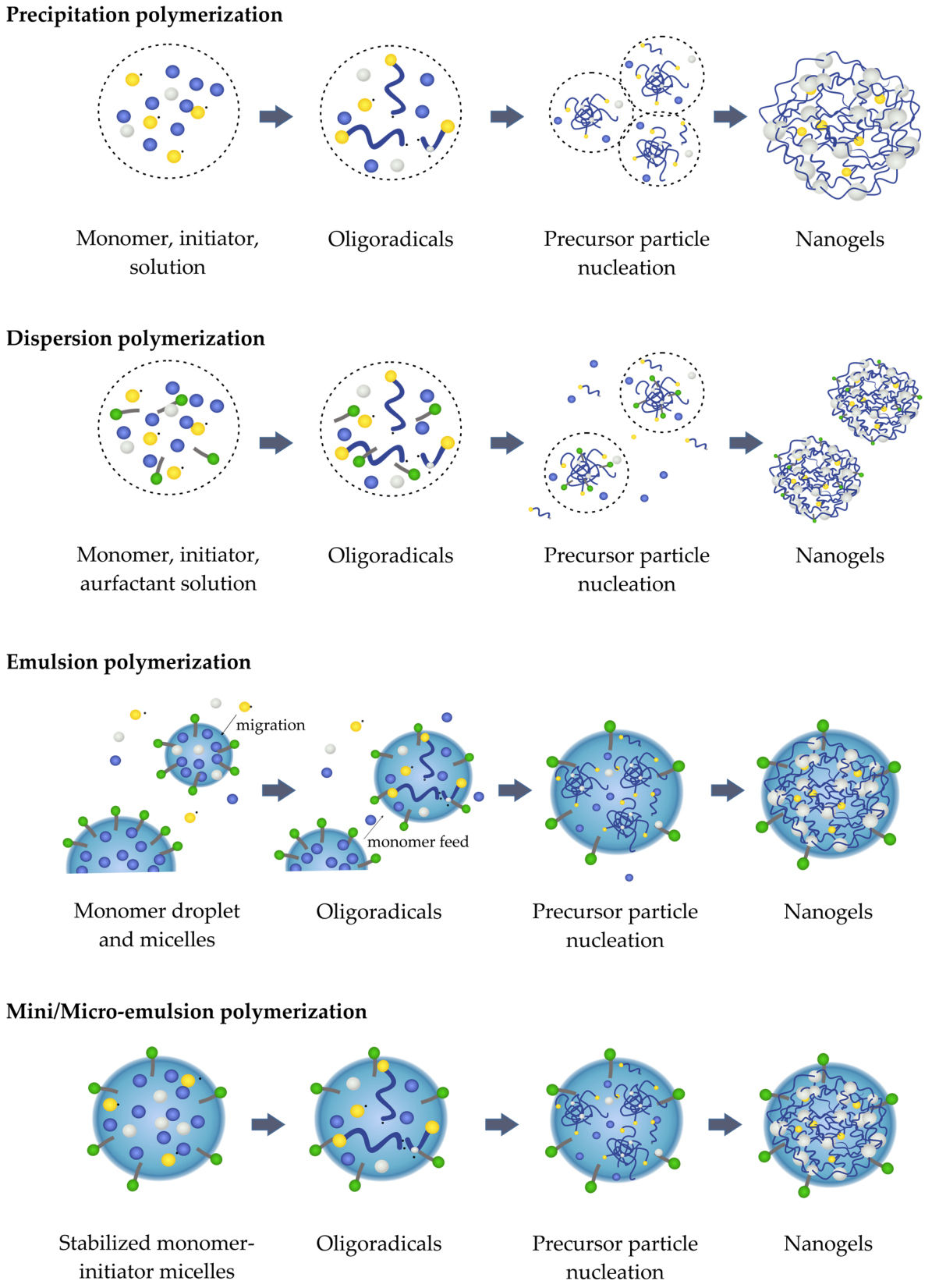

Figure 7. Different polymerization techniques and underlying mechanism for the generation of nanogels.

Both methods are frequently used for the formation of thermo-responsive nanogels based on LCST polymers. This is because a temperature dependent solubility only occurs for polymer chains from a certain chain length while the monomers and short oligomers do not change their solvation state. Thus, the reaction temperature is a key parameter to transform the solvent (in most cases water) at temperature above the LCST to a non-solvent for the growing polymer chains, resulting in their precipitation when they reach a certain chain length.

The other option to limit the size of polymer networks during the polymerization is the use of emulsion polymerizations. In general, an emulsion describes the formation of a dispersion of one solvent (dispersed phase) in another (continuous phase). The most common emulsion is the oil in water (O/W) emulsion while for the generation of hydrophilic nanogels 'inverse' emulsions (W/O) are used. In a typical emulsion mechanism, first, monomer droplets and monomer containing micelles, which are formed and stabilized by surfactants, are dispersed in a continuous phase in which the initiator is soluble. The polymerization is then initiated by the migration of the initiator to a monomer containing micelle which grows through a constant monomer feed from the shrinking monomer droplets.[121]

For sizes, especially in the lower nanometer range, some modifications of this technique are required to prevent growing of the gels to a micrometer size range. Here, two methods yielded good results: mini- and microemulsion.[121-123] The mechanism for both polymerizations is similar. First, nano-sized droplets are produced and stabilized containing all components: monomer, cross-linker, and initiator. Then, in analogy to precipitation polymerization, the polymerization is initiated but the whole process of nucleation and growing is performed within the nanodroplet acting as a 'nano-reactor'. The size of the droplet is thereby the limiting factor for the size of the resulting gels.[122, 123] As a result, for both methods the generation of stable droplets of nano-size is the key parameter which need to be controlled.

In miniemulsions, kinetically stable droplets are formed through the application of high sheer stress or ultrasound.[123] To prevent the nanodroplets to aggregate and precipitate through

Ostwald ripening (diffusion based growing of the droplets) or coalescence leading to phase separation, surfactants soluble in the continuous phase, as well as co-stabilizer soluble in the dispersed phase, are required.[123] In contrast, in the microemulsion, thermodynamically stable nanodroplets are formed only through the addition of stabilizing surfactants without any application of shear stress.[122] The drawback of the emulsion techniques, in comparison to the precipitation or dispersion polymerization, is the use of high amounts of surfactants which often complicate the purification of the resulting nanoparticles. In addition, in the precipitation polymerization of thermo-responsive polymers only water and no other organic solvents are required, which is beneficial in the context of their intended use for biomedical applications as well as under environmental aspects.

1.5 COMBINATION THERAPY

The molecular complexity of many diseases require combinational therapy approaches in order to increase treatment outcomes and decrease undesirable side-effects, particularly in long-term treatments. Classical combination therapy in cancer refers to the simultaneous administration of two or more pharmaceutical actives or the combination of different treatment modalities like chemotherapy and radiotherapy.[124] The simple co-formulation of chemotherapeutic actives often increases toxic side effects and may lack compatibility of the pharmacokinetic profiles of the two drugs. Therefore, smart drug delivery systems are in the focus for combinational delivery of drugs ensuring their transport and release to the same target.[125] The advances made in the development of multifunctional polymeric nanomaterials allow not only the loading of several drugs into the same carrier, but also the inclusion of particles, e.g. metallic or magnetic nanoparticles, or functional materials that bring in new features and treatment modalities. Carriers which combine different materials are thereby referred to as hybrid or composite materials. In particular, hybrid nanogels with multifunctionality and novel properties emerged as promising platforms to perform controlled drug delivery in combination with radiotherapy, photothermal therapy (PTT) or photodynamic therapy (PDT). In the best case, the materials are even equipped with imaging agents that allow a close integration of therapy and diagnostic (theranostic), which can be used for example in imaging guided therapy approaches.[33]

1.5.1 PHOTOTHERMAL THERAPY AND COMBINATION THERAPY WITH CHEMOTHERAPEUTICS

Thermal treatment approaches makes use of temperature-induced changes in the dynamics and viability of biological systems. Dependent on the rate of temperature elevation, we can distinguish between hyperthermia, with temperatures in the range of 41 – 47 °C, and irreversible injury treatments, occurring at temperatures above 48 °C. Hyperthermia is correlated with increased diffusional rates across membranes and enhanced susceptibility against chemo- and radiotherapy and is therefore used as an adjunct to these treatments. An irreversible damage of cells or tissue is only observed for very long-time hyperthermia treatments in the range of several hours or upon the application of high temperatures. At temperatures above 48 °C

structural protein denaturation leads to coagulative necrosis already after short exposure times of several minutes.[126] In classical thermal therapy increased temperatures are induced in parts or even the whole body. This has the drawback that besides the cancerous tissue also surrounding healthy tissue is exposed to the hyperthermic stimuli. Thus, intense effort has been made for the development of techniques to achieve a controlled and local heat generation only at the target site. Additionally, fundamental studies on the underlying mechanisms of the temperature induced cell killing have been explored.[126-128]

A promising tool for the local generation of heat are photothermal transducing agents which are able to absorb light and transform its energy into heat.[129] In particular, particles able to transform near-infrared (NIR) light, with wavelengths between 700-950 nm, attracted increased attention since biological tissue shows particularly low absorbance and scattering of light within this range. As a result, the penetration depth of NIR light into tissue is significantly greater than light of other wavelengths, e.g. light of the UV-visible range, and can reach up to several centimetres deep. Taking advantage of this deep penetration, NIR transducing materials offer minimally invasive approaches for cancer treatment. With the use of external laser irradiation they deliver high thermal energy to the cancerous tissue, allow adjustable energy dosing, and precise local control. This renders them into efficient agents for thermal ablation of tumors and yet minimizing harm to surrounding healthy tissue.[126, 129, 130] Important NIR transducing materials are noble metal nanoparticles, mainly anisotropic gold particles of different shapes and sizes,[131, 132] carbon based NIR transducers like graphene and carbon nanotubes,[87, 133, 134] small molecules e.g. indocyanine green,[135, 136] and semi-conducting polymers (Figure 8).

Metallic nanoparticles and in particular gold-based ones have been extensively studied for applications in PTT. Making use of the heat generated under exposure to NIR light, they could be successfully applied to ablate cancerous tissue.[126, 129, 137] Several studies additionally demonstrated NIR triggered-release and synergistic therapeutic effects upon incorporation of these particles into responsive nanogels delivering chemotherapeutic agents.[138, 139 140] In contrast, semi-conducing polymers are relatively new in the field with the first description of the use of

polyaniline (PANI) nanoparticles as NIR transducers for photothermal ablation of tumors in 2011 by Haam and co-workers.[141] Since then, further studies on PANI[142-145] and other semiconducting polymers like polypyrrole (PPY)[146-149] and poly(3,4-ethylenedioxythiophene) polystyrene sulphate (PEDOT:PSS)[150, 151] have been performed showing high photostability of the polymers and good outcomes upon their use in PTT.

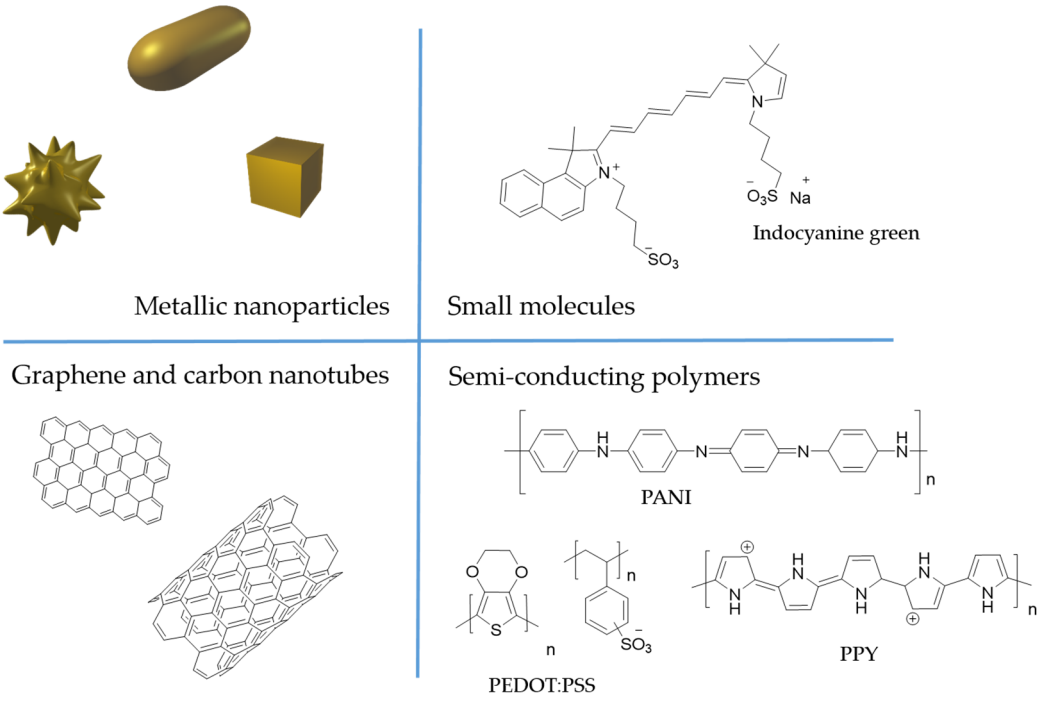

Figure 8. Classes of NIR transducing agents.

In particular, the polymer PPY has gained increased attention as it is has been used in biomedical applications and was demonstrated as biocompatible material suitable for biosensors,[152, 153] in tissue engineering,[154] and for neural prosthetics.[155-157] Almost contemporaneously the groups of Liu[147] and Zheng[158] reported the synthesis of PPY nanoparticles and demonstrated suitability for PTT of breast cancer xenografts implanted in mice. In both cases, efficient tumor reduction was achieved with temperature elevation to more than 50 °C at the tumor site. Thermal imaging upon the NIR exposure demonstrated good local control of the thermal treatment with only minimal temperature increases at the surrounding tissue close to the tumor site. The group of Zheng and co-workers additionally investigated the biodistribution profiles of the particles

showing that accumulation of the majority of PPY particles in the liver and the spleen after intravenous (i.v.) injection. To circumvent, respectively delay, particle recognition by the reticuloendothelial system (RES) the authors suggested the implementation of stealth functionalization of the particle surface. This is commonly achieved through the conjugation of polyethylene glycol (PEG) or similar polymers to the surface of particles, which reduce the opsonisation of proteins and thus the recognition of the particles by phagocytes.[25] Indeed, Dai and co-workers[159] found increased accumulation up to 18%ID/g tumor for PEGylated PPY particles. This accumulated concentration was found to a suitable to slow down tumor growth after i.v. administration and NIR exposure for 10 minutes. In addition, the authors functionalized the particles with a gadolinium chelate as contrast agent for magnetic resonance imaging, which they could use for time-dependent visualization of particle accumulation at the tumor site.[159]

Cooperative effects between PTT using PPY particles and radiotherapy was recently shown by Shi et al.[160] Interestingly, the authors found higher efficiency for the sequence using first PTT and then radiotherapy compared to the reversed order indicating that PTT helps to sensitize tumor cells for the following therapy. Synergistic effects with the chemotherapeutic agent Doxorubicin was reported for iron oxide-PPY core-shell particles showing decreased tumor volumes for the combinational therapy whereas for the single treatments only a decelerated growth was found.[161] Similar results were reported by Tang and co-workers,[162] who employed the same approach, but instead of using a core-shell structure dissolved the iron-oxide core prior loading of Doxorubicin. The resulting hollow particles had a spindle-like shape, which the authors could correlate with increased cellular internalization and efficient delivery of the drug upon NIR exposure.

As PPY in its pure form is water insoluble, particle stabilization is crucial. In the above-mentioned reports for PPY particles for PTT applications, stabilization was achieved by wrapping the final particles using the polymers polyvinyl pyrrolidone (PVP) or polyvinyl alcohol (PVA) which were added during the polymerization process.[146, 147] With the good results

achieved for other photothermal agents like gold nanoparticles, it stands to reason that a rational design of the stabilizing matrix, e.g. equipping them with stimuli responsive materials, can implement new functionalities for the use of the particles in combinational therapy approaches or for the inclusion of imaging modalities.

One possible option is the incorporation of PPY into hydrophilic nanogels. A preliminary work by Calderón et al., shows the feasibility of thermo-responsive nanogels as a stabilizing matrix for the photothermal transducing polymer PANI. Additionally, they could demonstrate the applicability of the resulting nanogels as PTT agent able to slow down the tumor growth of ovarian tumor xenografts.[144] For the introduction of PANI they used semi-interpenetration method. Semi-interpenetration is defined as the physical entanglement of a linear polymer in a cross-linked polymeric network and is typically achieved through the formation of one system in presence of the other.[163, 164] It emerged as an elegant tool for the inclusion of new capabilities to nanogels through the penetration with functional polymers. The great advantage of the semi-interpenetration method is that the individual properties of both the nanogels and the interpenetrating polymer are retained by their non-covalent linkage. For a potential use of the semi-interpenetrated materials as drug delivery agent, a proper understanding of the interpenetrating process and resulting structure, e.g. the localization of the interpenetrating polymer within the nanogels, is important. In the case of stimuli-responsive nanogels, additionally a thorough understanding of structural changes influencing the particles properties under exposure to the stimulus is relevant to determine suitable candidates for an application *in vivo*.

So far, only one report on PPY incorporated into smart, temperature-responsive nanogels has been published.[165] The authors used thermo-responsive PNIPAM mixed with chitosan and incorporated PPY by *in situ* polymerization of pyrrole during nanogel formation. The release of loaded Doxorubicin was efficiently increased under NIR exposure and temperature elevation of the tumor site post to nanogel injections indicated suitability of the nanogels for PTT.

Nevertheless, the presented study lacks of a full evaluation of the therapeutic efficiency and biodistribution of the nanogels.

1.5.2 PHOTOACOUSTIC IMAGING

Another beneficial aspect of photothermally active materials and their incorporation into drug delivery systems is that their photothermal response translate them into excellent photoacoustic (PA) imaging enhancers. PA imaging is an emerging non-invasive technique that provides 3D images of absorption-based contrast with high spatial resolution and allows a comparative and quantitative image intensity analysis.[129] PA imaging typically uses short (nanoseconds) optical excitation pulses to induce local thermal expansion of the tissue which translates into acoustic waves (Figure 9). The spatial distribution of the optical absorption, and hence the local abundance of chromophores, is encoded onto the time-course of the waves, which are detected outside the organism or sample. From these data sets, three-dimensional images are reconstructed that show the spatial distribution of the absorbing chromophores within the illuminated volume. As a result, light-to-heat transducing materials increase the PA signal intensity translating these materials into intrinsic theranostic devices enabling imaging guided therapy approaches.

The suitability of pure PPY nanoparticles as PA contrast agent was demonstrated by Dai and coworkers.[166] They showed the ability to visualize the particles down to a depth of 4 cm in muscle tissue upon exposure to laser light of 808 nm. The feasibility to follow the particles in real-time after administration was recently demonstrated in the same group.[159] Using dual imaging modalities of PA and magnetic resonance imaging and a good correlation between both imaging techniques, they could demonstrate the possibility to use PA imaging to monitor the accumulation of the particles at the tumor site.

Intrinsic imaging modalities additionally are advantageous for the determination of biodistribution profiles of new materials, which is a key parameter for the evaluation of new

drug delivery agents. With a label-free detection of the particles, one can disclaim additional synthetic modifications which could alter occurring biological interactions after administration.

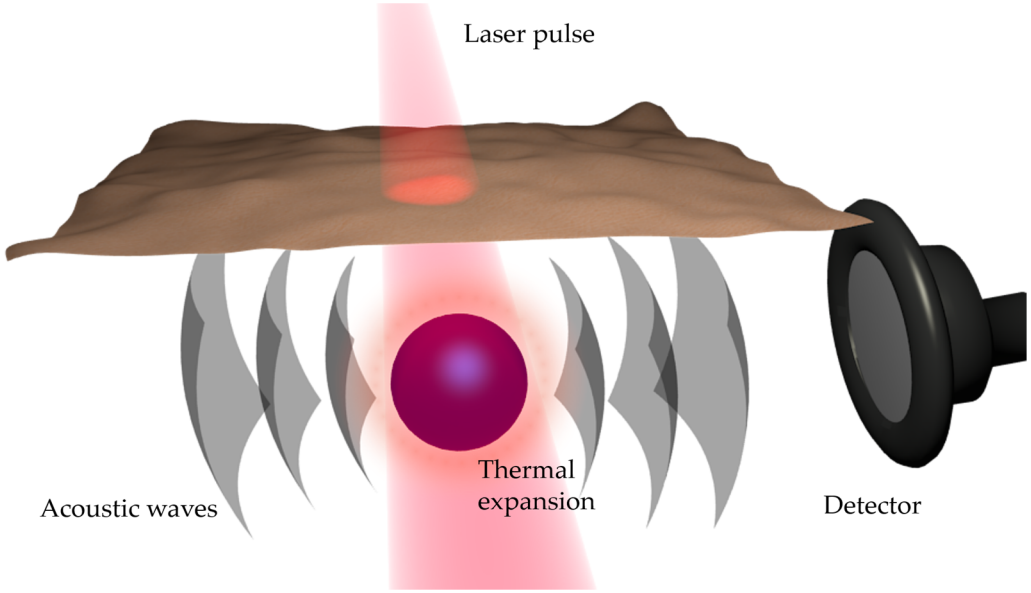

Figure 9. Principle of photoacoustic signalling enhanced by heat generation of an NIR-light absorber.

2 MOTIVATION & OBJECTIVES

Nano-sized smart drug delivery agents have the potential to protect therapeutic actives and release them upon a certain trigger. With the ability of a targeted delivery, they can efficiently increase pharmacokinetic profiles of conventional drugs, overcome dose limits, and reduce the occurrence of toxic side effects. Polymeric nanogels evolved as promising delivery platform due to their good biocompatibility, high loading capacities and the possibility of responsive behaviour. However, the complexity of the occurring diseases and the huge variability of possible therapeutic actives, ranging from small molecules to therapeutic proteins, make it necessary to adapt the carrier to the specific requirements. The control over properties and structure of the nanogels, such as network density, hydrophilic/hydrophobic character, responsiveness, charge, and size, and the knowledge of appropriate tuning pathways are therefore indispensable for the generation of efficient delivery systems. The main objective of this thesis is the development of concepts to adapt responsive nanogels in order to achieve efficient delivery of pharmaceutic actives, including small molecular weight drugs as well as therapeutic proteins, and broaden their range of applications from dermal, to mucosal, and systemic administration. The identification of key synthetic parameters to gain control of the network structure and the nanogels' properties with regard to the specific requirements of the drugs form the basis of this work. Building upon this, the translation into multi-responsive systems is targeted to generate tunable delivery platforms with advanced properties for a variety of applications (Figure 10).

To address an efficient delivery of therapeutic proteins in dermal applications, overcoming the skin barrier and penetrating into viable skin layers is vital and shall be approached with the aid of thermo-responsive nanogels as smart carriers. The structural properties of the nanogels, such as swelling degree and network density, are key factors for an efficient encapsulation and retention of the proteins within the nanogels during their transport. In addition, the regulation

of the volume phase transition temperature (VPTT) of the nanogels is crucial to enable a temperature-triggered release. Thus, it should be explored whether the thermo-responsive polymer *poly*-N-isopropyl methacrylamide (PNIPMAM) and the copolymerization with *poly*-N-isopropyl acrylamide (PNIPAM) allows tuning of the resulting nanogels' VPTT.

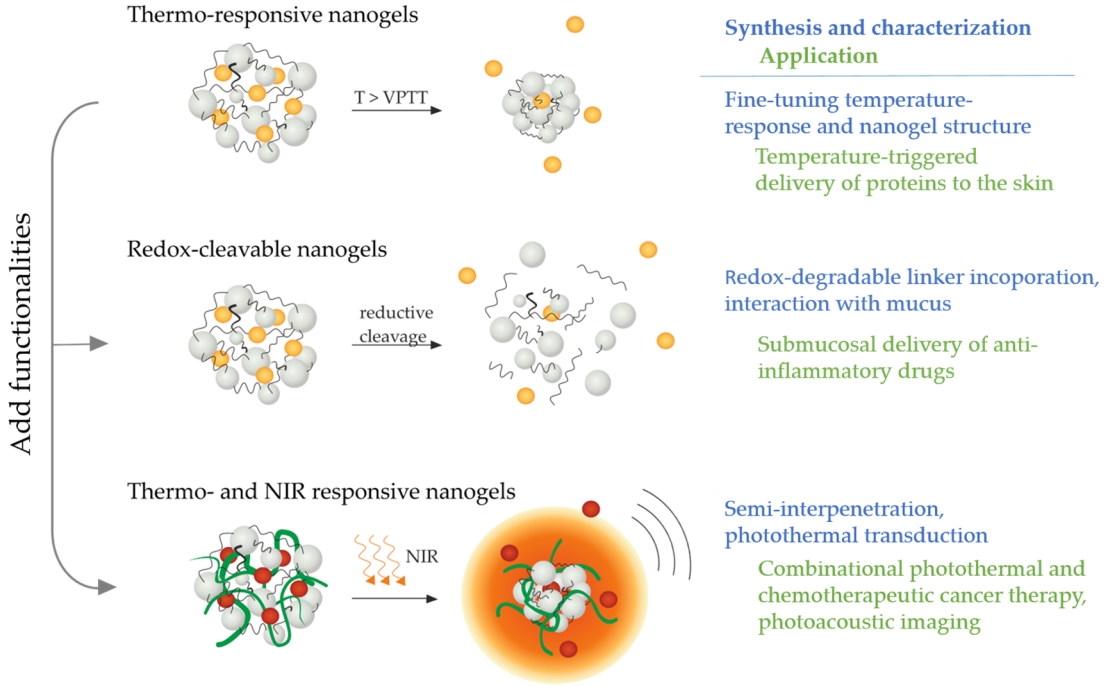

Figure 10. Research objectives presented in this thesis: Development of thermo-responsive nanogels and fine-tuning of their temperature response and structure as a basis for further functionalization of the nanogels with redox-cleavable moieties or NIR-transducing polymers.

In chapter 4.1.1, a thorough screening of reaction conditions and an evaluation of the resulting nanogels' properties, as well as a detailed analysis of the processes during nanogel formation, shall be performed to reveal the key parameters influencing the nanogel structure. In particular, the reaction kinetic of the two thermo-responsive polymers with acrylated dendritic polyglycerol (dPG) as crosslinker shall be studied. The nanogels' constitution, size, swelling ability and reaction conversion will be determined at different time points during the polymerization. Based on these results, in chapter 4.2.1, optimized candidates should be evaluated regarding their ability to encapsulate the model protein bovine serum albumin (BSA)

and to release it in a temperature-triggered fashion. Special attention shall be paid to the structural integrity of the proteins as the alteration can lead to a loss of their biological function. With the generation of nanogels with different VPTT, a comparison between dermal protein delivery performance induced by the natural temperature gradient in the skin and externally triggered temperature increase shall be evaluated.

The assessed thermo-responsive nanogels should be adapted for the delivery of anti-inflammatory drugs to submucosal cells. The implementation of disulfides should enable the nanogels to overcome the mucosal clearance mechanisms and thus increase the therapeutic efficiency of the loaded drugs against chronic inflammations such as Crohn's disease. Therefore, in section 4.1.2, a redox-degradable disulfide unit shall be introduced to the nanogel's polymer network. To maintain the flexibility to generate a variety of thermo-responsive nanogels using different monomers, the degradable unit shall be incorporated into the cross-linker. Thus, a degradable linker design will be employed which allows first its conjugation to dPG and then the reaction with the thermo-responsive polymers in a precipitation polymerization. As a proof of successful disulfide integration, degradation profiles of the resulting nanogels will be determined in reductive environments. In addition, the interaction with *ex vivo* native mucus shall be evaluated. Here, effects of the occurring interactions on the nanogels' structure shall be employed. In addition, the ability of the nanogels to counteract the mucosal clearance should be studied *ex vivo*, which forms the base for an efficient delivery of drugs to submucosal cell layers.

In chapter 4.2.2, the redox-degradable nanogels shall be evaluated for capability to encapsulate anti-inflammatory drugs of different nature, namely the small molecular weight drug Budesonide (BUD) and the therapeutic protein Etanercept (ETN). To check the retention of the therapeutic activity of ETN upon encapsulation, the structural integrity of ETN and the ability to bind to TNF-α will be tested *in vitro*.

Finally, a near-infrared (NIR)-transducing polymer will be incorporated into thermo-responsive nanogels to form new hybrid nanogels, applicable in combinational therapy approaches of cancer. Improvements in therapeutic efficiency should be gained through controlled delivery of

a chemotherapeutic drug in combination with photothermal therapy (PTT). To this end, the introduction of the NIR-transducing polymer polypyrrole (PPY) into the network of the thermo-responsive nanogels will be performed using the semi-interpenetration method. This should allow using the heat generated by the PPY chains under NIR exposure for photothermal ablation of cancerous tissue as well as to trigger the thermo-responsive network and the release of an encapsulated drug.

In chapter 4.1.3, studies to understand the interpenetration process and the resulting interpenetrated structure will be carried out to determine suitable candidates for an application. Particularly, the structural changes influencing the nanogels' properties under exposure to NIR and temperature stimuli will be investigated. The thermo-responsive nanogels should stabilize the water-insoluble PPY preventing its aggregation and implement long-term stability. The nanogels shall be optimized in size for a potential accumulation in tumor tissue by the enhanced permeation and retention (EPR) effect, as well as efficient NIR-light-to-heat transduction.

In section 4.2.3, the evaluation of the nanogels' ability to treat cancer shall be investigated *in vitro* and *in vivo.* The integration of PPY into the nanogels endows a dual functionality as chemotherapeutic delivery agent and photothermal transducers. In addition, the presence of PPY might potentially increase the loading capacity of small molecular weight drugs like Methotrexate (MTX) due to beneficial interactions and a reduction of the mesh size of the interpenetrated nanogels. With the generation of nanogels with different VPTTs, the influence of the hydration state of the nanogels on the biodistribution shall be investigated. Therefore, *ex vivo* photoacoustic imaging shall be performed and a novel method for the determination of the biodistribution based on the photothermal response of the nanogels shall be developed and validated. With this method at hand, the tumor accumulation behaviour will be studied to reveal the optimal time span between intravenous administration of the nanogels and application of the NIR trigger. The comparison between mono-therapeutic approaches and the combination of both therapies shall reveal the potential of the nanogels to improve the therapeutic performance.

3 EXPERIMENTAL PART

3.1 MATERIALS

Chemicals used for the synthesis of nanogels are listed in Table 1. In Table 2 all used solvents are specified. The therapeutic actives and model drugs evaluated in thesis are given in Table 3. In Table 4 manufacturers of the used materials are listed.

Table 1. Chemicals used for nanogel synthesis in this thesis. *recrystallized in n-hexane prior use.

Chemical	Abbreviation	CAS No	Manufacturer	Purity
2,2′-Bipyridyl	-	366-18-7	Sigma-Aldrich	≥ 99%
3-(Ethyliminomethyleneamino)-N,N-dimethylpropan-1-amine	EDCI	1892-57-5	Carbolution	99%
4-Dimethylaminopyridine	DMAP	1122-58-3	Carbolution	99%
Acryloyl chloride	Ac-Cl	814-68-6	Sigma-Aldrich	97%
Aminoguanidine hydrochloride	-	1937-19-5	Sigma-Aldrich	≥ 98%
Ammonium persulfate	APS	7727-54-0	Sigma-Aldrich	98%
Anhydrous sodium sulphate	-	7757-82-6	Carl Roth	99%
Copper sulfate pentahydrate	-	7758-99-8	Sigma-Aldrich	≥ 98%
Cystamine dihydrochloride	-	56-17-7	Sigma-Aldrich	96%
Dendritic polyglycerol	dPG	-	Nanopartica	PDI 1.3 (10 kDa)
Dicyclohexylcarbodiimide	DCC	538-75-0	Sigma-Aldrich	99%
Di-tert-butyl dicarbonate		24424-99-5	Sigma-Aldrich	≥ 98%
Dry N,N-dimethylformamide	DMF	68-12-2	Fisher Scientific	99.8%
Hydrochloric acid	HCl	7647-01-0	Fisher Chemical	37%
L-cysteine	Cys	52-90-4	Sigma-Aldrich	97%
Methacryloyl chloride	-	920-46-7	Sigma-Aldrich	97%

Methanesulfonyl chloride	-	124-63-0	Sigma-Aldrich	≥ 99.7%
N,N,N′,N′-Tetramethyl-ethylenediamine	TEMED	110-18-9	Sigma-Aldrich	≥ 99.5%
N,N-Diisopropylethylamine	DIPEA	7087-68-5	Carl Roth	99%
N-isopropyl acrylamide *	NIPAM	2210-25-5	Sigma-Aldrich	99%
N-isopropyl methacrylamide*	NIPMAM	13749-61-6	Sigma-Aldrich	97%
p-Methoxyphenol	-	150-76-5	Sigma-Aldrich	99%
Potassium persulfate	KPS	7727-21-1	Merck	≥ 99%
Propiolic acid	-	471-25-0	Sigma-Aldrich	95%
Pyrrole	-	109-97-7	Sigma-Aldrich	98%
Reduced glutathione	GSH	70-18-8	Sigma-Aldrich	≥ 98%
Rhodamine B (RhodB)	RhodB	81-88-9	Fisher Scientific	98%
Sodium azide	-	26628-22-8	Sigma-Aldrich	≥ 99.5%
Sodium chloride (sat. solution)	-	7647-14-5	VWR	99.9%
Sodium dihydrogen phosphate	-	7558-80-7	Merck	99%
Sodium dodecyl sulphate	SDS	151-21-3	Sigma-Aldrich	≥ 98%
Sodium hydroxid	NaOH	1310-73-2	Fisher Chemical	≥ 99%
Sodium L-ascorbate	-	134-03-2	Sigma-Aldrich	≥ 98%
Triethylamine	TEA	121-44-8	Acros	99%
Trifluoroacetic acid	TFA	76-05-1	Sigma-Aldrich	99%

Table 2. Solvents used in this thesis. *distilled prior use.

Solvent	**Abbreviation**	**CAS No.**	**Manufacturer**	**Purity**
Dichloromethane	DCM	75-09-2	Fisher Chemical	100%
Diethyl ether		60-29-7	VWR	100%
Ethyl acetate*		141-78-6	own bottling	-
Methanol	MeOH	67-56-1	Fisher Chemical	99.9%
n-Hexane*		110-54-3	own bottling	-

Table 3. Evaluated drugs for this thesis.

Drug (Abbreviation)	Manufacturer	Purity
Bovine serum albumin (BSA)	Sigma-Aldrich	-
FITC conjugated bovine serum albumin (BSA-FITC)	Sigma-Aldrich	-
Budesonide (BUD)	Sigma-Aldrich	≥ 99%
Etanercept (ETN)	Shanghai TheraMabs	-
Methotrexate (MTX)	Sigma-Aldrich	≥ 98%

Table 4. Materials used in this thesis.

Materials	Manufacturer
Sephadex G25 fine	GE Healthcare
Dialysis membranes regenerated cellulose (RC)	Carl Roth
Sephadex G25 PD-10 prepacked columns	GE Healthcare
Float-A-Lyzer G2	GE Healthcare
Vivaspin centrifugal device (MWCO 300 kDa)	Sartorius AG
Silica gel 60M	Machery Nagel
Celite 535 coarse	Sigma-Aldrich
TLC plates silica gel 60 F_{254}	Merck

3.2 ANALYTICAL METHODS

NMR spectroscopy. Spectra were recorded on a Jeol ECX 500 spectrometer operating at 400 MHz, Joel Eclipse spectrometer (500 MHz) and Bruker AVANCE III 700 (700MHz). Data was recorded in ppm and referenced to the mentioned solvents. All spectra were recorded at room temperature and were analyzed with MestReNova software.

FT-IR Spectroscopy. Spectra were recorded as a film on diamond on a Nicolet Avatar 320 FT-IR operating from 4000 to 400 cm^{-1}.

Raman Spectroscopy. Measurements were performed on the dry nanogels by using a modified OLYMPUSBX 41 microscope with a 100 standard (MPLN) objective. Raman excitation was carried out using a 532 nm CW laser (Millennia, Spectra Physics). Detection is accomplished by a fiber-coupled 80 cm DILOR XY800 spectrometer (HORIBA-JOBIN YVON, Bensheim, Germany) using three 1800 l mm^{-1} gratings in the subtractive mode along with a Synapse Si CCD-detector cooled to -66 °C. The laser power was limited to 12 mW in order to avoid laser-induced degradation of the samples. The spectral resolution of the Raman spectra was of the order of 2 cm^{-1}, using a 0.2 mm entrance slit.

Dynamic Light Scattering (DLS). The nanogels particle sizes, dispersity, VPTT, and ζ-Potential were measured at various temperatures by DLS using Malvern Zetasizer Nano-ZS 90 (Malvern Instruments) equipped with a red He-Ne laser (λ = 633 nm, 4.0 mW) or a green DPSS laser (λ = 532 nm, 50.0 mW) under a scattering angle of 173°. All samples were maintained for stabilization at the desired temperature for 2 – 5 min before testing. Particle sizes and size distributions (PDI) are given as the average of 3 measurements from the intensity distribution curves. For the determination of the VPTT, the sizes of the nanogels measured in a temperature range of 25 – 55 °C (step size 0.5 °C) was plotted against the temperature. The VPTT is defined as the temperature at the inflection point of the normalized size curve. The swelling degree of the nanogels is defined as the ratio between particle volume in the swollen state (25 °C) and the

collapsed state (55 °C).

UV-VIS and Fluorescence Spectroscopy. UV-VIS absorbance was measured in 96-well plates using a Tecan Infinite M200Pro microplate reader.

Transmission Electron Microscopy (TEM). Samples for TEM were prepared on carbon-coated copper grids (300 mesh, Quantifoil). When necessary, the nanogels were stained with uranyl acetate for better contrast. Visualization was performed using the TEM mode of the Hitachi Scanning Electron Microscope (SU8030) (20 kV).

Circular Dichroism (CD) Spectroscopy. Protein secondary structure determination was investigated on a Jasco J-810 spectropolarimeter. Protein solutions in the presence of nanogels are background corrected by corresponding nanogel solution. Temperature dependent measurements were conducted raising the temperature 1 °C/min.

3.3 SYNTHETIC PROTOCOLS

Synthesis of Acrylated dPG (dPG-Ac). dPG was dried under high vacuum at 80 °C overnight prior use. In order to obtain different acrylation degrees in dPG, the desired molar fraction (%) of available OH groups in dPG were set to 1 equivalent. Acrylation was achieved by adding Ac-Cl (1.3 eq.) dropwise to a cooled (0 °C) solution of dPG (1 eq.) and TEA (2 eq.) in dry DMF. The reaction was left stirring at r.t. for at least 4 h and the product was purified by dialysis (regenerated cellulose (RC), molecular weight cut-off (MWCO) 1 kDa) in deionized water for two days. The acrylated dPG was preferably used directly after purification. Otherwise, the product was stored at 6-8 °C in the presence of p-methoxyphenol and dialyzed before usage. Yield 85-90%. 1H-NMR (500 MHz, D2O), δ: 3.1 – 4.4 (m, 5 H, polyglycerol scaffold protons), 5.98 – 6.12 (m, 1 H, vinyl), 6.18–6.32 (m, 1 H, vinyl), 6.45 – 6.53 (m, 1 H, vinyl).

Synthesis of Thermo-responsive Nanogels. Thermo-responsive nanogels based on PNIPAM, PNIPMAM or their copolymers were synthesized according to previously reported methodologies with minor changes.[62] Different feeding ratios of acrylated dPG as well as different acrylation degrees were screened for PNIPAM and PNIPMAM based nanogels. In addition, different ratios of NIPAM and NIPMAM feed were investigated. In a typical reaction, 100 mg of monomers (dPG-Ac and NIPAM, NIPMAM or a mixture of NIPAM and NIPMAM) and SDS (1.8 mg) were dissolved in 4 mL distilled water. The reaction mixture was purged with argon for at least 15 min before transferred to a hot bath at 70 °C. After 5 min, an aqueous solution of KPS (3.3 mg, 1 mL) was added quickly to initiate the polymerization. The mixture was left stirring at 70 °C for 3 h, followed by purification via dialysis (RC, MWCO 50 kDa) in water. After lyophilisation, the product was obtained as a white cotton-like solid. Yield 80-90%.

FT-IR of PNIPAM-dPG nanogels: ν (cm^{-1}) = 3100-3500 (OH, dPG), 2971, 2931, 2874, 1732, 1643 (C=O amide), 1540 (amide), 1458, 1387 (CH isopropyl group), 1366 (CH isopropyl group), 1226, 1172, 1129, 1074, 979, 927, 880, 839.

FT-IR of PNIPMAM-dPG nanogels: ν (cm^{-1}) = 3100-3500 (OH, dPG), 2970, 2932, 2874, 1732, 1633 (C=O amide), 1516 (amide), 1457, 1386 (CH isopropyl group), 1365 (CH isopropyl group), 1321, 1260, 1197, 1128, 1077, 962, 928, 883, 840.

FT-IR of Co-dPG nanogels: ν (cm^{-1}) = 3100-3500 (OH, dPG), 2971, 2931, 2874, 1732, 1645 (C=O amide), 1526 (amide), 1458, 1386 (CH isopropyl group), 1366 (CH isopropyl group), 1220, 1173, 1129, 1077, 965, 927, 884, 840.

^{1}H-NMR of PNIPAM-dPG nanogels: (500 MHz, D2O), δ: 1.16 (s, 6 H, isopropyl groups of NIPAM), 1.57 (2 H, polymer backbone), 2.04 (1 H, polymer backbone), 3.35 – 4.10 (6 H, polyglycerol scaffold protons + 1 H NIPAM).

1H-NMR of PNIPMAM-dPG nanogels: (500 MHz, D2O), δ: 0.98 (s, 3 H, methyl group of NIPMAM), 1.15 (s, 6 H, isopropyl groups of NIPMAM), 1.78 (2 H, polymer backbone), 3.35 – 4.10 (6 H, polyglycerol scaffold protons + 1 H NIPMAM).

^{1}H-NMR of Co-dPG nanogels: (500 MHz, D2O), δ: 9.98 (s, 3 H, methyl group of NIPMAM), 1.16 (s, 6 H, isopropyl groups of NIPAM and NIPMAM), 1.57-2.15 (m, 3 H polymer backbone NIPAM + 2 H polymer backbone NIPMAM), 3.35 – 4.10 (7 H, polyglycerol scaffold protons + 1 H NIPAM + 1H NIPMAM).

Synthesis of Degradable Linker (N-methacryloyl N'-propargyoxylcystamine, D). The degradable linker was synthesized in 4 steps by modifying synthetic method reported by Takeuchi and co-workers for the synthesis of a bifunctional cystamine based linker (Scheme 1).[167]

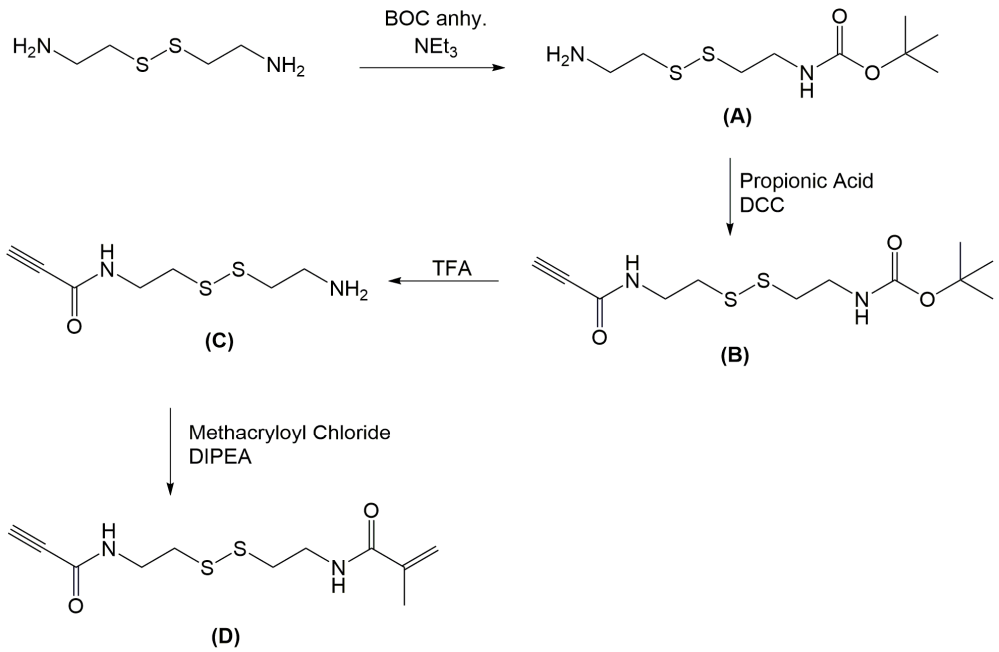

Scheme 1. Synthetic procedure of degradable cystamine based linker end-functionalized with methacryl and alkyne group.[167]

Synthesis of N-tert-butoxycarbonyl cystamine (A). The synthetic procedure followed an earlier published report.[167] Briefly, cystamine dihydrochloride (5 g, 22.2 mmol) and TEA (9.3 mL, 66.6 mmol) were dissolved in methanol (50 mL) and cooled in an ice bath. Into the reaction mixture ice cold methanolic solution (20 mL) of di-tert-butyl dicarbonate (2.42 g, 11.1 mmol) was added. The reaction mixture was then stirred for 6 h at 0 °C, after which the solution was dried under reduced pressure. 1 M sodium dihydrogen phosphate was added to the white residue and the solution was washed with diethyl ether (20 mL, 3 times) to remove N,N′-di-tert-butoxycarbonyl-cystamine. The aqueous solution was adjusted to pH 9 by addition of 5 M NaOH while stirring, followed by extraction with ethyl acetate (20 mL, 3 times). To the combined organic phases, 5 g anhydrous sodium sulfate was added and the solution was dried under reduced pressure. The resulting yellow oil was dried overnight in vacuum to yield N-tert-butoxycarbonyl cystamine (A). Yield: 2.1 g (37.5%). TLC: Rf 0.35 (MeOH).

^{1}H-NMR (400 MHz, $CDCl_3$): δ = 5.04 (b, 1H, NH-Boc), 3.41 (q, 2H, C(=O)-$NHCH_2$), 2.98 (t, 2H, CH_2NH_2), 2.75 (q, 4H, CH_2SSCH_2), 1.41 (s, 9H, CH_3).

Synthesis of N'-propargyoxylcystamine (C). N'-propargyoxylcystamine was synthesized following previously reported literature.[167] To a stirred solution of DCC (1.8 g, 8.72 mmol) in 20 mL of anhydrous DCM, under argon, at 0 °C, propiolic acid (0.51 mL, 8.32 mmol) was added. After 10 min, N-tert-butyloxycarbonyl cystamine (A) (2 g, 7.92 mmol) dissolved in 20 mL of anhydrous DCM was added dropwise and the resulting mixture stirred for 1 h at 0 °C and for 1 h at room temperature. The mixture was then filtered, and the solution was evaporated under reduced pressure. The crude product was purified by flash chromatography on silica gel using ethyl acetate/hexane (1:1) as eluent. The obtained pure compound (B) (2.1 g, yield 87%) was concentrated in reduced pressure and used immediately for the next step without further characterization.

The compound (B) was dissolved in 20 mL of DCM and cooled to 0 °C. TFA (10 mL) was added and the mixture was stirred until only a single spot was obtained on TLC. Upon completion, the reaction mixture was dried using vacuum, mixed with milli-Q water (10 mL, 3 times) and dried under vacuum to remove the residual TFA from the obtained compound N'-propargyoxylcystamine (C) as trifluoroacetate salt in high purity. The obtained compound was immediately used for the next step without any characterizations.

Synthesis of N-methacryloyl N'-propargyoxylcystamine (D). N′-propargyoxylcystamine (C) (1 g, 3.14 mmol) and DIPEA (1 mL, 6.28 mmol) were dissolved in anhydrous DCM (20 mL), cooled on ice and followed by addition of methacryloyl chloride (0.399 mL, 4.08 mmol) solution in anhydrous DCM (10 mL). The reaction mixture was stirred for 24 h at 0 °C, after which the reaction solution was washed with brine. The organic phase was evaporated and purified by silica gel column chromatography using ethyl acetate/hexane (1:1). Purified compound (D) was concentrated under reduced pressure and dried overnight under high vacuum yielding a yellow solid (0.76 g, 89.5%).

TLC: R_f 0.4 (ethyl acetate: hexane = 1:1).

^{1}H-NMR (400 MHz, $CDCl_3$): δ = 6.93 (b, 1H, C(=O)-N*H*), 6.39 (C(=O)-N*H*), 5.75 (s, 1H,C=CH_2), 5.37 (s, 1H,C=CH_2), 3.64 (t, 4H, CH_2S-S-CH_2), 2.87 (t, 4H, NHCH_2), 2.81 (s, 1H, *H*C≡C), 1.97 (s, 3H, CH_3).

Synthesis of dPG-azide. Azide functionalization of dPG was performed in two steps as described in Scheme 2 following reported methodology.[168]

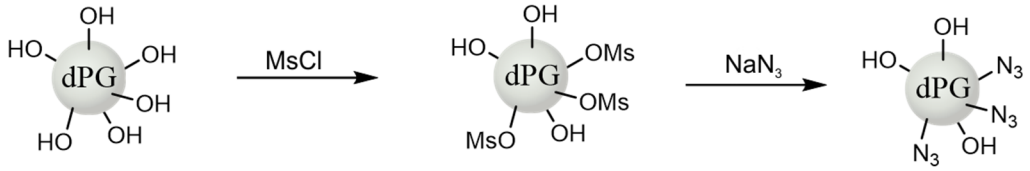

Scheme 2. Synthesis of dPG azide in two steps via mesylation and azidation.

Synthesis of mesylated dPG. Mesylated dPG was obtained by dissolving dry dPG (1 g, 13.5 mmol OH groups, 10% OH's groups = 1 eq.) and TEA (374 µl, 2.7 mmol, 2 eq.) in anhydrous DMF (20 mL). The reaction mixture was cooled on ice followed by addition of methanesulfonyl chloride (115 µl, 1.49 mmol, 1.1 eq.). The reaction mixture was stirred for 5 h at r.t. and then dried using reduced pressure. Purification was done by dialysis in methanol using 1 kDa MWCO membrane for 1 day. The dialyzed solution was dried under vacuum to obtain the product as yellow viscous liquid.

^{1}H-NMR (400 MHz, CD3OD): δ = 3.3 – 4.1 (m, dPG backbone, 5 H), 3.1 (s, mesyl-CH_3, 3H).

Sythesis of dPG-azide. Mesylated dPG (3.0 g, 8.1 mmol mesyl groups) and sodium azide (2.11 g, 32.4 mmol, 4 eq.) were added in 100 mL anhydrous DMF. The reaction mixture was stirred at 90 °C for 24 h and then another 72 h at 60 °C. The reaction mixture was then cooled down to room temperature and filtered using celite. DMF was evaporated under reduced pressure and the product was dialyzed (RC, MWCO 1 kDa) for 72 h in methanol. The dialyzed solution was dried under vacuum to obtain dPG-azide.

FT-IR: N3-peak at 2100 cm^{-1}.

^{1}H-NMR (400 MHz, CD3OD): δ = 3.3 – 4.1 (m, dPG backbone, 5 H).

Synthesis of RhodB labeled dPG-azide. Anhydrous dPG-azide (479.0 mg, 0.048 mmol, 1 eq.), RhodB (91.0 mg, 0.192 mmol, 4 eq.), EDCI (20.2 mg, 0.105 mmol, 2.2 eq.) and DMAP (1 mg, 8 μmol, cat.) were added in anhydrous DMF in presence of argon and stirred at room temperature for 24 h. Then, the reaction mixture was dialyzed against methanol for 2 days (RC, 1 kDa MWCO). The dialyzed solution was concentrated under reduced pressure and purified using sephadex G-25 fine. The colored RhodB-grafted dPG-Azide was collected, dried under vacuum and used for conjugation to the degradable linker.

Synthesis of degradable dPG-(S-S)-methacrylate using Cu(I) mediated alkyne-azide cycloaddition. The synthesis procedure was adopted from earlier reported literature.[169] dPG-azide or RhodB-dPG-azide (375 mg, 0.405 mmol N_3 groups) was dissolved in 1 mL milli-Q water followed by addition of copper sulfate (12.9 mg, 0.081 mmol, 0.2 eq.) and aminoguanidine hydrochloride (30 g, 0.405 mmol, 1 eq.) and slowly mixed with 4 mL DMF solution of the degradable linker (125 mg, 0.486 mmol, 1.2 eq.) and 2,2′ bipyridyl (25.3 mg, 0.162 mmol, 0.4 eq.). The reaction mixture was purged with argon for 30 min followed by addition of sodium ascorbate (32 mg, 0.162 mmol, 0.4 eq.). The reaction mixture changed the color to dark brown due to Cu(I) formation. The reaction was stirred at room temperature overnight followed by column purification using sephadex G-25 fine. Yield 260 mg.

^{1}H-NMR (500 MHz, $CDCl_3$), δ : 8.44 (b, 1H, triazole), 5.69 (s, 1H,C=CH_2), 5.43 (s, 1H,C=CH_2), 3.3-4.1 (m, dPG backbone, 5 H), 2.93 (b, 4H, NHCH_2), 1.90 (s, 3H, CH_3).

Synthesis of Redox-Degradable Nanogels. The synthesis of degradable nanogels was adapted from previously reported method using precipitation polymerization.[72, 170] Briefly, 100 mg of monomers (NIPAM and /or NIPMAM), dPG-(S-S)-methacrylate, SDS (1.8 mg, 6.2 μM), and APS (2.8 mg, 12.3 μM) were dissolved in 5 mL of distilled water. Argon was bubbled into the reaction mixture for 30 min. Then, the reaction mixture was transferred into a hot bath at 70 °C and after 5 min polymerization was activated by addition of a catalytic amount of TEMED (0.75 μL,

0.582 mg, 5.01 μM). The mixture was stirred at 300 rpm for 3 h. The products were purified by dialysis (RC, MWCO 50 kDa) in water for 48 h and then lyophilized to yield the nanogels. Alternatively, nanogels with RhodB label were synthesized in similar manner as described above using RhodB labeled PG-(S-S)-methacrylate as cross-linker. Non-degradable analogues for each nanogel were synthesized as described above.

^{1}H-NMR of PNIPAM-(S-S)-dPG nanogels: (400 MHz, D2O), δ: 1.13 (s, 6 H, isopropyl groups of NIPAM), 1.57 (2 H, polymer backbone), 2.00 (1 H, polymer backbone), 3.35 – 4.10 (6 H, polyglycerol scaffold protons + 1H NIPAM).

^{1}H-NMR of PNIPAM-co-PNIPAM-(S-S)-dPG (Co-(S-S)-dPG) nanogels: (400 MHz, D2O), δ: 0.98 (s, 3 H, methyl group of NIPMAM), 1.15 (s, 6 H, isopropyl groups of NIPMAM), 1.78 (2 H, polymer backbone), 3.35 – 4.10 (6 H, polyglycerol scaffold protons + 1 H NIPMAM).

^{1}H-NMR PNIPMAM-(S-S)-dPG nanogels: (400 MHz, D2O), δ: 1.13 (s, 6H, isopropyl groups of NIPAM), 1.57 (2 H, polymer backbone), 2.00 (1 H, polymer backbone), 3.35 – 4.10 (6 H, polyglycerol scaffold protons + 1H NIPAM).

Semi-interpenetration of thermo-responsive nanogels. Dry nanogels were swollen in a solution of pyrrole·HCl with a nanogel concentration of 10 mg/mL. After complete dissolution, the polymerization process was initiated by quickly adding an APS solution (same molarity than pyrrole·HCl, half the volume of swelling solution). After 30 min polymerization was finished and the PPY nanogels were transferred into a dialysis bag (RC, MWCO 50 kDa) and dialysed in demineralized water for at least 3 days. The nanogels were stored in solution; concentrations were adjusted by dialysis against concentrated polyethylene glycol (100 kDa) solution.

3.4 EXPERIMENTAL PROCEDURES

Polymerization Kinetics. Analysis of the polymerization kinetics was assayed by stopping the polymerization process at certain time points by cooling down the sampling volume in an ice bath and bubbling air through the solution to quench the formation of radicals. Unreacted reagents were removed by dialysis (Float-A-Lyzer G2, 30 kDa) and the obtained products were lyophilized and analysed for of weight, size (DLS) and constitution (NMR). In the NMR analysis for each time point the integral of PNIPAM respectively PNIPMAM signal was set to 9 respectively 11 protons and the ratio between integral of dPG signal and PNIP(M)AM signal was calculated.

Encapsulation and Release of BSA in Thermo-Responsive Nanogels. Protein encapsulation and release behaviour of the different nanogels was studied using BSA-FITC as a model drug. To encapsulate the protein in the nanogels, dry nanogels were swollen in a solution of BSA-FITC (1 mg/mL, pH 7.4, PBS) for at least 24 h at 6-8 °C. The solutions were purified using Vivaspin 300 kDa centrifugal device (10 min at 6000 rpm). The concentration of encapsulated BSA-FITC was determined by absorbance at 492 nm. Encapsulation efficiency (EE%) was calculated using the following equation:

$$EE(\%) = \frac{m\,(BSA_{init}) - m\left(BSA_{free}\right)}{m\,(BSA_{init})} * 100 \qquad (1)$$

For the release study, 10 mg of nanogels (10 mg/mL) with encapsulated BSA-FITC were placed in a Vivaspin 300 kDa device and diluted with acceptor medium (PBS, pH 7.4) to 10 mL. At certain time intervals, the samples were centrifuged (5 min, 5000 rpm) and the filtrate was taken for analysis (absorbance at 492 nm) and the sampled volume was replaced with fresh buffer.

Cytotoxicity of Thermo-responsive Nanogels on Human Dermal Fibroblasts and HeLa Cells. Human dermal fibroblasts isolated from juvenile foreskin were isolated in accordance to local

ethics and biosafety regulations (ethical approval EA1/345/14 by the Charité ethical committee). HeLa cells (#ACC-57) were obtained from Leibnitz Institute DSMZ- German collection of Microorganisms and Cell Cultures. To assess cell viability, 10000 cells per well were seeded into 96-well-plates (Sarstedt) in 100 µL/well Roswell Park Memorial Institute (RPMI) medium (for HeLa) or Dulbecco's Modified Eagle Medium (DMEM) (for fibroblasts) (Gibco, Thermo Fisher Scientific) containing 10% fetal bovine serum (FBS), (FBS Superior, Merck), 1% Penicillin/Streptomycin and 1% MEM non-essential amino acids (NEAA, RPMI only) (Thermo Fisher Scientific). The cells were incubated at 37 °C and 5% CO_2 overnight. Then, medium was replaced with fresh medium containing various dilutions of the corresponding nanogel in duplicates and cells were incubated for 48 h at 37 °C and 5% CO_2. The cell culture supernatant was removed and cells were washed twice with PBS (200 µL/well). Then, 100 µL/well fresh full medium including 10 µL/well MTT (Sigma-Aldrich, 5 mg/mL in PBS) were added and incubated for another 4 h at 37 °C. After development of formazan crystals, the cell culture supernatant was removed and crystals were dissolved by addition of 100 µL/well of isopropanol containing 0.04 M HCl. Absorbance was read at 590 nm in a Tecan Infinite M200 Pro microplate reader. Relative viabilities were calculated by dividing average absorbance values of wells with treated cells by values of untreated cells (=100% viability). All tests were repeated 3 times independently and errors were expressed as SEM.

Skin Penetration. To evaluate temperature-triggered delivery of encapsulated BSA into excised human skin, penetration studies were performed on barrier-impaired skin in two different setups: a) temperature ramp from 32 – 37 °C modelling the natural temperature gradient in the skin and b) increasing the skin surface temperature up 41 °C by local irradiation with an infrared (IR) lamp. All experiments were conducted on excised abdominal skin from healthy male patients, who underwent plastic surgery and upon signed consent from each patient (ethical approval EA1/345/14 by the Charité ethical committee). Skin samples were obtained in accordance with the guidelines of Helsinki Declaration with ethical approval.

Temperature Ramp

Excised human skin (freshly obtained 3h after surgery or frozen for less than 6 months) was stretched on a metal block then tape stripped 50 times to disrupt the stratum corneum (SC) in order to mimic an impaired barrier integrity in diseased skin (e.g. skin inflammatory, infectious diseases). Skin punches of 15 mm diameter were taken and placed in 6-well inserts (Falcon® Cell Culture Inserts, 3 μm, HD, PET membrane). The inserts were placed in 6 well plates, each filled with 2 mL PBS. The explants were then treated with protein loaded nanogels to a final concentration of 20 μg/cm² of loaded BSA (6.8 mg/mL nanogels stock solution with a ~10wt% BSA-FITC loading). Afterwards the treated skin biopsies were incubated for 6 h applying a temperature ramp of 32 °C, 34 °C to 37 °C over the first 3 h. Skin punches treated either with PBS or 20 μg/cm² BSA solution served as control.

IR Irradiation

Skin explants were tape-stripped and treated with thermo-responsive nanogels as described above. Here, the skin punches were incubated for 1 h at room temperature in the dark, followed by irradiation with an IR lamp (Efbe-Schott infrared lamp equipped with Philips pulp 150 W, Bad-Blankenburg, Germany) to increase the temperature of the skin surface to 41 °C. The IR lamp was fixed at a 40 cm distance from the treated skin biopsies expressing a light intensity dose of 150 kJ/cm² measured by power density measuring device (HBM 1, Hydrosun GmbH, Mülheim, Germany). The irradiation persisted for 120 s until skin surface reached a maximum temperature of 41 ± 1 °C. Photos were taken before and after irradiation using a thermal IR camera (FLIR E4 camera, FLIR Systems GmbH, Frankfurt, Germany). After the irradiation, the skin punches were incubated for another 60 min with the nanogels. Control experiments of skin biopsies treated with nanogels at room temperature for 2 h in the dark served as controls.

Cryosectioning and Microscopy Imaging of Skin Punches

At the end of each experiment, skin punches were cleaned and subsequently embedded in freezing medium (Leica Biosystems, Nussloch, Germany). After 24 h at 80 °C, the tissues were cut at 6 μm thickness using a CM1510 S Cryotome (Leica Biosystems, Nussloch Germany). The

mounted cryosections on the poly-l-lysine coated slides were then fixed with 4% paraformaldehyde (Roti® Histofix 4%, Carl Roth GmbH, Karlsruhe, Germany), rinsed with phosphate-buffered saline (PBS, pH 7.4) and stained with DAPI mounting solution (Roti®-Mount FluorCare DAPI, Carl Roth GmbH, Karlsruhe, Germany). Slides were then sealed with a cover slip and stored in the dark at 4 °C. Cryosections were then subjected to fluorescence microscopy (BZ-8000, zoom 20×, Plan-Apo, DIC N2, Keyence, Neu-Isenburg, Germany, equipped with objective 20×/0.75, Nikon, Japan). Mean fluorescence intensity (MFI) of FITC-labeled BSA was quantified by its distribution area within epidermal layers using Image-J[171, 172] for at least three skin sections per sample. Experiments and subsequent analysis were repeated using skin from three different donors.

Redox-Degradation Studies. Degradation profiles of the nanogels were assayed using time dependent size measurements by DLS post incubation with different reducing solutions and buffers of different pH.

Interactions of Redox-Degradable Nanogels with Native Mucus. To investigate mucus-nanogel interactions, mucus gel was isolated from juvenile pig's ileum. Briefly, the small intestine was freshly excised from the proximal region of 4 months old farm pigs, sacrifice for research purposes. The excised jejunum was immediately sectioned into 25 cm pieces, each was opened longitudinally and carefully rinsed with ice-cold PBS (pH 7.4). Therefore, a syringe was used to allow food debris and other waste to be gently removed without damaging the tissue or losing the loose mucus layer covering the surface. The mucus gel was then carefully scraped off with a spatula and stored at -20 °C until usage.[173] To explore mucus-related degradation of the nanogels, 5 mg/mL of RhodB labeled PNIPMAM-(S-S)-dPG and PNIPMAM-dPG were mixed with 100 mg native mucus gel then incubated for 1, 3, 6, 12, and 24 h at 37 °C. After incubation, samples were centrifuged for 30 min at 16.100 xg, supernatants were then collected, snap-frozen in liquid nitrogen and freeze-dried (-80 °C at 0.1 mbar). Gel permeation chromatography (GPC) was conducted on a Shimadzu Prominenze-i LC-2030 liquid chromatography system. The lyophilized samples were solved in 1ml mobile phase (PBS, pH 7.4), then 50 µL of each were

injected and analyzed at a flow rate of 1 mL/min. Shodex OHpak SB-806M HQ column was used with OHpak SB-G 6B as guard pre-column. The columns were operated at r.t. with the UV-visible detector set to 567 nm wavelength. Negative controls for this conduct included the mucus gel as well as the labeled nanogels. As a parallel control study of degradation, the PNIPMAM-(S-S)-dPG degradation profile was analysed after incubation at various time points and with different concentrations of GSH.

Mucopenetration. The nanogels potential for mucopenetration was investigated *ex vivo* using a Franz-cell setup adapting previously reported scheme.[174] Freshly excised porcine intestinal punches (diameter: 15-16 mm) were incubated at 37 °C on a nylon membrane over the receptor compartment at 37 °C. The receptor chambers were filled with oxygenated Krebs-Ringer-buffer (12 mL). The Franz-cells were sealed and the tissue punches were left 10 min at 37 °C to equilibrate. Afterwards, 50 µL of 10 mg/mL Rhod-B labeled nanogels in PBS solution (pH 7.4) were added to the donor compartments. After 1 h and 3 h, the biopsies were removed, their surface was gently rinsed with PBS (3x 100 µL) and snap frozen in liquid nitrogen. Untreated biopsies at each time point served as controls. Cryo-sections of 5 µm thickness were cut using a CM1510 S Cryotom (Leica Biosystems, Nussloch Germany). Afterwards, the tissue sections were fixed with 4% paraformaldehyde (Roti® Histofix 4%, Carl Roth GmbH, Karlsruhe, Germany), mounted with 1 drop of DAPI mounting solution (Roti®-Mount FluorCare DAPI, Carl Roth GmbH, Karlsruhe, Germany), sealed with a cover slide, and stored in the dark at 4 °C until visualization on a fluorescence microscope (BZ-8000, objective 20×/0.75, zoom 10×, Plan-Apo, DIC N2, Keyence, Neu-Isenburg, Germany).

Cytotoxicity to Submucosal Endothelial Cells. Cell lines were purchased from ATCC (Manassas, VA, USA); VK2/E6E7 (ATCC CRL-2616) is derived from normal vaginal mucosal tissue of a premenopausal woman undergoing anterior-posterior vaginal repair surgery, and Ect1/E6E7 (ATCC CRL-2614) were taken from normal epithelial tissue of a premenopausal woman undergoing hysterectomy for endometriosis.[175] The cell lines were cultured in keratinocyte-serum free medium (K-SFM) from GIBCO (Thermo Fisher Scientific, USA)

supplemented with 0.1 ng/mL human recombinant epidermal growth factor (EGF) and 0.05 mg/mL bovine pituitary extract. The nanogels influence on epithelial cell viability of the female genital tract was investigated by MTT assay.[176] 1× 10^4 cells/well were seeded in 96 well-plates and incubated at 37 °C and 5% CO_2. After 24 h, cells were treated with 1.0, 2.5 or 5.0 mg/mL of both, degradable and non-degradable, nanogel stock solutions of 50 mg/mL in PBS. After 24 h or 48 h, MTT solution (5 mg/mL) was added and incubated at 37 °C for 4 h. The supernatant was removed and the formed formazan salt was solubilized with 50 µl/well of dimethyl sulfoxide (DMSO). The optical density (OD) at 570 nm was measured with FLUOstar Optima, BMG LABTECH GmbH, Ortenberg, Germany). SDS (0.001 mg/mL) served as a positive control; untreated cells as a negative control. Each sample was tested in triplicate and the experiments were repeated three times, respectively. Data were normalized against the untreated control. Cell viability ≤ 70% predicted cytotoxicity.

Cytotoxicity and Internalization into Macrophages. Human monocytes were isolated from human whole blood and differentiated to macrophages. Potential cytotoxicity to the macrophages was assayed by Annexin V-FITC/ PI assay after 3 h and 24 h incubation with RhodB labeled nanogels (1 mg/mL). Viable cells were identified by flow cytometry on 1x10^4 cells from each test sample using a CytoFLEX flow cytometer (Beckman Coulter GmbH, Germany).
To investigate the nanogels ability to induce active endocytosis into macrophages, RhodB labeled nanogels (1mg/mL) were incubated with macrophages for 3 h at 37 °C and 4 °C (where active endocytosis processes are inactivated). Afterwards, the uptake into the cells was measured by the cells fluorescence using flow cytometry. Untreated cells exposed to PBS served as negative control. The experiment was repeated three times, each time with two different negative controls for each temperature condition.

Encapsulation of Budesonide and Etanercept. Encapsulation of a small molecular drug into redox-degradable nanogels was assayed using BUD as model drug. In brief, 10 mg nanogels were dissolved in 2 mL MilliQ water and incubated at 50 °C in order to collapse the nanogels and increase their hydrophobicity. Then, 5 mg BUD were added and the mixture was sonicated

(30 min) and stirred at r.t. overnight. Non-encapsulated BUD was removed by filtration (syringe filter, RC, 0.45 mm) and encapsulation efficiency was determined by LC-MS/MS using deuterated Budesonide (BUD-d8) as standard.

Protein encapsulation was studied using Etanercept (ETN; Shanghai TheraMabs Bio-Technology). To encapsulate ETN in the nanogels, dry nanogels were swollen in a solution of ETN (1 mg/mL, pH 7.4, PBS) for at least 24 h at 6-8 °C. The solutions were purified using Vivaspin 300 kDa centrifugal device (10 min at 6000 rpm; Sartorius AG, Göttingen, Germany). The concentration of encapsulated ETN was determined by Bradford assay according to standard procedure.[177]

Integrity of Encapsulated and Released ETN. As indication for ETN stability upon encapsulation and release from the nanogels, the secondary structure of the proteins was analysed by CD measurements. Protein solutions containing nanogels were background corrected by the corresponding nanogel solution without proteins.

Second, after two weeks of storage at 4 °C the TNF-α binding activity of ETN in the nanogels was tested by ELISA (ELISA kit, IG-AA102, Tani Medicals, Ankara, Turkey) according to the instructions of the manufacturer. For comparison, a benchmark control for ETN (stored 2 weeks at 4 °C) was included. All values were normalized to a solution of ETN maintained at -80 °C and freshly thawed for the assay.

Photothermal Effect of semi-interpenetrated PPY Nanogels. The heat production of the nanogels was measured at different concentrations placing a 20 μL sample in a transparent thin-walled microcentrifuge tube and irradiating with an infrared diode laser module (FC-D-785 CNI, λ = 785 nm, 500 mW) or NIR lamp (hydrosun® 750, Hydrosun Medizintechnik GmbH) equipped with a water filter and an additional band pass filter (721 nm -1000 nm, T>70%, FGL9, ThorLabs). During 5 min of irradiation, the temperature increase was monitored with an infrared camera (FLIR E30, 25° Optic, 60 Hz) at the outside of the tube, perpendicular to the laser beam direction. The effect of NIR irradiation on the size of the nanogels was assayed by

irradiating a 0.25 mg/mL or 0.1 mg/mL nanogel solution for 3 min and immediately measuring their size by DLS.

Encapsulation and Release of Methotrexate. The encapsulation efficiency of the thermo-responsive nanogels and semi-interpenetrated PPY nanogels was evaluated for the anti-cancer drug methotrexate (MTX). For nanogels which could be redissolved after drying (non-interpenetrated and PPY/PNIPMAM-dPG), encapsulation was achieved by swelling the dry nanogels in an aqueous solution of MTX (1 mg MTX/mg nanogel, c = 5 mg/mL). For all other nanogels, the nanogel solution was heated to 55 °C in a water bath for at least 30 min to collapse the nanogels. Then, a concentrated solution of MTX (1 mg MTX/mg nanogel, c = 30 mg/mL) was added and the mixture was cooled down in an ice bath to swell the nanogels. All nanogel-MTX solutions were stored in the fridge overnight prior purification by gel filtration (Sephadex G-25 PD-10, GE Healthcare). The amount of separated free MTX was determined by UV-VIS spectroscopy using absorbance at 380 nm. Encapsulation efficiency (EE%) was calculated using equation 1.

The release profiles of MTX from the nanogels was determined using dialysis method. The nanogel solution was transferred to a dialysis bag (Float-A-Lyzer G2, MWCO 300 kDa, VWR) with 6 mL of surrounding acceptor medium (PBS pH 7.4). At indicated time points the whole acceptor medium was collected and replaced by fresh buffer solution. The collected fraction was lyophilized, redissolved and MTX content was determined by UV-Vis spectroscopy using absorbance at 380 nm. NIR induced release was assayed applying 5 min of NIR irradiation (785 nm, 500 mW) on indicated time points.

Evaluation of Photothermal Ablation Ability and Combinational Therapy In Vitro. A549 cells (Leibniz Institute DSMZ – German Collection of Microorganisms and Cell Cultures, #ACC 107) were seeded into 96 well plates in DMEM (Thermo Fisher Scientific) with 10% FBS (Merck Millipore) and 1% Penicillin/Streptomycin (Thermo Fisher Scientific) at a density of 10000 cells/well. Cells were incubated with nanogel solutions with and without loaded MTX for 48 h. The nanogels concentrations of all applied solutions were adjusted according their absorbance

at 785 nm (0.42 mg/mL PPY/PNIPAM-dPG, 1.0 mg/mL PPY/Co-dPG and, 0.67 mg/mL PPY/PNIPMAM-dPG, MTX loaded nanogels as their non-loaded analogues). After incubation, half of the wells containing cells were irradiated for 6 min with an infrared diode laser module (FC-D-785 CNI, λ = 785 nm, 500 mW). After overnight incubation, cell viability was assessed by MTT test. For this, 10 µL/well MTT solution (5 mg/mL in PBS) was added in fresh medium to the cells and incubated for 4 h at 37 °C. Afterwards, the cell culture supernatant was removed and 100µL/well of isopropanol containing 0.04 M HCl was added. Absorbance was read at 570 nm in a Tecan Infinite M200Pro microplate reader. Relative cell viabilities were calculated by dividing absorbance values of wells with treated cells by the values of untreated cells (100%). Two replicate wells were run for each sample and the experiment was repeated twice.

Tolerability of Semi-Interpenetrated PPY Nanogels In Vivo. All animal studies were performed in accordance to national and local guidelines and regulations as described in the approved Tierversuchsantrag G 0030/15 (Landesamt Berlin für Gesundheit) from 20.09.2018 for the EPO GmbH Berlin-Buch.

In the first part of the study, healthy 6-8 weeks old female nude (NMRI, nu/nu) mice were injected with increasing doses (10, 20, 40, 70 or 100 mg/kg) of nanogels into their tail vein and body weight changes were monitored over the course of 2 weeks. In the second part of the study, the maximum tolerated dose found in the first part (100 mg/kg) was injected on five consecutive days and the tolerability was monitored by body weight for two weeks. One day, respective 14 days after the last injection, selected organs were collected and fixed in formalin for 24 h.

Hematoxylin and Eosin (H&E) stained slides prepared from formalin-fixed paraffin embedded tissue samples of liver, lung, kidney, spleen and heart of treated and untreated mice were examined by pathologists at EPO GmbH Berlin-Buch.

Biodistribution. Biodistribution profiles of the nanogels were generated *ex vivo* using the photothermal response of the nanogels present in the organs and the results were validated by photoacoustic imaging. For the evaluation of tumor accumulation, 6 – 8 week old female nude

(NMRI, nu/nu) mice bearing A549 lung cancer xenografts (average tumor volume 0.13 cm^3 at day 7 after subcutaneous (s.c.) cell inoculation) were treated once with an intravenous (i.v.) injection of 100 mg/kg of nanogels or PBS *via* tail vein. 2 h, 6 h, 12 h, 24 h, and 48 h after the injections 3 mice per group were sacrificed and organs were sampled and snap-frozen or formalin-fixed.

Photothermal Response. Photothermal response of organ samples was measured in two ways. First, in order to validate and establish the method, formalin fixed full organs were irradiated with a NIR lamp (hydrosun 750, Medizintechnik GmbH) equipped with a water filter and additional band pass filter (721 nm - 1000 nm, T >70%, FGL9, ThorLabs, d = 10 cm). The temperature increase within 5 min irradiation was recorded by an IR camera. Second, organs were homogenized (Homogenisator, VDI) and diluted in PBS (pH 7.4), and 20 µL samples were irradiated with infrared diode laser module (FC-D-785 CNI, λ = 785 nm, 500 mW). For quantitative analysis, a standard curve was prepared of temperature vs concentration values of nanogel solutions irradiated in the same way. The temperature values of irradiated organ samples were corrected by values of irradiated untreated organs and concentrations were obtained from exponential fit of the calibration curve. Values are given as average of three different organs expressed as percent of injected dose (%ID) per organ or per g of organ and calculated using following equations:

$$\%ID = \frac{\frac{c}{DF} \cdot V}{ID} \cdot 100 \quad (2)$$

$$ID = dx \cdot BW \quad (3)$$

Here, c is defined as particle concentration, DF is the dilution factor, V sample volume after homogenisation, d is the dose per injection, x reflects the number of injections, and BW is the bodyweight at the day of first injection.

Photoacoustic Imaging. Tomographic 3D PA images of formalin-fixed organs and snap-frozen tumors were acquired *ex vivo* using a Fabry-Perot-based ultrasound scanner.[178, 179] The organs were placed on the scanner and acoustically coupled with PBS. PA signals were generated using excitation pulses of 8 ns duration at two different wavelengths (620 nm and 800 nm) provided

by an OPO laser (Innolas Spitlight 1000 OPO). The pulse energies were 8 mJ and 13 mJ, respectively. The samples were illuminated by a Gaussian beam of approximately 20 mm diameter ($1/e^2$).

3D image data sets of organs were acquired over an *x-y* scan area of 16.2 x 16.2 mm^2 with a step size of $dx = dy = 180$ μm. Tumours were measured over a 20.0 x 20.0 mm^2 scan area ($dx = dy = 200$ μm). The time-resolved PA signals comprising the data sets were recorded using 20 MHz detection bandwidth and 15 μs acquisition length. 3D PA images were reconstructed using the time-reversal algorithm of the k-Wave toolbox[180] and the data sets were two-fold upsampled before reconstruction to improve lateral resolution.[181] The intensities of the images were normalised with respect to the pulse energy at the two excitation wavelengths. To allow a quantitative comparison, *x-y* maximum intensity projections (MIP) of the 3D images were calculated. Regions of interest (ROI) corresponding to the organ shapes were manually segmented using polygons and the average signal intensities of the MIPs and the standard deviations inside the ROIs were calculated.

Anti-Tumor Efficiency. 6-8 weeks old female nu/nu mice were injected subcutaneously with $1x10^7$ A549 cells to form xenograft tumors in the flank. Treatments were started when the tumor volume (TV) reached approximately 100 mm^3 which was designated as day = 0 (d0). Mice were homogenously distributed into 11 groups (n = 6 per group). The tumor bearing mice were treated intratumorally (i.t.) with injections of 30 μL nanogel solutions (10 mg/mL) of PPY/PNIPAM-dPG or PPY/Co-dPG, purely or loaded with MTX (10 wt%), followed by irradiation of the tumor site with infrared diode laser module (FC-D-785 CNI, $\lambda = 785$ nm, 500 mW) for 5 min. The remaining 7 groups including untreated mice (PBS (i.t.)), NIR exposed mice (PBS (i.t.) + laser), MTX treated mice (10 mg/kg every 3 days, i.p.), PPY/PNIPAM-dPG and PPY/Co-dPG without NIR irradiation, and MTX loaded PYY/PNIPAM-dPG and PPY/Co-dPG without laser served as controls. Temperature changes at the tumor site were monitored using an IR camera (FLIR E30, 25° Optic, 60 Hz). Tumor sizes were determined with a calliper and was calculated as $TV = (LxW^2)/2$, where L is tumor length and W is tumor width.

For analysis of mild photothermal treatment i.t. (temperature at the tumor site limited to a maximum of 45 °C) and tumor inhibition after i.v. administration of the nanogels, mice bearing A549 tumors (TV 300 mm^3) were used. Here, the day of laser treatment after last nanogel injection was designated as d0. Tumor bearing mice were treated either i.t. with PPY/Co-dPG nanogel solutions (10 mg/mL; 1 mg/TV) or i.v. (100 mg/kg) for 5 consecutive days. For mice treated i.t., NIR irradiation of the tumor site was performed immediately after injection for 5 min, or 15 min respectively (n=3). PBS treated mice (i.t.) served as control. For i.v. treatment with PPY/Co-dPG nanogels mice were separated in 2 groups (n=3) and irradiated for 5 min after the 3^{rd} injection of nanogels and after the 5^{th}, or only once after 5^{th} injection.

4 RESULTS AND DISCUSSION

4.1 SYNTHESIS AND CHARACTERIZATION OF NANOGELS

4.1.1 THERMO-RESPONSIVE NANOGELS FINE-TUNED FOR PROTEIN DELIVERY APPLICATIONS

This chapter is based on the paper "Critical parameters for the controlled synthesis of nanogels suitable for temperature-triggered protein delivery", which has been partially modified. The link to the published form is given in Appendix 7.2. Author Contributions: All synthesis and characterizations of nanogels were performed by me. TEM images were recorded by Julián Bergueiro Álvarez and Emanuel Glitscher. I wrote the manuscript. All authors contributed to the final version of the manuscript.

To address an efficient delivery of therapeutic proteins in dermal applications, thermo-responsive nanogels are promising candidates to overcome the skin barrier and facilitate deep penetration of their cargos into viable skin layers. The regulation of the VPTT of the nanogels is thereby crucial to achieve a temperature-triggered release. In dermal applications, nanogels with VPTTs below 37 °C can take advantage of the natural temperature gradient in the skin for the release of their cargo. In contrast, with VPTTs above 37 °C, nanogels might be suitable as well as they allow a temporal and local control over the release in combination with an external heating source. In addition, such nanogels are feasible candidates for systemic applications where the nanogels are exposed to 37 °C body temperature immediately after administration.

The two polymers PNIPAM and PNIPMAM have an almost identical structure with the difference of PNIPMAM bearing a methyl group in its polymeric backbone and thus have a higher transition temperature than PNIPAM.[170] Thus, it should be explored whether the thermo-responsive polymer PNIPMAM and the copolymerization with PNIPAM allows the tuning of

the VPTT of the thermo-responsive nanogels (Figure 11). In addition, structural properties of the nanogels, such as swelling degree and network density, are key factors for an efficient encapsulation and retention of the drugs within the nanogels during their transport. Studies to reveal the main parameters to control the structure of thermo-responsive nanogels should be therefore performed allowing a precise adaption to required features.

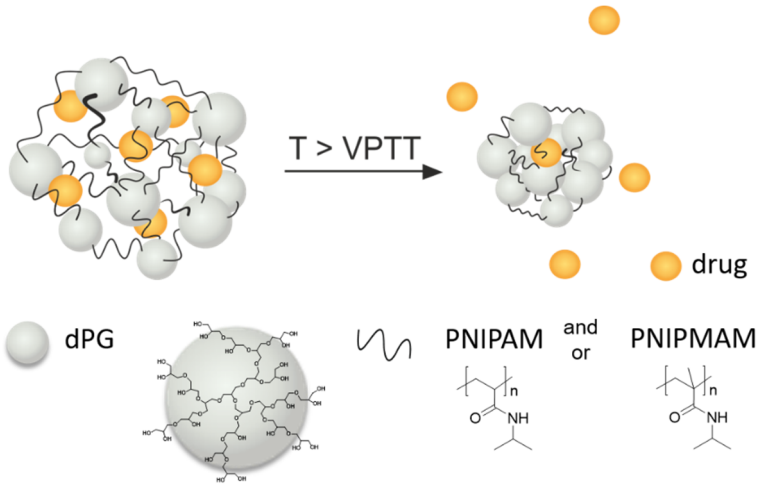

Figure 11. Schematic representation of temperature triggered release of an encapsulated drug from thermo-responsive nanogels based on dendritic polyglycerol (dPG) and poly-N-isopropyl acrylamide (PNIPAM) and/or poly-N-isopropyl methacrylamide (PNIPMAM) and chemical structures of dPG, PNIPAM and PNIPMAM.

In a first approach, it was aimed to synthesize thermo-responsive nanogels using previously reported methodology[62] of the two homopolymers PNIPAM and PNIPMAM cross-linked with dPG as macromolecular cross-linker. Interestingly, it was found that the initiator system APS/TEMED is working for PNIPAM based nanogels but yields polydisperse aggregates for PNIPMAM. A screening of different initiator systems revealed, that particles with low polydispersity for PNIPMAM could only be obtained using KPS or APS without TEMED (Table 5). We assumed that the reason for this might be evoked by different polymerization kinetics including different kinetics of the initiation as well as different polymerization rates of the used monomers. Therefore, we performed a kinetic analysis of the polymerization reaction

monitoring the size development and swelling ability of the particles via DLS, consumption of monomers by ^{1}H-NMR and reaction conversion by weight.

The comparison of different initiator systems for the nanogel synthesis revealed that initiation by KPS and APS is very similar, showing almost the same increase in nanogels size in the beginning of the polymerization (Figure 12). For both polymers, nanogels obtained by polymerization with KPS appear to be slightly smaller than their APS initiated analogues. In addition, for PNIPAM-dPG nanogels, additive TEMED accelerates the reaction and final particles size is reached quicker (Figure 12). We found that the more TEMED is used, leading to faster initiation, the smaller the size of the final nanogels (Table 5).

This is in good agreement with reported kinetics for acrylamides by Qiu et al.,[182] who demonstrated that TEMED accelerates the reaction and leads to fast conversion but at the same time yields linear polymer chains with lower molecular weight. As the nanogels are a three-dimensional cross-linked network of polymer chains, the TEMED induced decrease in the polymeric chain length between the dPG-cross-linker appears in smaller nanogel sizes. However, for PNIPMAM-dPG, we observe the formation of polydisperse particles in the presence of TEMED regardless of the initiator used. Only using KPS or APS alone as initiator yielded nanogels with low polydispersity for both, PNIPAM and PNIPMAM. These results denote that the reaction rates between initiator and monomers have to be balanced out in order to induce a nanogel formation.

Therefore, we performed kinetic studies of the monomer consumption via ^{1}H-NMR of NIPAM respectively NIPMAM and dPG during the polymerization. In good agreement with polymerization kinetics reported in the literature,[75, 183] we found that NIPAM reacts faster than NIPMAM with full conversion after 30 min (NIPAM) or 60 min (NIPMAM), respectively (Figure 13A). For both systems, the consumption of dPG is faster than the formation of the temperature-responsive polymers yielding a high ratio of dPG to polymer in the beginning of

the polymerization (Figure 13B). This is much more pronounced for the slower forming PNIPMAM nanogels with convergence to the final ratio of dPG:polymer of 0.3 after 45 – 60 min (10 – 15 min for PNIPAM). These results indicate that probably APS/TEMED and KPS/TEMED initiation is so fast that mainly dPG reacts with itself and almost no or only very short PNIPMAM chains are getting cross-linked leading to the formation of linear PNIPMAM aggregates. In contrast, NIPAM reacts faster than NIPMAM and therefore nanogels are obtained with accelerated initiation getting smaller with higher TEMED amount due to shorter chain lengths between the dPG.

Table 5. Characterization of PNIPAM-dPG and PNIPMAM-dPG nanogels synthesized with varied initiator systems and concentrations, and PNIPAM-BIS and PNIPMAM-BIS nanogels**.**

Nanogel system	initiator system	[init] (μmol) /100 mg monomers	[init]/[TEMED]	Size (d.nm) at 25 °C	PDI
PNIPAM-dPG	APS	12.2	-	200	0.088
	APS/TEMED	12.2	0.1	191	0.128
	APS/TEMED	12.2	0.5	169	0.125
	APS/TEMED	12.2	1	152	0.201
	KPS	12.2	-	186	0.137
	KPS/TEMED	12.2	0.1	165	0.122
	KPS/TEMED	12.2	0.5	151	0.165
	KPS/TEMED	12.2	1	135	0.195
PNIPMAM-dPG	APS	12.2	-	141	0.183
	APS/TEMED	12.2	0.1–1	polydisp.	>0.5
	KPS	12.2	-	123	0.205
	KPS/TEMED	12.2	0.1–1	polydisp.	>0.5

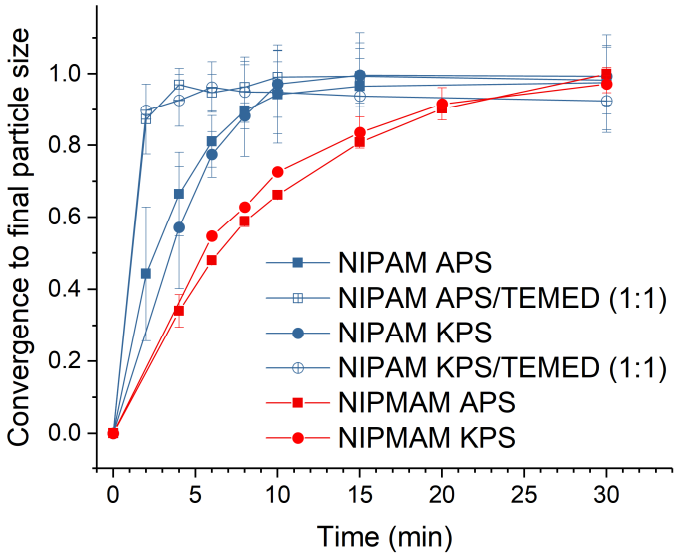

Figure 12. Normalized particle size development during polymerization with different initiator systems for NIPAM and NIPMAM based nanogels.

Interestingly, comparing the size of nanogels initiated with KPS (or APS) we found smaller diameters of the PNIPMAM-dPG nanogels than for PNIPAM based ones even though NIPMAM is reacting slower than NIPAM. These findings are in contrast to reported nano- and microgels of PNIPAM and PNIPMAM cross-linked with di-acrylates like BIS and/or (1,2,-dihydroxylethylene)bisacrylamide (DHEA).[96, 184]

Nevertheless, different reaction kinetics of NIPAM and NIPMAM in comparison with the cross-linker is reported to play a crucial role for particle architecture.[96, 184] In addition, Lyon et al.[184] demonstrated that hydrophilicity of the cross-linker is an important factor for the gel structure as the nucleation process is driven by hydrophobic polymer-to-polymer interactions. The hydrophilic character of dPG in combination with the differences in polymerization rate could provide an explanation for the smaller particle diameter of PNIPMAM nanogels (Figure 13C). As dPG will react much faster than NIPMAM, it can form hydrophilic oligomers which, when incorporated to the hydrophobic precursors, will be probably located more on the outside of the precursor particles. This seems to stabilize the growing particles resulting in colloidal stability at earlier stages of the polymerization and therefore formation of smaller particles. This assumption is supported by lower ability to swell for PNIPMAM based systems indicating

higher cross-link(er) density (Figure 13D). To verify that assumption, we performed surfactant free nanogel synthesis of NIPAM and NIPMAM with dPG. Indeed, the resulting nanogels showed smaller diameters than reported BIS cross-linked analogues supporting the notion that dPG can act as a stabilizing agent (Table 6).[75, 96]

Table 6. Characterization of surfactant free PNIPAM-dPG and PNIPMAM-dPG nanogels. Given size values are intensity values of DLS measurements. The swelling ratio is defined as ratio between volumes in swollen (25 °C) and shrunken state (55 °C).

Nanogel	Hydrodynamic size (d.nm) at 25 °C (PDI)	Hydrodynamic size (d.nm) at 55 °C (PDI)	swelling ratio	VPTT
PNIPAM-dPG	348 (0.124)	171 (0.109)	8.4	33 °C
PNIPMAM-dPG	187 (0.223)	88 (0.086)	9.6	45.5 °C

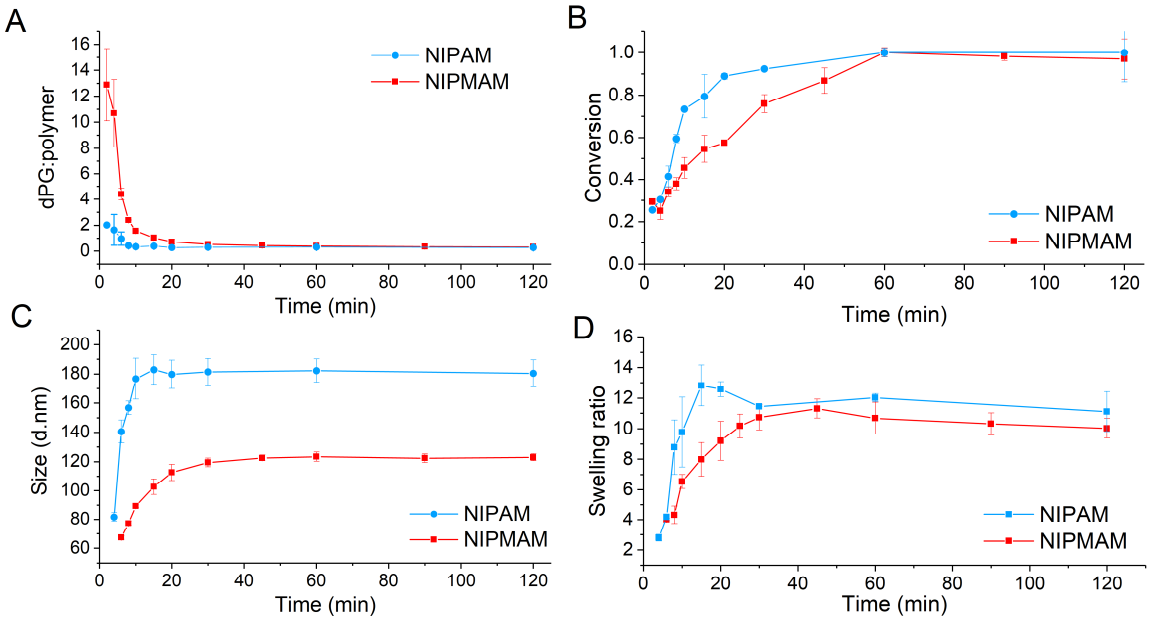

Figure 13. (A) Consumption of NIPAM or NIPMAM and dPG during polymerization visualized by the ratio between dPG to PNIPAM or PNIPMAM obtained from 1H-NMR analysis. (B) Time dependent conversion of the polymerization from NIPAM or NIPMAM with dPG by weight. (C) Hydrodynamic diameter of the nanogel particles dependent on reaction time. (D) Time evolution of the swelling ratio of the nanogels (defined as ratio between particle volumes in swollen (25 °C) and collapsed state (55 °C).

Another aspect coming to the field upon using dPG as a cross-linker is its multi-functionality. In comparison to small molecular bi-functional BIS, each dPG molecule has several cross-linking points depending on the functionalization degree (e.g. 7% acrylates correspond to 10 cross-linking units per dPG with a M_w of 10 kDa). This multi-functionality could explain our finding that the final size (Figure 13C) of the nanogels is reached earlier than the final weight (Figure 13A) indicating that after consumption of the majority of cross-linker, further polymerization takes place mainly at the inside of the growing particles. We assume that once incorporated into the growing precursor particle, several other unreacted cross-linking points of the dPG are locally "trapped", facilitating the connection of remaining free cross-linking points in the course of the polymerization. This assumption is supported by the fact that the swelling ratio during the polymerization process first reaches a maximum contemporaneously with gaining final particle size and then drops to reach final swelling ratio by the time of full conversion (Figure 13D). This effect is more pronounced for NIPAM based nanogels, probably due to the faster reaction rate.

In order to achieve a triggered release of encapsulated therapeutics from the nanogels gaining control over cross-linking density is crucial. Therefore, we screened the effect of the cross-linker on nanogels size and swelling ability. Due to its multi-functionality, dPG allows to tune the potential cross-linking degree in two ways: first, by varying the cross-linker feed and second, different functionalization degrees per macro-cross-linker. It is reported that using small, low molecular weight BIS, nanogel sizes increase with higher cross-linker feeds.[183, 185] In contrast, we observe for both, PNIPAM and PNIPMAM nanogels, a decrease in size with higher dPG feed (Figure 14A,B). At the same time, the swelling ability decreases (Figure 14C) with higher dPG feeds showing an increase of rigidity indicating that the overall cross-linking density is increased with more cross-linker present. In addition, as discussed above, due to the hydrophilicity of dPG we expect dPG to stabilize the nanogels during polymerization leading to smaller final particle sizes the higher the dPG content, similar to results reported for higher surfactant concentrations.[62, 75, 186] Caused by the slower reaction kinetics of NIPMAM, the size of PNIPMAM-dPG nanogels is for all dPG feeding ratios about 80-100 nm smaller than their PNIPAM-dPG analogues and show lower swelling abilities.

Remarkably, the impact of the functionalization degree of the dPG seems to be less prominent than the feeding ratio of cross-linking molecules. Nevertheless, both nanogel systems showed sensitivity against the acrylation degree with only a small window of functionalization percentage yielding in particles with a narrow polydispersity. Already for acrylation degrees larger than 13% (PNIPAM) or 10% (PNIPMAM), we obtained large aggregates probably due to the formation of cross-links between individual nanogel particles and decrease of the hydrophilicity of dPG. Interestingly, both nanogels show minima in their hydrodynamic radii for acrylation degrees in the range of 7% to 9% independent of the dPG feed (Figure 14A,B). Comparing the swelling abilities of nanogels with same dPG feed but different acrylation percentages, no major influence of the functionalization degree is observed (Figure 14C). These results imply that within the suitable window of functionalization degree we found for nanogel formation, the additional cross-links due to higher functionalization do not significantly influence the rigidity of the network and thus the main parameter to control the nanogels' cross-linking density is the PG feed.

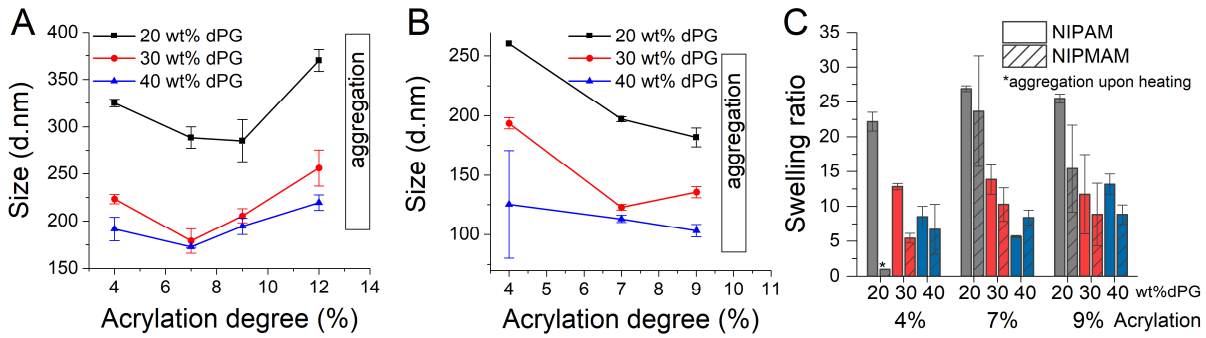

Figure 14. Correlation of the hydrodynamic diameter of (A) PNIPAM-dPG and (B) PNIPMAM-dPG nanogels with dPG-Ac feed and acrylation degree. (C) Swelling ratio of the nanogels dependent on dPG feed in wt% and acrylation degree (%).

For a triggered release of bioactives from the nanogels, we aim for nanogels showing significant shrinkage upon a temperature trigger but at the same time have a dense enough network to prevent premature cargo diffusion. In addition, for better comparability hydrodynamic radii of the nanogels should be as similar as possible. Therefore, we decided to continue to evaluate the

features as a drug delivery system with the nanogels showing an intermediate swelling ratio of around 10, which we obtained from dPG with 7% acrylation and a 30%-feed of the cross-linker.

Tuning the VPTT

Djopké and Vogt[95] reported the phase transition behaviour of linear copolymers from NIPAM and NIPMAM showing a linear dependence of the transition temperature with the ratio between different monomer feeds. These results motivated us to synthesize a range of copolymeric nanogels in order to find the conditions to fine tune the VPTT and find a suitable candidate for drug delivery in systemic applications.

In fact, we obtain nanogels with VPTTs between 32 °C and 47 °C depending on the ratio between NIPAM and NIPMAM (Figure 15A, Table 7). The size of the obtained nanogels correlate linearly to weight ratio between the two monomers. In addition, temperature dependent size measurements show a relatively sharp transition for all nanogels (Figure 15B). Successful incorporation of both monomers was proven by ^{1}H-NMR even though a quantitative evaluation of the ratio between the monomers was not possible due to strong overlap of the signals (Figure 16). TEM images (Figure 17) revealed that all nanogels show spherical shape with low polydispersity and a size around 70-100 nm, which is similar to the diameter obtained from DLS for nanogels in the shrunken state.

Interestingly, in comparison to BIS cross-linked particles, using dPG as cross-linker, in the TEM images the nanogel shape appears a bit "knobbly", which may be attributed to the spherical shape of the dPG itself. As discussed above, we aimed to synthesize nanogels with higher VPTT without affecting other physico-chemical properties too much, in particular without affecting the surface charge of the nanogels. Therefore, measurements of the ζ-potential were performed with all nanogels. Indeed, we find neutral ζ-potentials for both homopolymeric as well as for all copolymeric nanogels below and above their transition temperature (Table 7).

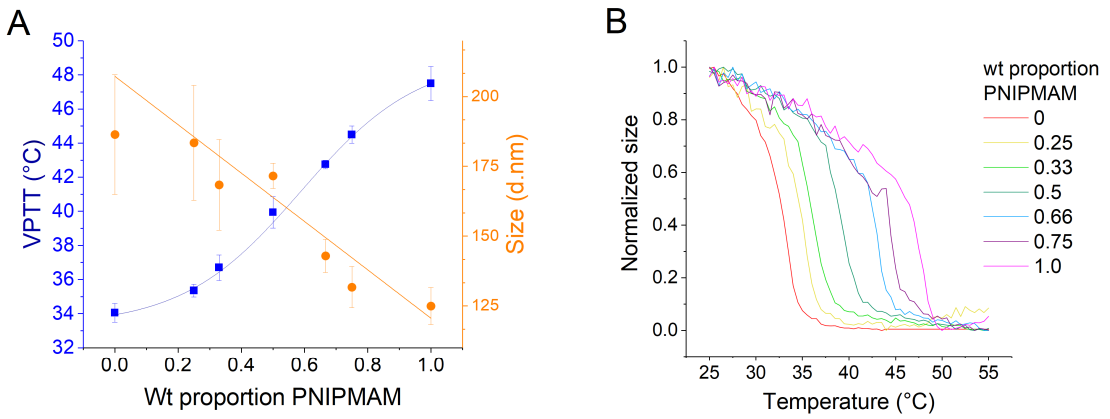

Figure 15. (A) VPTT and hydrodynamic diameters for PNIPAM-co-PNIPMAM-dPG nanogels dependent on weight proportion of PNIPMAM in monomer feed and (B) temperature dependent shrinkage of these nanogels.

Table 7. Characterization of NIPAM, NIPMAM and copolymeric nanogels: sizes values obtained from DLS measurement (intensity), Zeta-Potentials and VPTTs (DLS).

Thermo-responsive Monomers (wt%)		Size (d.nm) at 25 °C (PDI)	Size (d.nm) at 50 °C (PDI)	ζ at 25 °C	ζ at 50 °C	VPTT (°C)
NIPAM	NIPMAM					
100	0	186 (0.137)	87 (0.093)	-1.13	-3.66	34.1
75	25	183 (0.170)	75 (0.067)	-1.2	-2.74	35.4
67	33	168 (0.153)	72 (0.066)	-1.0	-2.83	36.7
50	50	172 (0.146)	86 (0.088)	-0.54	-2.00	39.9
33	67	143 (0.193)	75 (0.162)	-2.74	-4.42	42.7
25	75	132 (0.209)	81 (0.157)	-2.64	-3.07	44.5
0	100	131 (0.205)	61 (0.058)	-2.23	-2.15	47.5

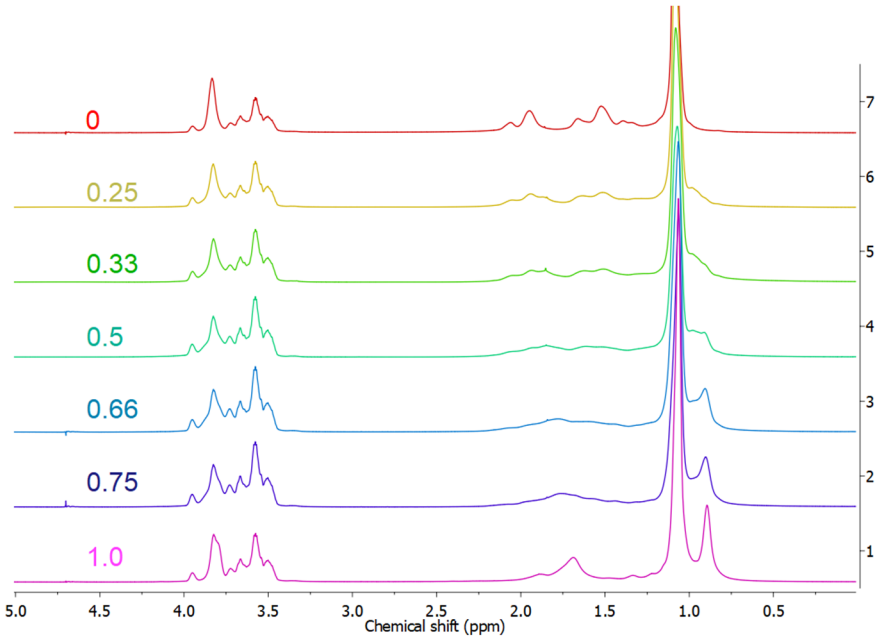

Figure 16. ^{1}H-NMR spectra of PNIPAM-co-PNIPMAM and both homopolymeric nanogels with increasing ratio of PNIPMAM (top to bottom). Numbers indicate the amount of NIPMAM feed of the total weight.

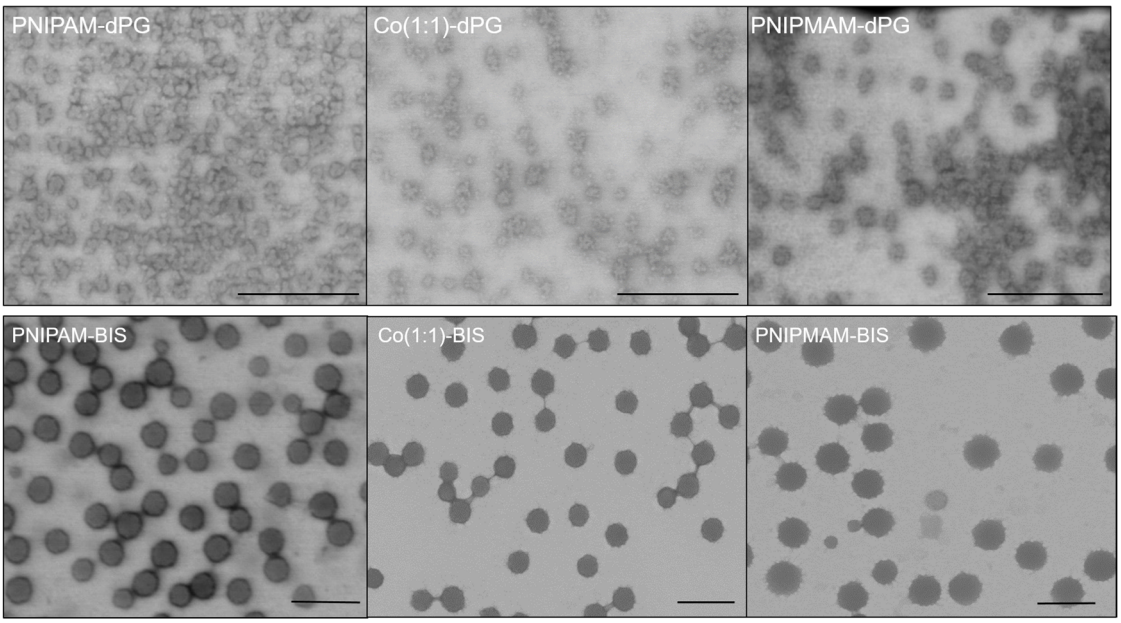

Figure 17. TEM images of PNIPAM-dPG, Co (1:1)-dPG and PNIPMAM-dPG nanogels and their BIS cross-linked analogues. Scale bar = 500 nm.

For systemic applications with for example intravenous administration of the nanogels, a VPTT slightly higher than 37 °C body temperature is desirable. The (1:1)-copolymeric nanogel is therefore a suitable candidate, as it has a VPTT of 40 °C. At 37 °C it is still in a highly hydrophilic swollen state, but already from temperatures of 41 °C it is almost completely collapsed (Figure 15B). In addition, knowing the good performance of PNIPAM-dPG as dermal delivery system and expecting the collapse of the nanogels crucial for this, the copolymeric nanogels are interesting candidates to evaluate the efficiency of an externally triggered topical delivery system. Stability of the nanogels was evaluated by DLS, showing no alterations in the hydrodynamic radii of all nanogels directly after redispersion and after a period of 2 months (Figure 18).

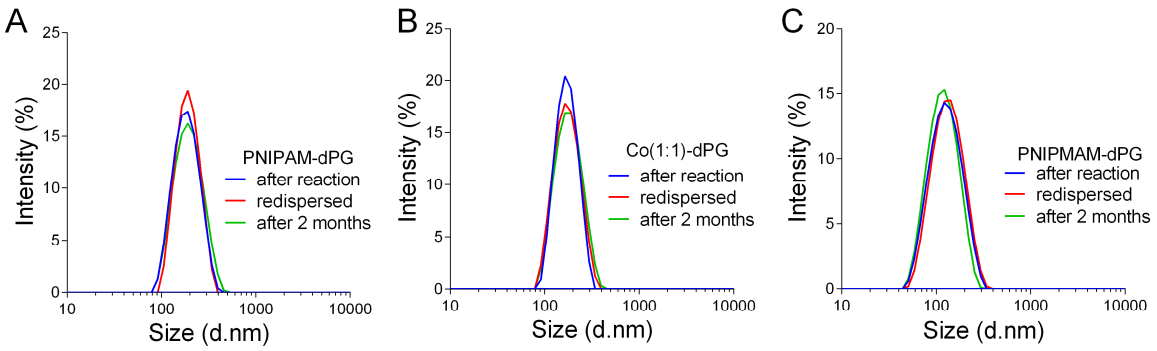

Figure 18. Stability of nanogels determined by DLS measurements after redispersing and after 2 months.

4.1.2 REDOX-DEGRADABLE NANOGELS

Author Contributions: Degradable linker design and nanogel synthesis was performed in close collaboration by Mritjunjoy Kar and me. Degradation studies by DLS were performed by me. GPC analysis was performed by Rawan Charbaji, we discussed the results and I wrote the manuscript. TEM images were recorded by Julián Bergueiro Álvarez.

Besides swelling and deswelling, the major trigger used in controlled drug delivery by polymeric nanogels is a controlled degradation.[42, 187] In most cases, a degradable unit is incorporated in the cross-links of the carrier leading to a loss of its three dimensional network connection upon cleaving these bridges and a burst release of encapsulated cargos. While the carriers are designed to have sizes too large for recognition by the RES, their fragments are much smaller after degradation and thus are more easily cleared from the body. Disulfides are redox-responsive moieties excellent for their use in systemic applications as they cleave into free thiols under redox potentials physiological available, e.g. within the cytosol of cells.

In addition, thiol bearing materials recently gained increased interest due to their ability to overcome mucosal clearance and thus to deliver drugs to submucosal layers in sufficient concentrations.[111, 112] So far, only free thiol bearing materials have been employed for submucosal delivery of drugs. However, in aqueous environment disulfides and thiols are in a dynamic equilibrium resulting in the occasionally presence of free thiols for disulfide containing materials as well. We thus hypothesize, that disulfide containing materials will perform in a similar manner to thiol bearing particles and are exciting candidates to overcome the mucosal barrier and deliver therapeutic actives to submucosal cells (Figure 19).

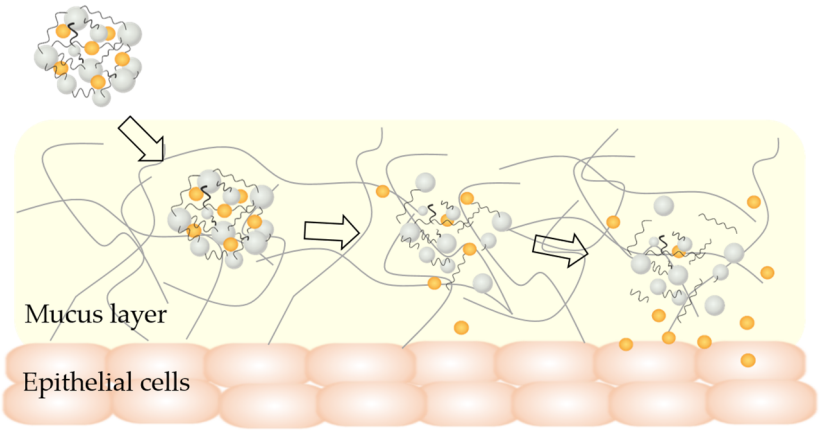

Figure 19. Schematic representation of submucosal delivery of therapeutic actives (yellow spheres) through interaction of disulfide-containing nanogels.

We were therefore interested in the introduction of degradable disulfide moieties into our thermo-responsive nanogels and in the employment of their ability to interact with mucus. In order to do be able to generate a variety of nanogels using different monomers and apply the knowledge we gained about the key parameters in the synthesis of thermo-responsive nanogels, we aimed for a modification of the cross-linker dPG for the integration of the degradable unit. We designed a cystamine based degradable linker functionalized with heterogenous end-functionalization: On one end the linker bears a methacrylate for the polymerization with the thermo-responsive monomers and the other end an alkyne group is attached for an easy and fast coupling to dPG-azide via copper catalyzed *click* chemistry (Scheme 3).

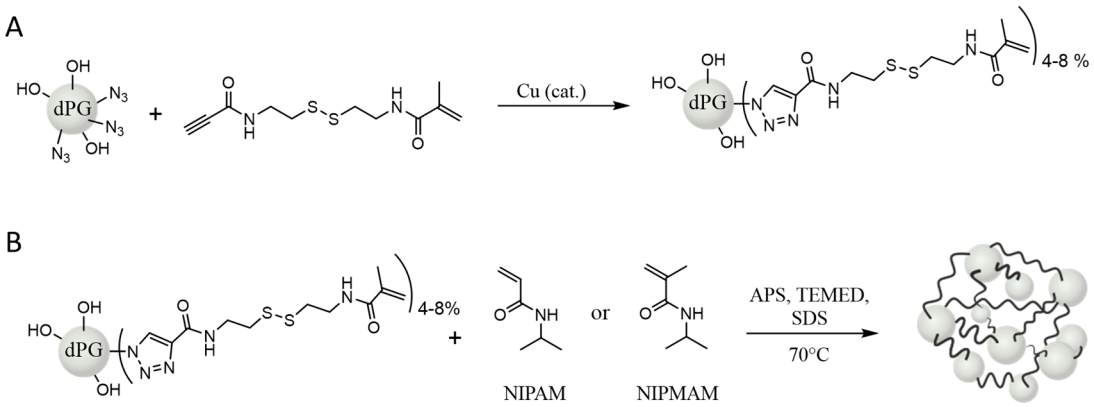

Scheme 3. (A) Conjugation of degradable linker to dPG-azide via copper promoted cycloaddtion and (B) synthesis of degradable nanogels.

The degradable linker was synthesized in a 4 steps procedure using modified method reported by Takeuchi and co-workers (Scheme 4).[167] In brief, cystamine was used as starting material and was mono- tert-butyl oxycarbonly (BOC) protected in the first step using BOC anhydride in the presence of a base. This allowed the carbodiimide-promoted amide coupling of alkyne bearing propionic acid via the formation of an activated ester in the second step. After deprotection of BOC in acidic conditions, the resulting free amine can be reacted with methacryloyl chloride to yield the degradable linker.

The obtained linker was coupled to azide-functionalized dPG using copper promoted azide-alkyne cycloaddition (Scheme 3A). Successful coupling was proven by ^{1}H-NMR analysis of the purified conjugate showing the signals of both, dPG backbone (Figure 20, peak h) and the linker (peaks b,d,a) as well as a shift of the signal from the alkyne (g) to lower field due to the formation of the triazole upon the alkyne azide cycloaddition. In addition, FT-IR analysis of the conjugate showed complete reduction of the signature peak of the azide at 2100 cm^{-1} proving successful reaction (Figure 21). As the copper catalysed coupling reaction worked quantitatively, the grafting density of degradable linkers per dPG could be tuned between 4-8% directly by percentage of azide functionalization on the dPG.

With this degradable cross-linker in hand, nanogel synthesis was performed in analogy to the thermo-responsive nanogels (Chapter 4.1.1) using precipitation polymerization with NIPAM and NIPMAM as monomers (Scheme 3B). With the variation of dPG and monomer feeding ratio the size of the nanogels could be tuned between 100–250 nm (PNIPAM-(S-S)-dPG) and 45 –170 nm (PNIPMAM-(S-S)-dPG), respectively (Table 8). For PNIPMAM based nanogels, we found increased PDI values for nanogels synthesized with higher dPG feed ratio. We therefore selected nanogels with a monomer:dPG ratio of 90:10 showing lowest PDI and size of 166 nm for further studies. Using NIPAM as monomer, in all tested conditions, nanogels with a low PDI below 0.2 were obtained. We therefore chose the nanogel with a similar hydrodynamic size of 160 nm (70:30 monomer:dPG) for the evaluation of the degradation profiles and the interaction with mucus.

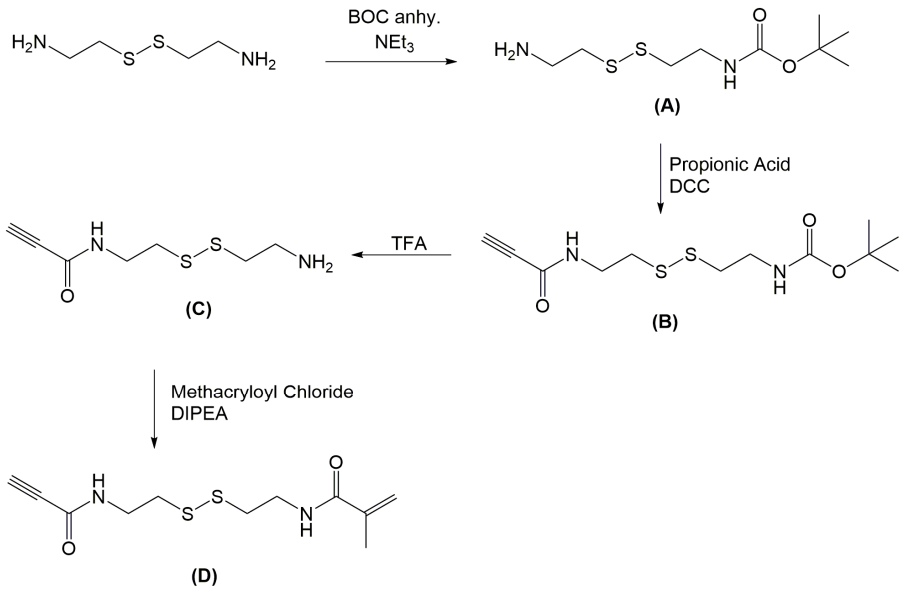

Scheme 4. Synthetic procedure of the degradable cystamine based linker end-functionalized with methacryl and alkyne group.

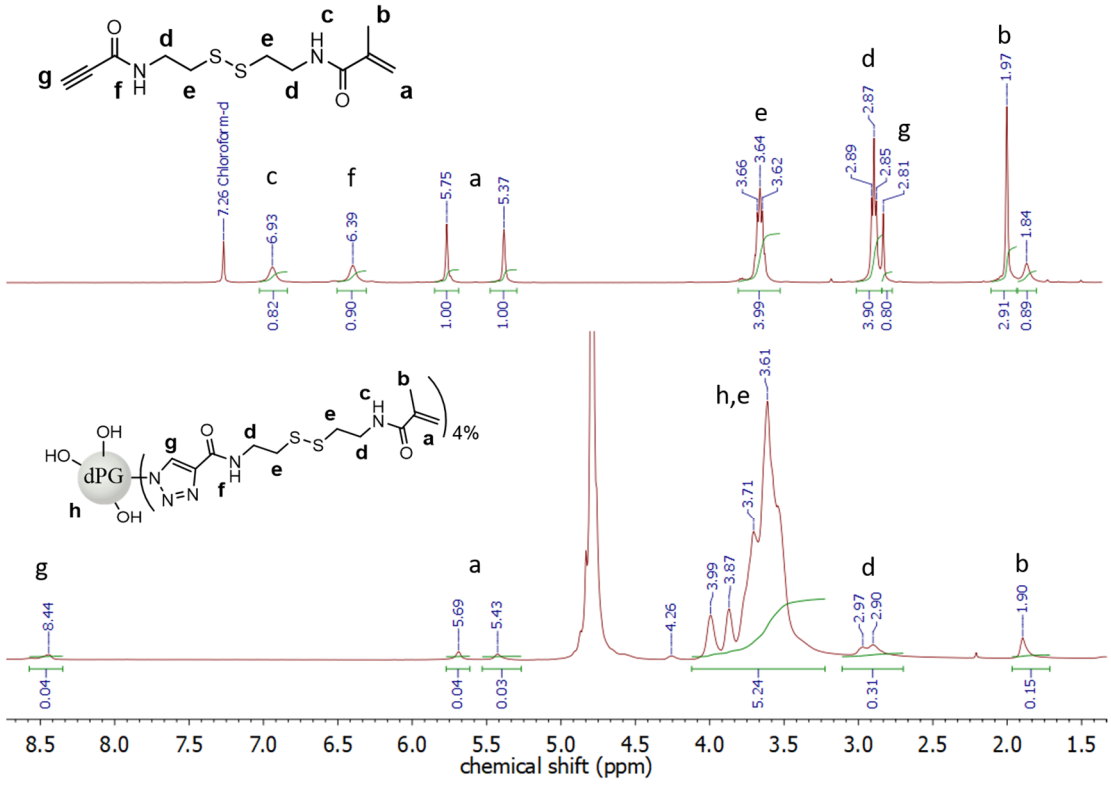

Figure 20. [1]H-NMR spectra of the degradable linker and the corresponding dPG (grafting density 4% per dPG) conjugate proving successful coupling.

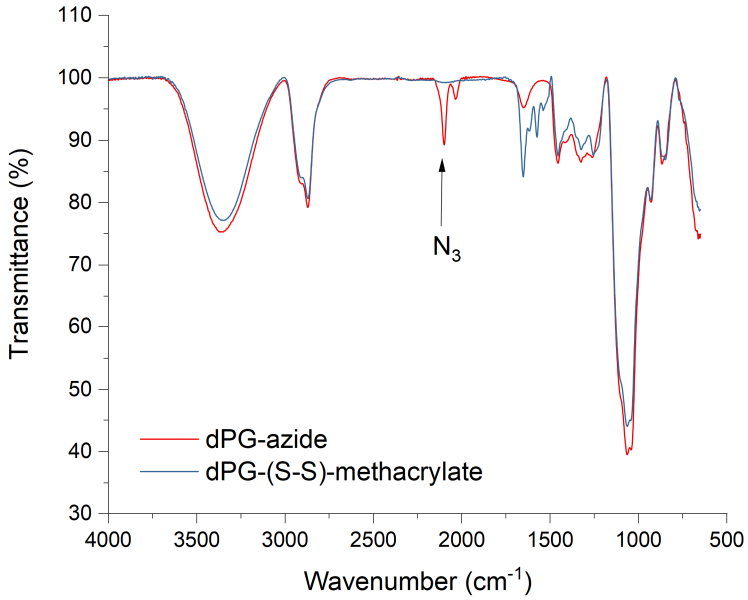

Figure 21. FT-IR spectra of dPG-azide and dPG conjugated with the degradable linker (dPG-(S-S)-methacrylate) showing complete removal of azide signal at 2100 cm^{-1} proving successful coupling.

Table 8. Hydrodynamic sizes (d.nm) and PDI of degradable nanogels with different composition determined by DLS at 25°C.

Monomer	wt% monomer	wt% dPG	Size (d.nm) at 25°C	PDI at 25°C
NIPMAM	90	10	166	0.218
	80	20	97	0.241
	70	30	80	0.433
	60	40	46	0.396
NIPAM	90	10	250	0.132
	80	20	185	0.116
	70	30	159	0.144
	60	40	100	0.172

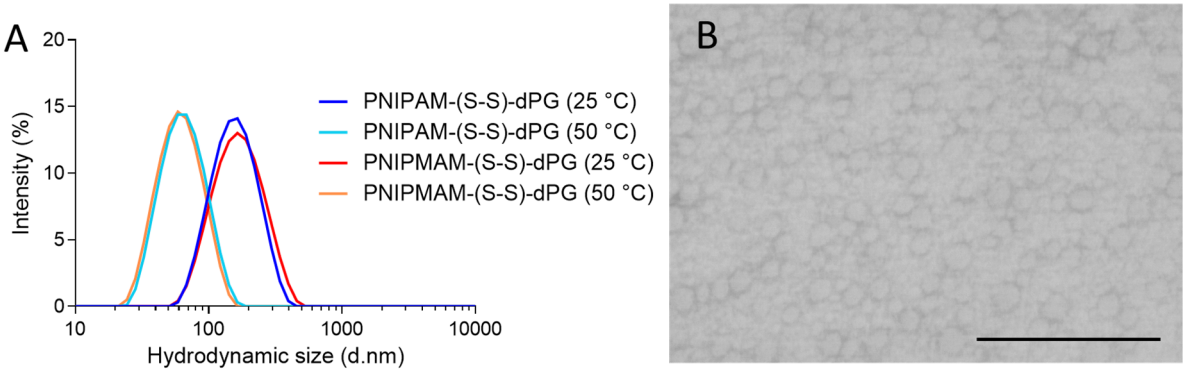

Figure 22. (A) Size distribution of selected nanogels PNIPAM-(S-S)-dPG and PNIPMAM-(S-S)-dPG obtained by DLS at 25 °C and 50 °C (B) TEM image of PNIPMAM-(S-S)-dPG. Scale bar 200 nm.

Temperature response of both nanogels was examined using DLS measurement. Both nanogels showed a size decrease down to 65 nm upon incubation at elevated temperature above the transition temperature of the polymers (Figure 22A). Analysis of the morphology by TEM revealed spherical shape and low polydispersity of selected nanogels (Figure 22B).

Due to the important role of disulfide bonds for the folding process and stabilization of proteins, a number of redox active enzymes and compartments with altered redox potential are prominent within the body. For instance, it was found that the redox-potential within different cell compartments of eukaryotic cells is significantly increased due to high concentrations (2-10 mM) of the molecule glutathione (GSH).[188, 189] Thus, upon internalization the presence of GSH can be used to reduce the disulfides bonds leading to a cleavage of the nanogels.

We therefore investigated the degradability of the nanogels to proof the presence of the disulfides. We monitored time and concentration dependent changes of their sizes by DLS upon incubation with GSH (Figure 23). For PNIPMAM-(S-S)-dPG a very fast degradation with high GSH concentrations (2 and 5 mM) was observed showing almost complete degradation within the first 4 h of incubation (Figure 23A,B). With longer incubation times in 5 mM GSH, a broad signal of larger size emerged from 12 h onwards indicating the formation of aggregates. For lower concentration of GSH (0.5 mM), which corresponds to extracellular concentrations, no size

decreases of the nanogels was observed. Only a slight decrease in the intensity and minor broadening of the signal was found for long incubation times.

We assume this is due to the cleavage of some disulfides leading to a partial loosening of the network structure allowing the nanogels to swell slightly (Figure 23C). This is in good agreement with the behaviour of periodate sensitive microgels reported by Lyon et al.[184] and macro-sized disulfide based hydrogels by Kar et. al.,[190] which both showed swelling of the gels before full disintegration. We assume the same degradation mechanism is valid for our disulfide based PNIPMAM-(S-S)-dPG nanogels, however due to the fast degradation kinetics with higher GSH concentrations the swelling phenomenon cannot be observed in our system.

To our surprise, we found the PNIPAM-(S-S)-dPG nanogels to be non-degradable even in high GSH concentrations. Here, only a slight decrease in intensity and broadening of the signal could be observed (Figure 23D). This indicated that there might be some disulfide bridges cleaved inducing the swelling of the nanogels in similarity to PNIPMAM-(S-S)-dPG in low GSH concentrations, but that the majority of the cross-links are still intact. In order to confirm whether the disulfides are still present in PNIPAM-(S-S)-dPG nanogels, we performed Raman spectroscopy. The comparison of PNIPMAM-(S-S)-dPG and PNIPAM-(S-S)-dPG (Figure 24) clearly shows the disulfide signal at 400 cm^{-1} for PNIPMAM based nanogels but no signal for PNIPAM-(S-S)-dPG. We therefore conclude, that in the case that NIPAM is used as monomer the disulfide linker is already broken during the polymerization process.

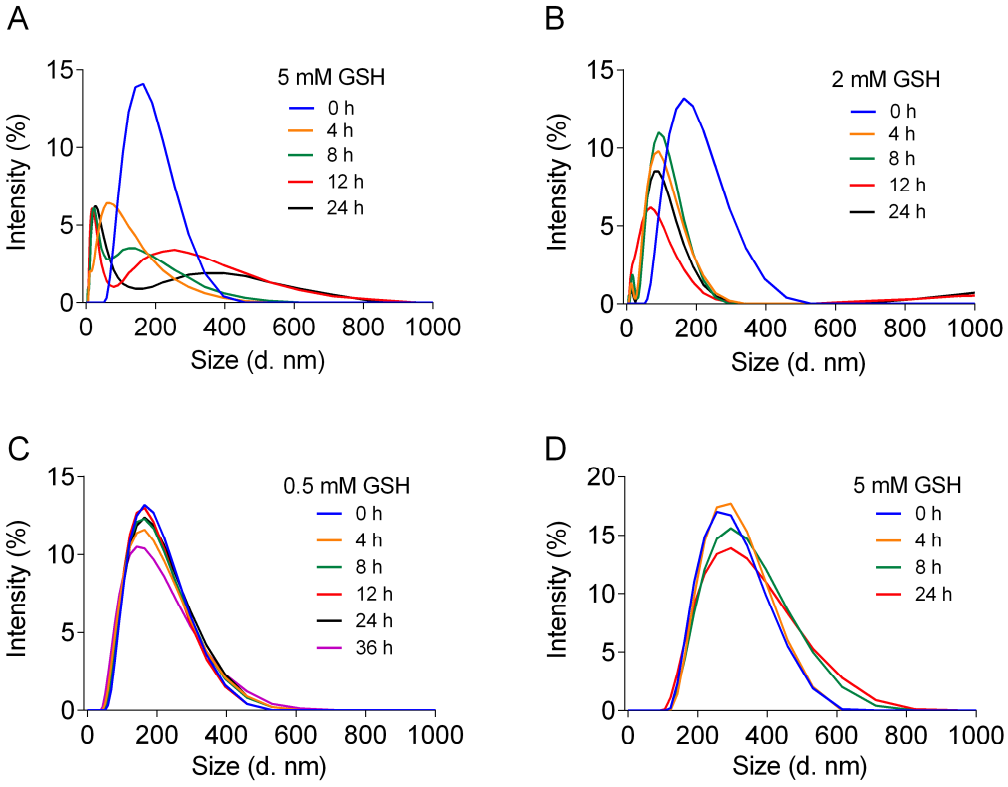

Figure 23. Redox induced degradation profiles of different nanogels. (A) Degradation of PNIPMAM-(S-S)-dPG nanogels in 5 mM GSH solution, (B) 2 mM GSH, and (C) 0.5 mM GSH, (D) degradation of PNIPAM-(S-S)-dPG in 5 mM GSH.

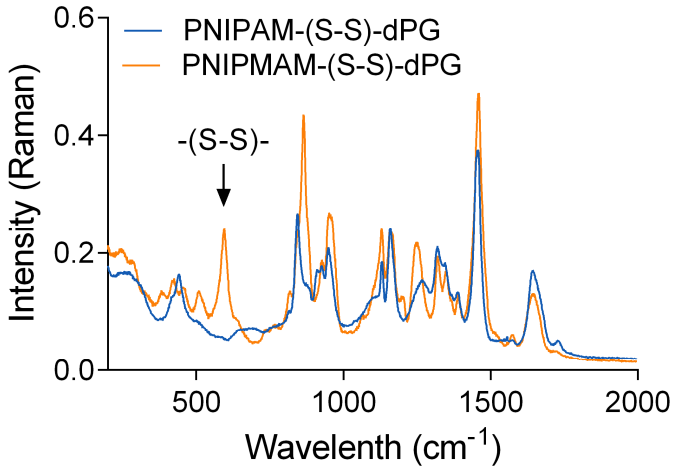

Figure 24. Raman spectra of PNIPAM-(S-S)-dPG and PNIPMAM-(S-S)-dPG nanogels.

We therefore prepared a macro hydrogel of the same constituents than the nanogel and studied its degradation by GSH. After incubation for 36 h with 5 mM GSH, we found the hydrogel completely disintegrated while incubation in PBS solution did not affect the hydrogel's structure (Figure 25). As the macrogels were synthesized at room temperature but the precipitation polymerization for the nanogel formation was performed at 70 °C, we assume that the reaction temperature could be a possible reason for the absence of disulfides in the nanogels. Nevertheless, the precipitation polymerization technique requires temperatures above the transition temperature of the thermo-responsive polymer. For PNIPAM the LCST is around 32 – 34 °C, making the formation of nanogels at room temperature impossible. We were thus interested in a gradual approximation to lower reaction temperatures and in an evaluation of the effects on the nanogels degradability.

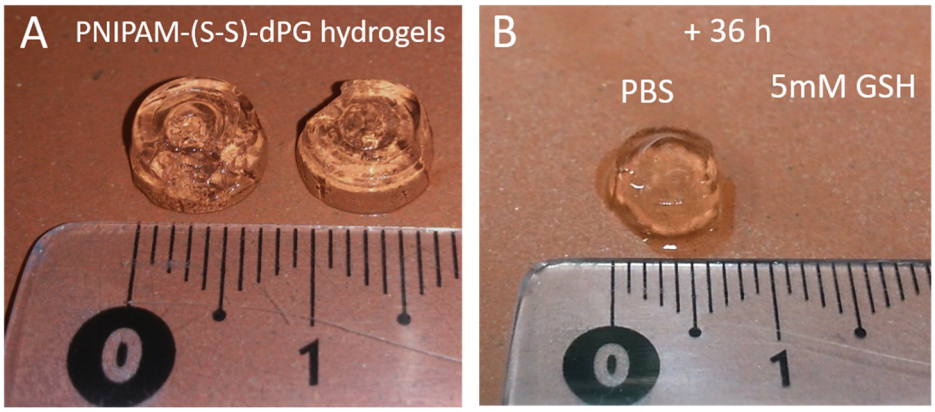

Figure 25. Hydrogel of PNIPAM-(S-S)-dPG (A) before and (B) after incubation with 5 mM GSH or PBS solution.

We screened the nanogel formation decreasing the reaction temperature stepwise down to 50 °C. We obtained nanogels with low PDI and sizes around 130 – 160 nm, but found none of them degrading in the presence of GSH (Table 9). So far, it is not clear to us why the use of NIPAM instead of NIPMAM affects the stability of the disulfide so drastically. We assume that the different reactivity of the radicals formed of the acrylate and the methacrylate in combination with higher temperatures are a possible explanation. The degradation behaviour of copolymeric nanogels with different ratios between PNIPAM and PNIPMAM (Figure 26) however

demonstrates that presence of NIPAM is decisive for the breakage of the disulfides during synthesis. With increasing NIPMAM content the nanogels swelling, visible as a signal broadening in the DLS measurements, gets more prominent until fragmentation into smaller particles appears from ratios of NIPMAM:NIPAM of 3:1 onwards.

Table 9. Variation of conditions for the synthesis of PNIPAM-(S-S)-dPG nanogels. No size changes upon incubation of the nanogels with 5 mM GSH solution for 24 h (measured by DLS) is defined as 'no degradability'.

Temperature (°C)	Initiator	Size (d.nm) at 25°C	PDI at 25°C	Degradability
70	APS/T	159	0.144	no
60	APS/T	136	0.090	no
55	APS/T	132	0.122	no
50	APS/T	141	0.090	no

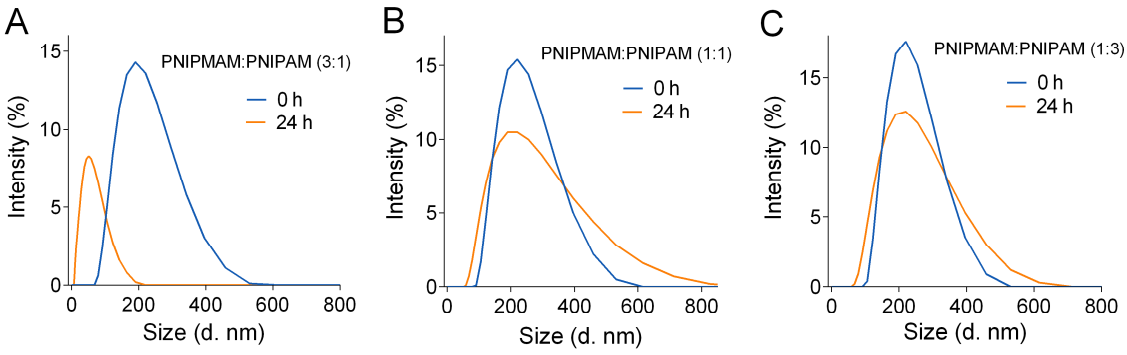

Figure 26. Degradation profiles of copolymeric nanogels in GSH solution (5mM) with different PNIPMAM : PNIPAM ratios: (A) 3:1, (B) 1:1, and (C) 1:3.

We hypothesized that due to a dynamic equilibrium between thiols and dithiols our nanogels will be able to interact with biological materials possessing as well either thiols or disulfides. Both are found in the mucosal layer due to the presence of mucins, which are glycoproteins with proteins backbones that contain around 25 domains of cysteine residues, where each domain has 10 invariant Cys residues.[191] We therefore evaluated the ability of PNIPMAM-(S-S)-dPG

nanogels to interact with cysteine and found a similar size reduction in a concentration dependent manner as for the incubation with GSH (Figure 27A-C). This demonstrated the ability of Cys to break the present disulfide bridges in the network of the nanogels.

The mucosal layer is slightly basic. In addition, as a potential drug delivery agent, the stability of the nanogels upon facing environments of different pH is crucial. We therefore investigated the effects of various pH on the nanogels. Time dependent size measurement showed that the nanogels are stable over 96 h in slightly acidic and neutral conditions (Figure 27D,E). At basic pH, a slow degradation is visible (Figure 27F) probably due to hydrolysis of some disulfide bonds reacting with the hydroxyl ions to form thiols and oxythiols.

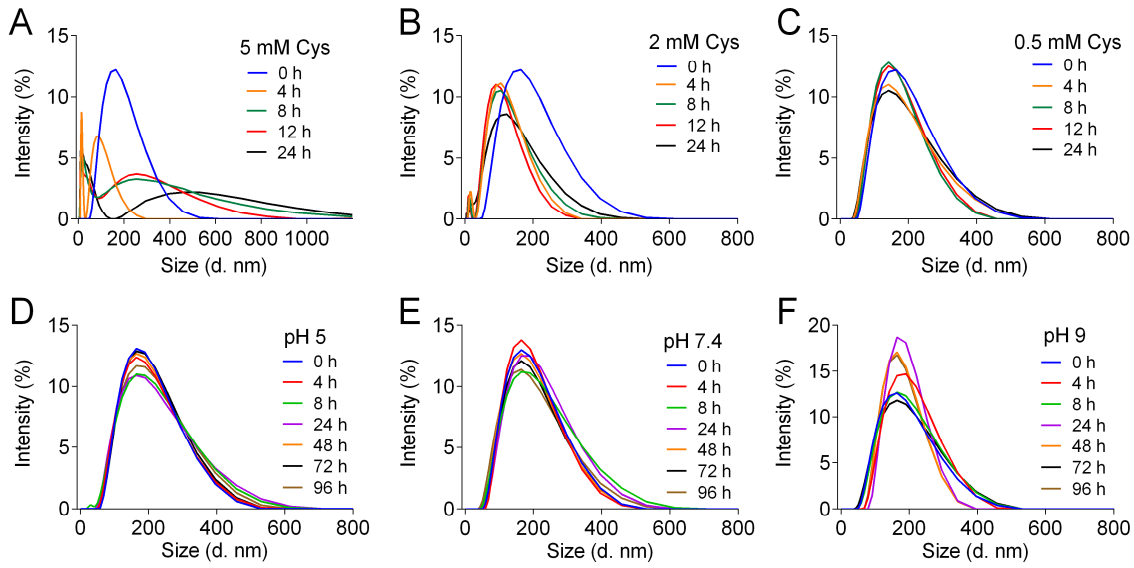

Figure 27. Degradation of PNIPMAM-(S-S)-dPG nanogels in presence of (A) 5 mM L-Cysteine (Cys), (B) 2 mM Cys or (C) 0.5 mM Cys and stability at different pH values: (D) pH 5, (E) pH 7.4 and (F) pH 9.

Interaction with mucus

To investigate interaction of the nanogels with mucus and effects on the nanogels structure, native porcine intestinal mucus gel was isolated and incubated with the PNIPMAM-(S-S)-dPG nanogels at 37 °C. Due to the complex composition of the mucus itself, analysis by DLS as for GSH and Cys induced degradation were not feasible. We therefore performed gel permeation

chromatography (GPC) connected to an UV-Vis absorbance measurement chamber. In order to be able to distinguish the nanogels from particles of the mucus, we labeled the nanogels with the dye RhodB conjugating it to the dPG. In case of a degradation of the nanogels, the retention time of the labeled materials is thus expected to converge to retention time of the dPG itself.

To validate this technique, we first explored this setup with the nanogels incubated with GSH. Indeed, we found increasing retention times with increasing incubation times, consistent with size decrease of the nanogels (Figure 28A), while the non-degradable PNIPAM-dPG control nanogels did not show any changes (Figure 28B). A convergence to the retention time of dPG was found for both, increasing incubation times (Figure 28C) or higher concentrations of the used GSH solution (Figure 28D). The results are in good agreement with the ones obtained by DLS measurements (Figure 23), showing that already after 4 h almost a full degradation is apparent. Thus, we investigated the interaction with mucus with the same RhodB labeled nanogels using the validated setup. Interestingly, we found a gradual reduction of the PNIPMAM-(S-S)-dPG nanogel in the mucus gel over time as well with 98% degradation after 12 h (Figure 28E,F). These results indicate that the cysteins present in the mucus are able to induce a cleavage of the disulfides in the nanogels.

To test whether the interaction with mucus enables the nanogels to overcome the mucosal barrier and reach underlying viable cell, we followed the nanogels after administration on freshly excised porcine jejunum. The viable tissue punches were mounted on a Franz-cell setup at 37 °C and treated with the RhodB labeled PNIPMAM-(S-S)-dPG and its non-degradable analogue for 1 h and 3 h. Snap frozen sections of the tissue were analysed using fluorescence microscopy (Figure 29). The resulting images showed efficient penetration of the degradable nanogels through the mucus layer reaching underlying epithelium. In contrast, the non-degradable PNIPMAM-dPG nanogels remained on top of the mucin layer and were almost entirely cleared by the mucus after 3 h. These results clearly demonstrate that the presence of disulfides enabled the nanogels to resist against the flow of the secreted mucus. They even move upstream and are thus able to infiltrate the submucosal tissue. The ability to overcome the mucosal clearance renders the disulfide containing nanogels in a promising candidate for the application as efficient submucosal drug delivery agent.

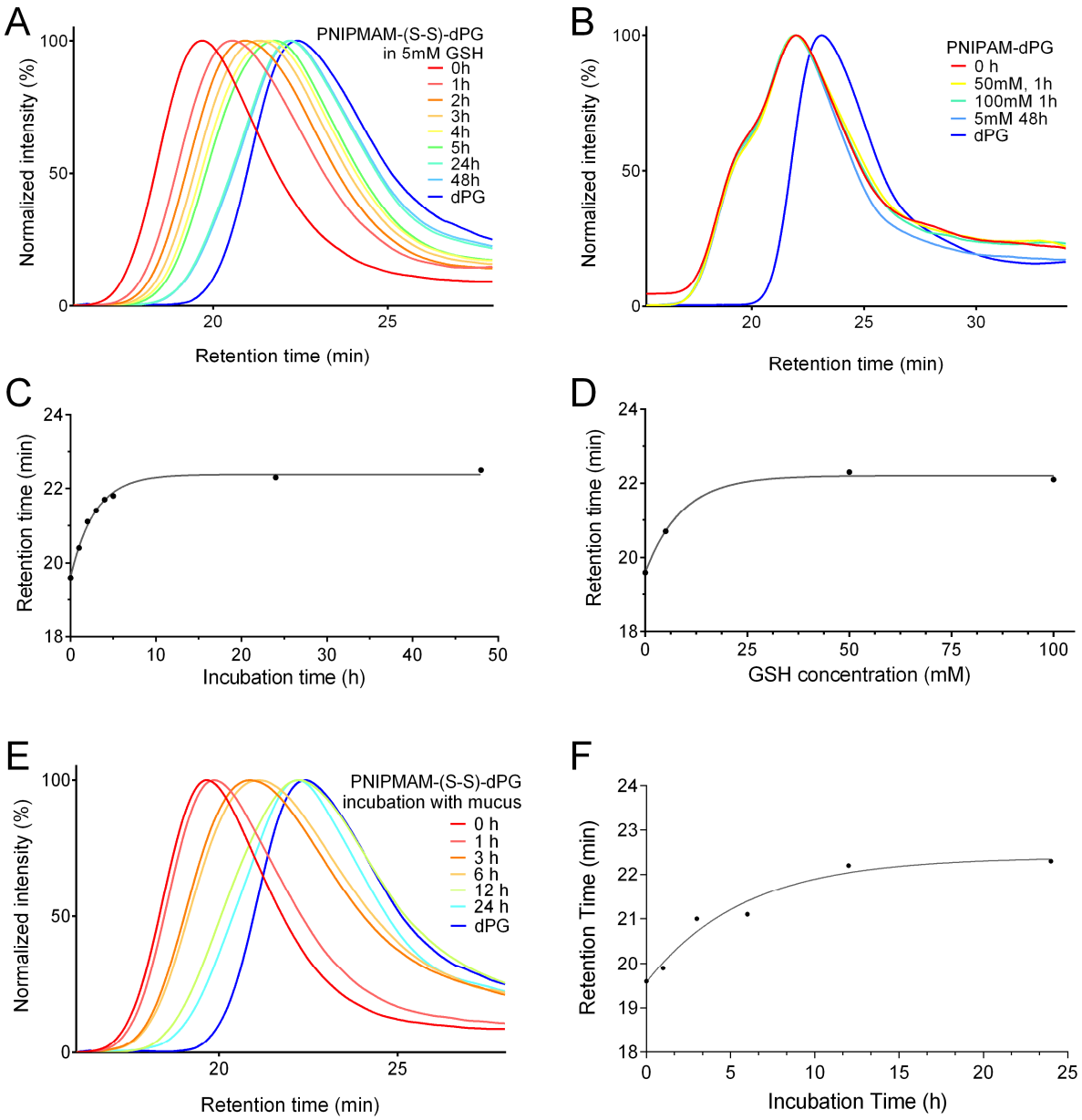

Figure 28. Degradation analysis upon incubation with GSH and mucus by GPC. (A) Retention profile of PNIPMAM-(S-S)-dPG post incubation in 5 mM GSH solution and pure dPG, (B) non-degradable controls in different concentrations of GSH and different incubation times, (C) mean retention time of PNIPMAM-(S-S)-dPG plotted versus incubation time in 5 mM GSH or (D) GSH concentration. (E) Retention profile and (F) mean retention time post incubation of PNIPMAM-(S-S)-dPG with mucus.

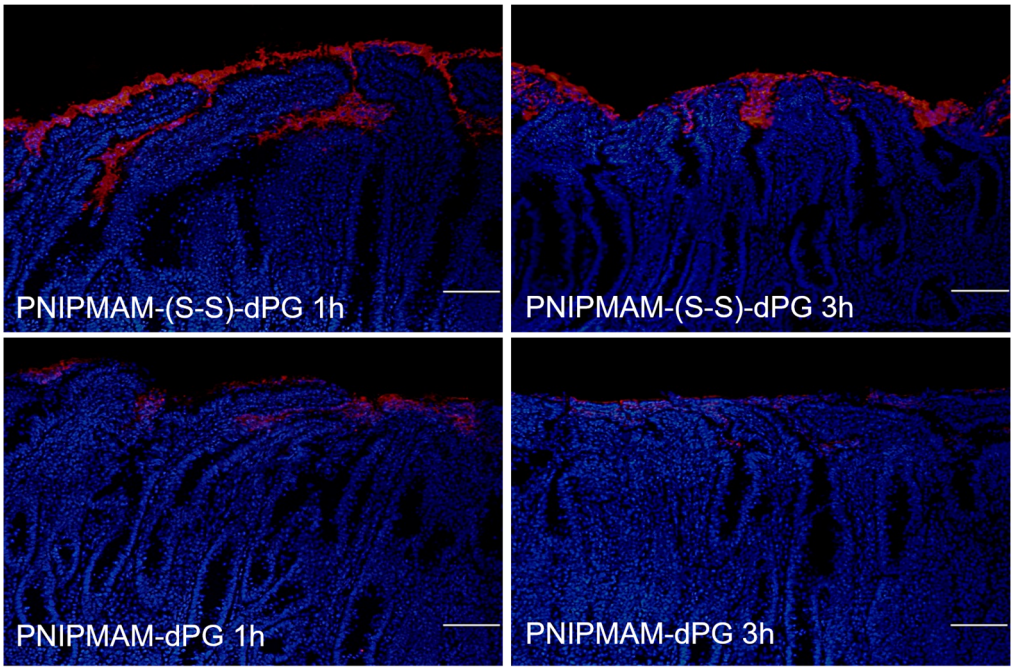

Figure 29. Representative fluorescence microscopy images of porcine jejunum cryosections (5 µm) after application of Rhod-B labeled (red) degradable disulfide-nanogel (PNIPMAM-(S-S)-dPG) and its non-degradable analogue (PNIPMAM-dPG) after 1 h and 3 h treatment. DAPI stained nuclei are shown in blue. Scale bar = 100 µm. N = 3.

4.1.3 NIR-TRANSDUCING SEMI-INTERPENETRATED NANOGELS

This chapter is based on the manuscript "NIR- and thermo-responsive semi-interpenetrated polypyrrole nanogels for imaging guided combinational photothermal and chemotherapy" (Appendix 7.3), which has been submitted to the Journal of Controlled Release. Contributions: Nanogel synthesis and full characterization was performed by me. TEM images were recorded by Julián Bergueiro Álvarez, size distribution analysis from the TEM images was done by me.

For the generation of dual NIR- and thermo-responsive nanogels suitable for imaging guided combinational photothermal and chemotherapy, we were interested in the use of thermo-responsive nanogels as 'smart' stabilizing matrix for the NIR transducing polymer PPY. To optimize the behaviour of resulting nanogels after systemic administration, particularly the influence of the hydration state of the thermo-responsive network on the biodistribution profile and the tumor accumulation should be evaluated. We therefore aimed to use thermo-responsive nanogels with similar physico-chemical properties but different hydration states at 37 °C body temperature.

In Chapter 4.1.1, the suitability of using the thermo-responsive polymers PNIPAM and PNIPMAM for the generation of thermo-responsive nanogels with variable VPTTs was demonstrated. PNIPAM-dPG nanogels exhibited a transition temperature of 34 °C and are thus in their collapse state at 37 °C. In contrast, copolymeric nanogels with a 1:1 wt. ratio of PNIPAM and PNIPMAM (Co-dPG) and PNIPMAM-dPG nanogels have their transition at 40 °C, respectively 47 °C. Thus, both are in a swollen state at 37 °C body temperature (Table 7). All nanogels had neutral zeta-potential, sizes between 130 – 180 nm and showed similar swelling-shrinking ratios rendering them into feasible candidates for a comparative evaluation of the hydration state influence on the nanogels behaviour.

First, we were interested in the ability of these nanogels to act as stabilizing matrix for PPY. To introduce PPY to the thermo-responsive nanogels we used semi-interpenetration. This was performed by swelling dry nanogels in an acidified solution of pyrrole and initiating its *in situ*

polymerization within the nanogels network with APS (Figure 30). The variation of the molarity of monomer solution revealed no major impact on the final particle size in hydrated state with sizes of all semi-interpenetrated nanogels of around 200 nm (Table 10). However, at higher molarity copolymeric and NIPMAM based PPY nanogels aggregated strongly upon crossing the VPTT of the thermo-responsive network making theses nanogels unsuitable for systemic administration.

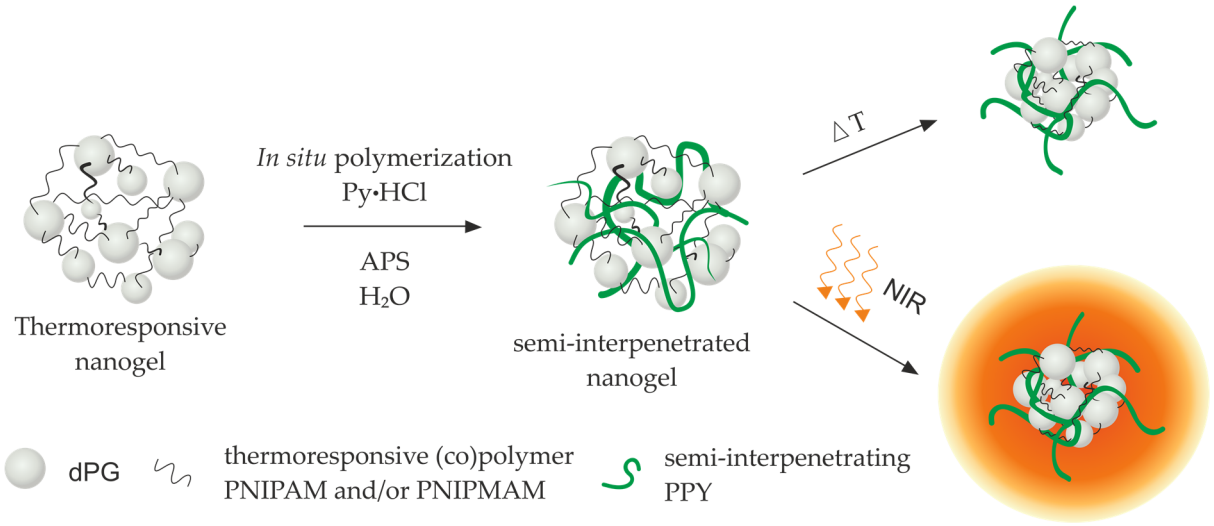

Figure 30. Synthesis of NIR and thermo-responsive nanogels by semi-interpenetration.

We found that for nanogels with higher VPTT (equating higher PNIPMAM content) stable nanogels are only obtained when lower molarity of pyrrole solution. A possible reason for this behaviour could be the size difference of the thermo-responsive nanogels with PNIPMAM-dPG nanogels being approximately 60 nm smaller than their PNIPAM analogues. As similar sizes after semi-interpenetration are reached for all nanogels, we hypothesize that a higher ratio of PPY chains will partially be outside or on the surface of the nanogel network in case of copolymeric and PNIPMAM based networks. We suppose that this ratio even will be increased upon crossing the transition temperature of the thermo-responsive network and its resulting contraction (Figure 30). This assumption is supported by our findings for semi-interpenetration of PNIPAM-dPG nanogels with charged polymers showing a change in the zeta-potential upon crossing the VPTT indicating the exposure of the inner semi-interpenetrating network.[192] Due to

the water-insolubility of the PPY, a high ratio of exposed PPY could lead to a loss of the stabilizing ability of the thermo-responsive network. Thus, a high PPY content and smaller size of the thermo-responsive network lead to aggregation of the resulting semi-interpenetrated nanogels at high temperatures.

In order to confirm the entanglement of PPY chains within the nanogels network, we performed the semi-interpenetration in a similar manner but in the macroscale using thermo-responsive hydrogels prepared with the same building blocks as used for the nanogels. In Figure 31A-E it can be nicely seen that the polymerization of pyrrole starts at the hydrogels surface. With time, the whole solution turns black forming PPY also outside the hydrogel structure. These non-interpenetrated PPY chains precipitated overnight (Figure 31F) in similar manner to polymerization performed in absence of a hydrogel (Figure 31 insets a,e,f). Short oligomeric pyrrole chains yielding a greenish colour of the solution can be sufficiently removed by dialysis while non-interpenetrated longer PPY chains precipitate (Figure 31G). After purification, a stable black hydrogel (Figure 31H) is obtained underlining the stabilizing ability of the gels network for PPY chains and successful interpenetration. Transferring this to the nanoscale, the absence of PPY precipitates indicate that PPY formation is only happening within the nanogels probably promoted by the greater surface area of the nanogels in comparison to the macroscopic gel and their dispersion in the whole solution. This is in good agreement with findings from Fernández-Barbero and coworkers who could demonstrate uniform distribution of PPY within micro-scale thermo-responsive gels when the penetration reaction was performed at temperatures below the VPTT of the microgels (in the swollen state).[193]

Another aspect which may influence the formation of stable interpenetrated nanogels could be the polymerization kinetic, which we found to be faster for the semi-interpenetration process performed at higher molarity of pyrrole (Figure 32A). Eventually, when the polymerization is progressing too fast, formed PPY chains are not sufficiently entangled or not located in the inside of the nanogel network, leading to an aggregation upon the shrinkage of the thermo-responsive network.

Table 10. Characterization of different thermo-responsive nanogels semi-interpenetrated with PPY with varied molarities of the monomer swelling solution. Hydrodynamic size (d.nm), corresponding PDI values and VPTTs were measured by DLS (intensity distribution).

	PPY/PNIPAM-dPG			PPY/Co-dPG			PPY/PNIPMAM-dPG		
Py·HCl	25 °C	50 °C	VPTT	25 °C	50 °C	VPTT	25 °C	50 °C	VPTT
0.1 M	200 (0.162)	118 (0.062)	33.0 °C	205 (0.119)	aggr.	-	241 (0.178)	aggr.	-
0.075 M	178 (0.191)	103 (0.097)	33.3 °C	249 (0.167)	136 (0.074)	39.5 °C	244 (0.213)	aggr.	-
0.05 M	176 (0.200)	103 (0.093)	33.3 °C	197 (0.164)	97 (0.075)	39.5 °C	204 (0.197)	147 (0.126)	47.0 °C

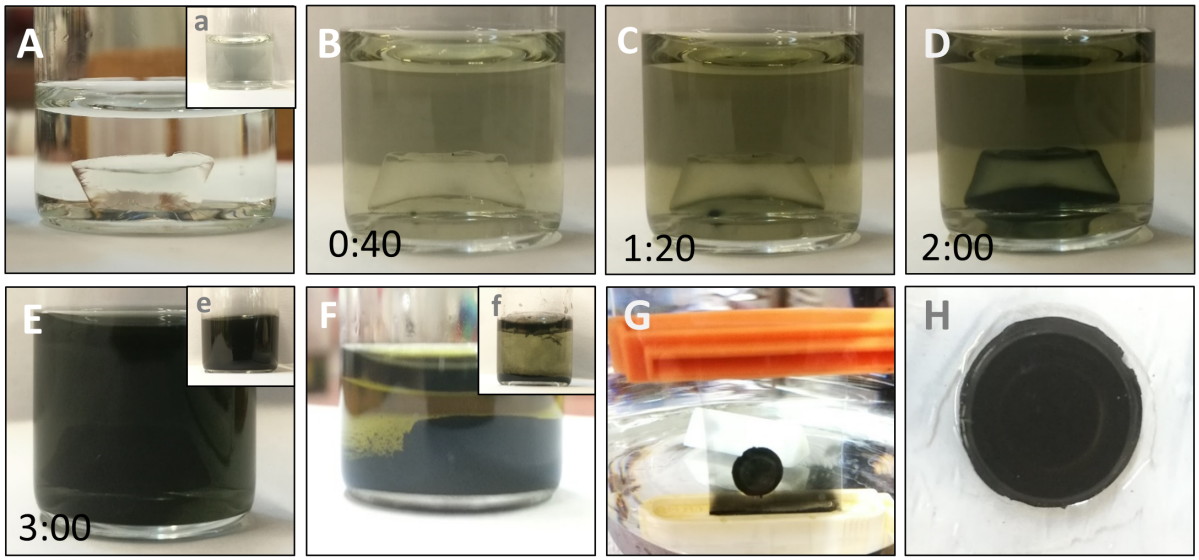

Figure 31. PPY polymerization process inside a hydrogel. A) PNIPAM-dPG hydrogel swollen in Py·HCl solution, B)-E) polymerization of PPY in presence of a hydrogel indicated over time (min:sec) and F) appearance of the reaction mixture on the next day, G) semi-interpenetrated hydrogel in the dialysis bag, H) semi-interpenetrated hydrogel after purification. Insets a), e), and f) show the respective state in the polymerization process of PPY in the absence of a hydrogel.

Absorbance spectra of the reaction mixture clearly show increasing absorbance in the NIR region due to increasing chain length of PPY (Figure 32B). After purification, the obtained nanogels show the characteristic absorbance spectrum of PPY demonstrating the successful

interpenetration (Figure 32C). As a result of the higher molarity of pyrrole solution used for PNIPAM-dPG nanogels, these nanogels have a higher PPY content than their copolymeric and NIPMAM based analogues. This is evidenced by a stronger absorbance for same nanogel concentration. Besides the stability upon heating, long-term stability of the nanogels over several months was assayed by frequently measuring their hydrodynamic size demonstrating stability of all PPY nanogels up to six months.

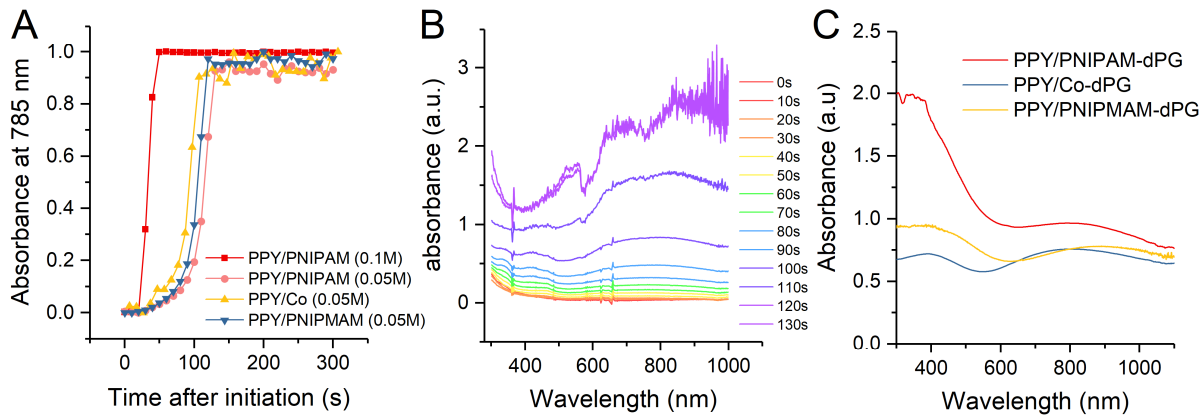

Figure 32. Semi-interpenetration process studied by UV-Vis spectroscopy. (A) Absorbance at 785 nm during first 5 min of polymerization, (B) UV-VIS spectra of PPY/PNIPMAM-dPG within the first 2 min after initiation, and (C) UV-VIS absorbance spectra of all three semi-interpenetrated PPY nanogels after purification in a concentration of 0.25 mg/mL.

As can be seen from in the TEM images, the resulting PPY-interpenetrated nanogels for all three thermo-responsive nanogels show spherical shape and low polydispersity (Figure 33). As expected, the temperature-responsive properties of the nanogels remain unaffected by the semi-interpenetration process with VPTT of 33 °C (PPY/PNIPAM-dPG), 39.5 °C (PPY/Co-dPG) and 47 °C (PPY/PNIPMAM-dPG) (Table 10, Figure 34). Interestingly, the size of the nanogels obtained from TEM is much smaller than the values obtained by DLS at swollen (25 °C) as well as shrunken (50 °C) state (Figure 35) indicating that the nanogels in shrunken state still contain a relatively high proportion of water.

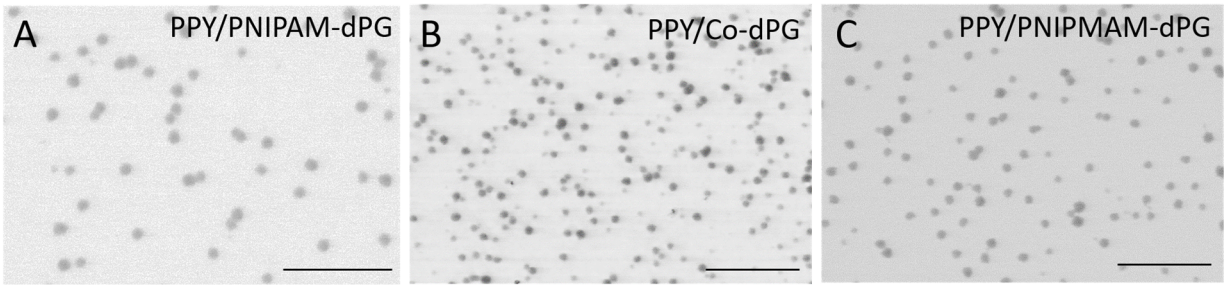

Figure 33. Morphology of semi-interpenetrated PPY nanogels as studied by TEM. (A) PPY/PNIPAM-dPG, (B) PPY/Co-dPG and (C) PPY/PNIPMAM-dPG. Scale bar 500 nm.

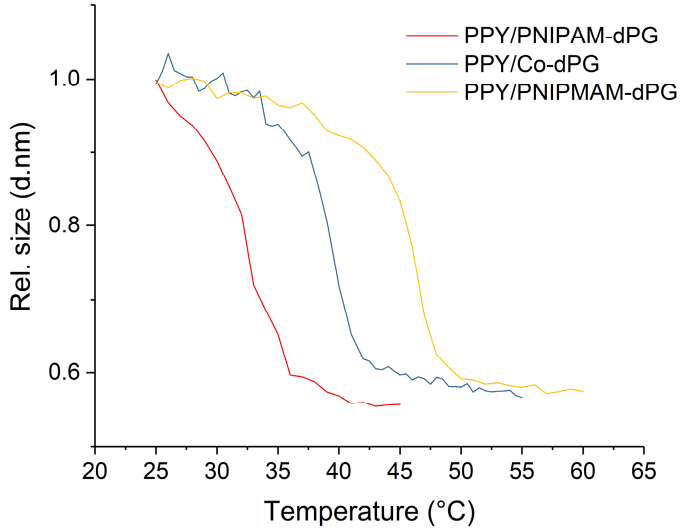

Figure 34. VPTT diagrams of all three semi-interpenetrated nanogels.

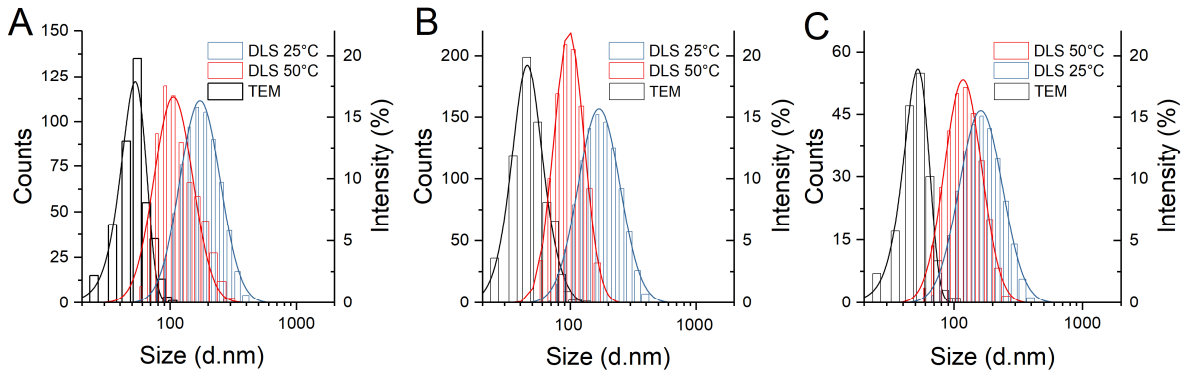

Figure 35. Size comparison of (A) PPY/PNIPAM-dPG, (B) PPY/Co-dPG, and (C) PPY/PNIPMAM-dPG in aqueous solution above and below the VPTT by DLS and in dry state by TEM.

Photothermal transducing ability and thermo-responsiveness under NIR trigger

Next, we investigated the ability of the formed PPY nanogels to transduce light of the NIR region into heat. For the application of the nanogels as drug delivery agent, stability of the particles is crucial. In addition, it is known that particles larger than 200 nm are more rapidly cleared from the body than smaller analogues.[25] We therefore chose PPY nanogels with sizes of a maximum of 200 nm and a PPY content assuring the retention of their stability upon heating (PPY/PNIPAM-dPG 0.1 M, PPY/Co-dPG 0.05 M, and PPY/PNIPMAM-dPG 0.05 M). The nanogel solutions were exposed to a NIR-Laser (785 nm, 500 mW) and temperature increase was monitored with an IR-camera. All nanogels showed concentration dependent heating reaching a temperature plateau after 120 – 150 s of irradiation (Figure 36). The PPY/PNIPAM-dPG nanogels show increased heating performance as they contain more PPY, but all three nanogels increase the temperature of more than 10 °C already at concentrations of 0.05 mg/mL or below (Figure 37B). Repeated cycles of NIR exposure and cooling (Figure 37C) demonstrate the excellent photostability of PPY in the interpenetrated nanogels.

To assess the nanogels' thermo-responsiveness during NIR irradiation and light-to-heat transduction, we measured the size of the nanogels immediately after NIR exposure. In all cases, we found a shrinkage of the nanogels and a reswelling to their original size within 5 min (Figure 37D). For PPY/PNIPAM-dPG nanogels, even in low concentrations, temperatures higher than 50 °C, far above the VPTT, were reached during irradiation. For the other two nanogels, temperatures around their VPTT are reached at this concentration, and only at higher concentrations the solutions were heated above their transition temperature.

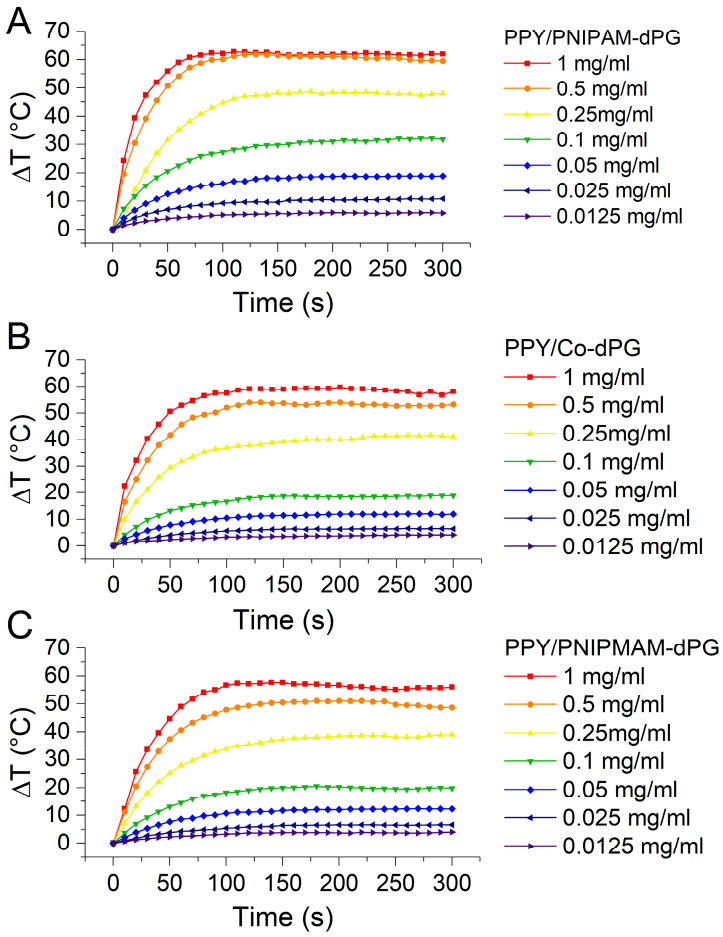

Figure 36. Temperature increase upon irradiation with a NIR laser (785nm, 500 mW) of A) PPY/PNIPAM-dPG, B) PPY/Co-dPG and C) PPY/PNIPMAM-dPG solution with different concentrations over time.

Surprisingly, we found that upon NIR irradiation the shrinkage of the nanogels is much more pronounced than only incubating them at the corresponding temperature (Figure 37E). For instance, PPY/PNIPAM-dPG reach a temperature of 53.5 °C upon NIR (starting from 25 °C). The incubation at this temperature let the nanogels shrink about 42% to a relative size of 0.58 in comparison to their swollen state. In contrast, upon NIR exposure the nanogels even shrink about 68%. Also for PPY/Co-dPG and PPY/PNIPMAM-dPG the size decrease after NIR expose is more pronounced than induced by heating the whole solution. Triggered by NIR light, the shrinkage is increased about 9% (PPY/Co-dPG), respectively 18% (PPY/PNIPMAM-dPG) in comparison to the temperature induced shrinkage in lower concentration of 0.1 mg/mL. This

effect is even more pronounced at higher concentrations (0.25 mg/mL) with 17%, respectively 31% more shrinkage upon NIR exposure.

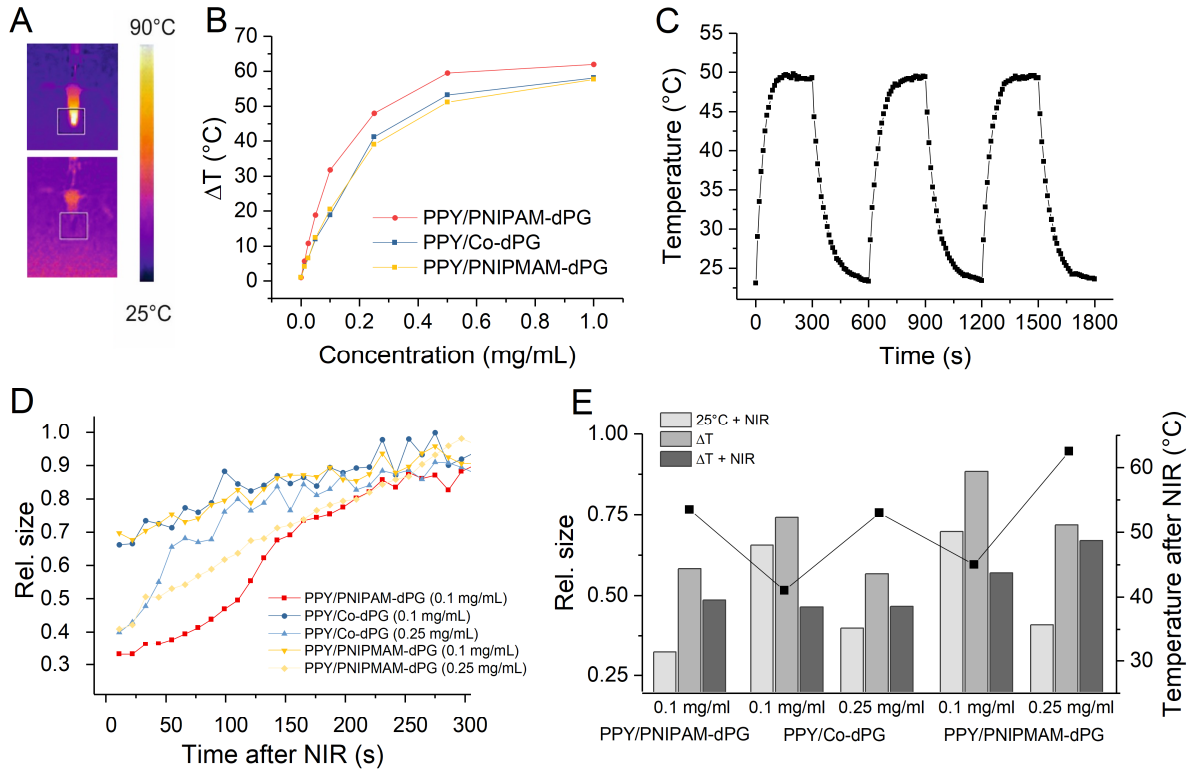

Figure 37. Photothermal activity and thermo-responsiveness of the semi-interpenetrated PPY nanogels. (A) IR pictures of a sample during irradiation, (B) concentration dependent temperature difference reached after 5 min NIR irradiation, (C) three heating and cooling cycles of PPY/Co-dPG solution, (D) relative size of semi-interpenetrated nanogels after exposing to NIR laser for three minutes (t0) and reswelling after removal of NIR trigger, (E) comparison of relative size to swollen state after: 3 min NIR at r.t., at the corresponding temperature reached upon NIR (ΔT), and 3 minutes NIR at corresponding ΔT.

As in the lower concentration for both nanogels the photothermal conversion only causes a temperature increase close to the VPTT, we reason that the local temperature elevation in close vicinity to the PPY chains is likely much higher than measured by the IR camera in the whole solution. Thus, a collapse of the nanogels is induced even if the solution appeared to not reach temperatures high enough (above VPTT). This strong heating in close vicinity to the transducer is also reported for other photo-thermal agents like gold nanorods and gold-decorated

upconversion nanoparticles along with a fast decay of the temperature with increasing distance to the particles surface.[194, 195]

Furthermore, the NIR irradiation seems to induce an additional shrinkage even over the maximal collapsed state caused by elevated temperature. In order to investigate this phenomenon, we irradiated nanogels while keeping the surrounding temperature as high as reached under NIR exposure at 25 °C. For example, PPY/PNIPAM-dPG nanogels were incubated at 53.5 °C as this was maximal temperature reached after 3 min of NIR exposure. As mentioned above, this temperature induce a size decrease of the nanogels about 42%. Then, the heated nanogel solution was additionally exposed to NIR and the size of the nanogels was measured immediately after 3 min of irradiation. We found an additional size decrease of 9% (Figure 37E). Similar effects showing additional size reduction of 5-9% were found for PPY/Co-dPG and PPY/PNIPMAM-dPG when the incubation temperature was above the VPTT of the corresponding nanogel.

Even stronger size reduction was found for PPY/Co-dPG (18%) and PPY/PNIPMAM-dPG (31%) nanogels in lower concentration, where the incubation temperature was close to the VPTT or below. Interestingly, the relative size reached for both nanogels under simultaneous application of temperature and NIR is similar and seems to be independent of the concentration. At both concentrations, the relative size is lower than what the heating of the solution above the transition temperature induce. Removing the NIR trigger, all nanogels re-swell to the size of the stage induced by the temperature applied (data not shown). We therefore conclude that upon local heat production under NIR exposure another portion of water is expelled from the nanogel procure an 'over-collapsed' state that only persists with the trigger applied.

Comparing the relative size of nanogels upon application of NIR we found that the 'over-collapse' is more prominent when the trigger is applied on swollen nanogels (incubated at 25 °C) and in concentrations reaching temperatures above the VPTT under irradiation than on collapsed nanogels (incubated above their VPTT). We correlate this to the formation of

stabilizing, inter-polymeric hydrogen bonds, which were demonstrated to be present above the transition temperature for linear PNIPAM and PNIPMAM by Dybal and coworkers,[94] acting against the additional size decrease when NIR exposure is applied on nanogels held above their VPTT.

Taken together, we can conclude that the semi-interpenetration of PPY into the thermo-responsive nanogels do not alter the general temperature-response of the resulting nanogels, but the local heat production upon photothermal conversion increase the shrinkage of the nanogels inducing the expulsion of additional interior water molecules.

4.2 EVALUATION OF NANOGELS AS DRUG DELIVERY SYSTEMS AND COMBINATIONAL THERAPEUTIC ACTIVES

4.2.1 TEMPERATURE-TRIGGERED DELIVERY OF PROTEINS

This chapter is based on the paper "Critical parameters for the controlled synthesis of nanogels suitable for temperature-triggered protein delivery", which has been partially modified. The link to the published form is given in Appendix 7.2. Author Contributions: All synthesis and characterizations of nanogels were performed by me. In vitro encapsulation and release profiles, as well as CD measurements and analysis were done by me. MTT cell viability was performed by Stefanie Wedepohl. Rawan Charbaji did all skin penetration studies. We discussed the results and I wrote the manuscript. All authors contributed to the final version of the manuscript.

In order to evaluate the ability of the thermo-responsive nanogels to deliver therapeutic active agents in a controlled fashion, bovine serum albumin labeled with FITC (BSA-FITC) was loaded to the nanogels and its release profile dependent on a temperature stimulus was studied. Therefore, the nanogels were swollen in a solution of BSA-FITC to encapsulate the BSA into the nanogels. Three different ratios between nanogels and protein were tested. For the lowest ratio (10:1 nanogel:protein) loading efficiency was ≥ 86% BSA loaded to the nanogels. For PNIPAM-dPG and Co-(1:1)-dPG these high loading efficiencies were also observed with higher ratios of protein:nanogels (Figure 38). Only for PNIPMAM-dPG nanogels there was a significant drop in the encapsulation efficiency from 80% (10:1 nanogel:BSA) to 50% with a 1:1 nanogel:BSA feeding ratio.

In order to see if the different nanogel size is a reason for this efficiency loss, we performed encapsulation studies with surfactant free synthesized PNIPMAM nanogels. These have a similar size to the PNIPAM and copolymeric ones with an average diameter of around 185 nm. Indeed, we observed a higher loading efficiency for these nanogels compared to the ones

synthesized in presence of SDS (Figure 38). Nevertheless, the encapsulation efficiency was reduced with higher PNIPMAM content of the nanogels. These results emphasize the importance of the nanogels size for protein loading, but as well indicate that slightly higher hydrophobicity or sterical demand of PNIPMAM counteracts protein encapsulation. However, it is worth noticing that for all tested nanogels, protein encapsulation is outstandingly high.

To evaluate protein stability upon encapsulation and release, circular dichroism (CD) of encapsulated BSA was measured. As depicted in Figure 39A, no significant spectra changes were observed for all nanogels indicating that the encapsulation process did not affect the secondary structure of the protein. As the nanogels are designed for the purpose of a temperature triggered release of their encapsulated cargo, stability of the used model protein BSA at different temperatures was analysed with and without nanogels present (Figure 39B,C). As reported previously, we found that BSA is stable until temperatures of around 50 °C and starts to unfold at higher temperatures.[196-198] Apparently, presence of the nanogels do not alter this behaviour. These results indicate that in principle all three nanogels are feasible for the temperature-triggered release of BSA, as their VPTT is below the temperature at which the protein starts to unfold.

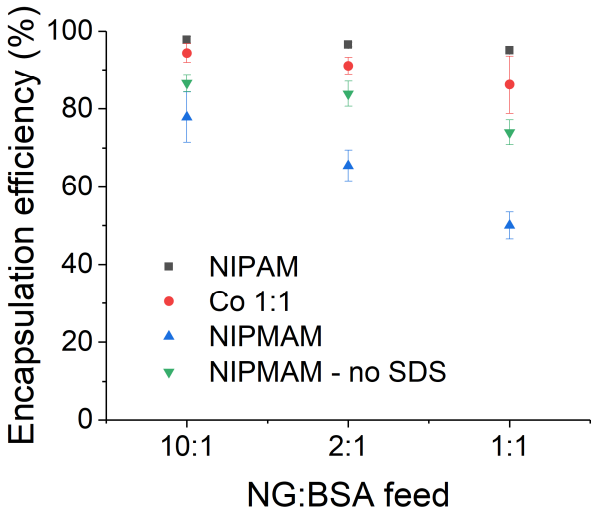

Figure 38. Encapsulation efficiency of BSA-FITC into different thermo-responsive nanogels determined by UV-VIS spectroscopy.

The release of BSA-FITC from all nanogels was studied at three different temperatures. For PNIPAM-dPG and Co(1:1)-dPG nanogels, a temperature triggered release could be observed showing a burst release of the encapsulated protein when the temperature is raised above the VPTT of the nanogels (Figure 40). For NIPAM based nanogels, a significant increase of released BSA from 21% (29 °C) to 90-96% (37 °C or 42 °C) after 72 h could be observed. Similar results were obtained for the copolymer of NIPAM and NIPMAM where the release was accelerated to 72% after 72 h above its VPTT of 40 °C, whereas at 29 °C and 37 °C only minor release of less than 20% was determined. As a control for the temperature dependent release mechanism, PNIPMAM-dPG nanogels were analysed as well, here all three tested temperatures were below the VPTT of the nanogels and we only expect minor release of encapsulated BSA. As the encapsulation efficiency was more similar to PNIPAM-dPG and Co(1:1)-dPG, the surfactant free synthesized nanogels was chosen for this study. Indeed, we observed only a minor release up to maximal 36% after 72 h for the NIPMAM-dPG nanogels. These results show that the release mechanism is indeed temperature triggered, in which the shrinkage of the nanogels lead to a burst release of encapsulated protein. We could also observe a contribution of diffusion processes to the overall release profile, as not all protein is released immediately and an accelerated temperature lead to increased release rates.

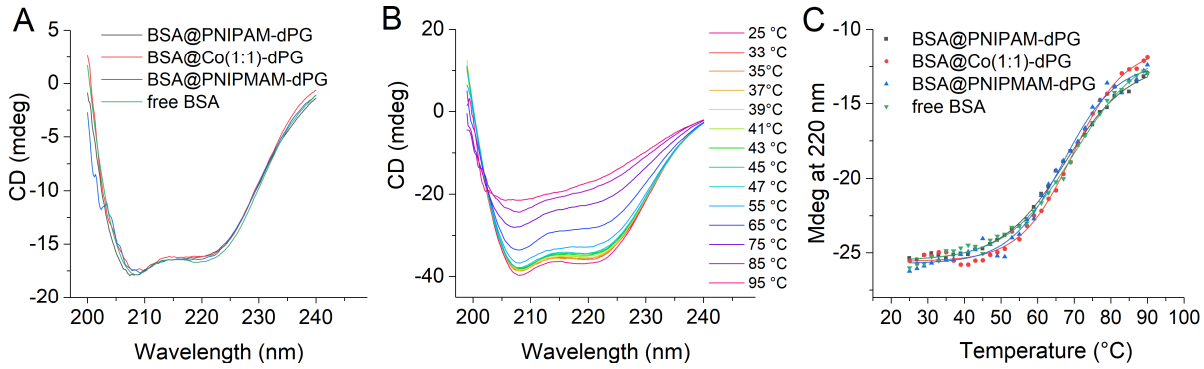

Figure 39. Structural integrity of BSA during encapsulation and thermally triggered release. (A) CD spectra of encapsulated BSA in all three nanogels at 25 °C, (B) CD spectra of a BSA solution at different temperatures, (C) intensity values from CD spectra of BSA free and encapsulated in the nanogels at 220 nm plotted against the temperature.

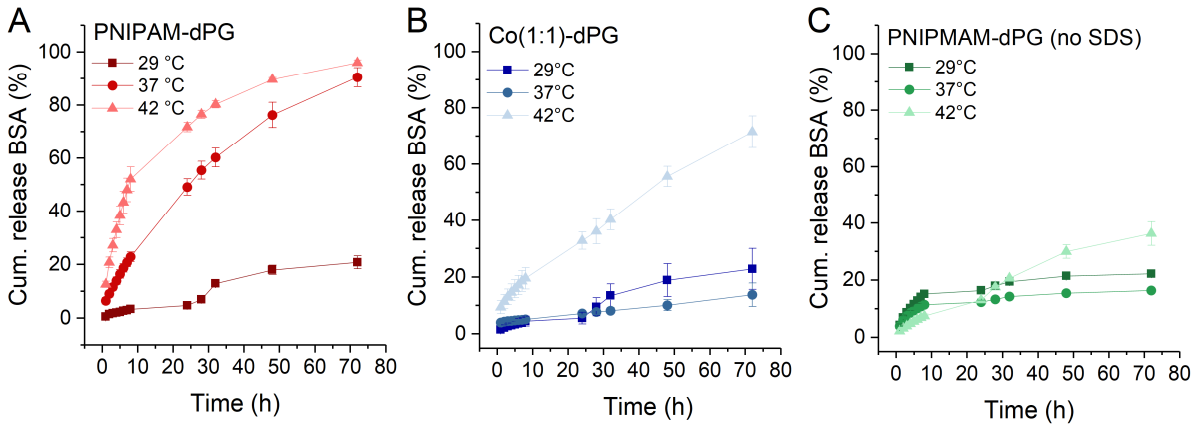

Figure 40. Release profiles of BSA-FITC from (A) PNIPAM-dPG, (B) Co(1:1)-dPG and (C) PNIPMAM-dPG (no SDS) at three different temperatures (29 °C, 37 °C, 42 °C).

Evaluation of cytocompatibility

Biocompatibility is an important issue for new materials for drug delivery applications. As a first indication thereof, we evaluated the compatibility of the bare thermo-responsive nanogels on primary human dermal fibroblasts and HeLa cells using MTT assay. In both cell lines the three nanogels did not affect the cell viability in concentrations up to 0.1 mg/mL (Fig. 9). Increasing polymer concentration to 1.0 mg/mL resulted in reduced cell viabilities of 60% on HeLa cells and 50% in fibroblasts after 48 h incubation.

In order to assess the suitability of our nanogels particularly designed for the delivery of therapeutic proteins, we have to consider the main factor that determines the concentration of nanogels that would be applied, the required dose of the chosen proteins to be delivered to achieve successful treatment. With over 130 proteins already approved for their clinical use, the variety of possible proteins and application modalities is quite high.[199] Doses for achieving efficient treatment are typically in the lower microgram range, but depend on the application, the selected protein and administration pathway. For the treatment of diseases that impair the skin barrier, the protein Etanercept for example is typically administered by subcutaneous injections.[200-202] Pharmacokinetics studies upon a 25 mg injection show an average maximum concentration of Etanercept in serum of 1.65 µg/mL.[203] Recent results from our group demonstrated efficient transdermal delivery of Etanercept from hydrophilic nanogels and anti-

inflammatory activity with 35 µg/cm² topically applied.[70] Another example for a therapeutic protein in dermal application is the protein Transglutaminase 1. It is reported to achieve successful mitigation on deficient skin barrier functions by supplementing the lacking proteins caused by genetic congenital ichthyosis disease.[72, 204] Here, protein concentrations of 5-10 µg/cm^{-2} delivered to the skin with the help of hydrophilic nanogels sufficiently improved the skins barrier function. Considering these examples and taking the high encapsulation efficiency of our nanogels of more than 80% (w/w) into account, the concentration of nanogels showing cytotoxic effects is about 100-1000 fold higher than what is expected to be required for potential applications.

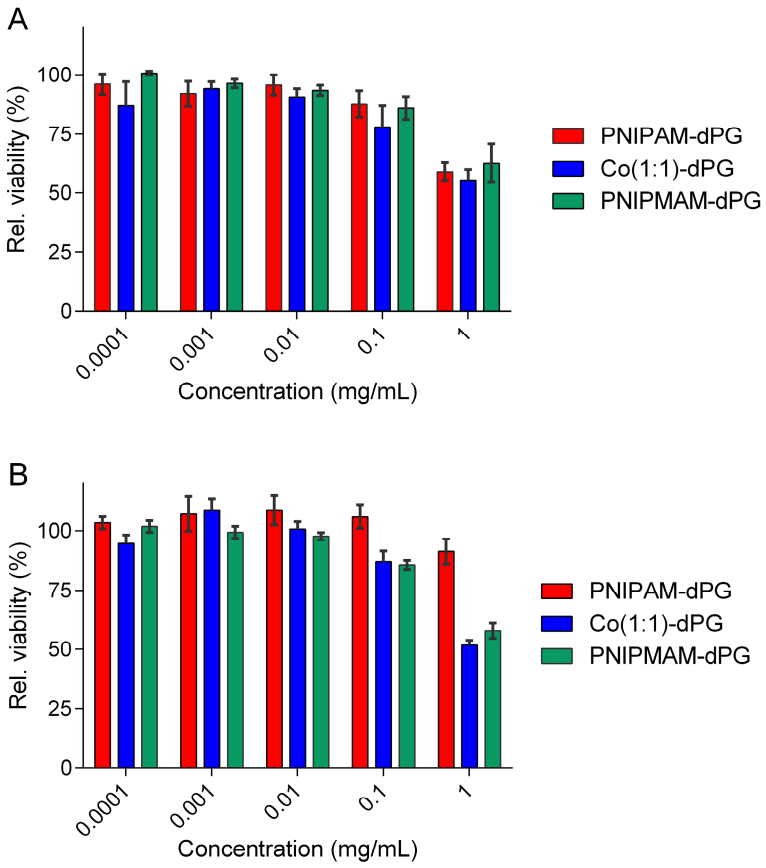

Figure 41. Effect of bare thermo-responsive nanogels on cell viability analysed by MTT assay on (A) HeLa cells and (B) fibroblast incubated with different nanogel concentrations of PNIPAM-dPG, Co(1:1)-dPG or PNIPMAM-dPG for 48 h.

Temperature dependent protein delivery to the skin

Recent results of our group demonstrate the good performance of nanogels with a VPTT of around 32-34 °C as dermal drug delivery system using the natural temperature gradient in human skin.[70, 72] In addition, the results indicate a correlation between collapse of nanogel and dermal penetration enhancement of encapsulated cargos. With the copolymeric nanogels, we now have the opportunity to evaluate temperature-dependent dermal delivery using an external trigger and compare the delivery profile to nanogels using the internal trigger caused by the temperature gradient in human skin (Figure 42). Therefore, we evaluated the temperature dependent release from NIPAM-dPG and Co(1:1)-dPG nanogels on *ex vivo* skin. In order to see the temperature dependency of the release and the effect of the external trigger, we used two different setups: first, a temperature ramp from 32-37 °C modelling the natural temperature gradient on skin and second, increasing the temperature for maximally 2 min up to 41 °C by irradiation with an IR lamp. For control, we also tested the delivery of BSA-FITC from PNIPMAM-dPG nanogels, which show a high VPTT and do not collapse under both conditions.

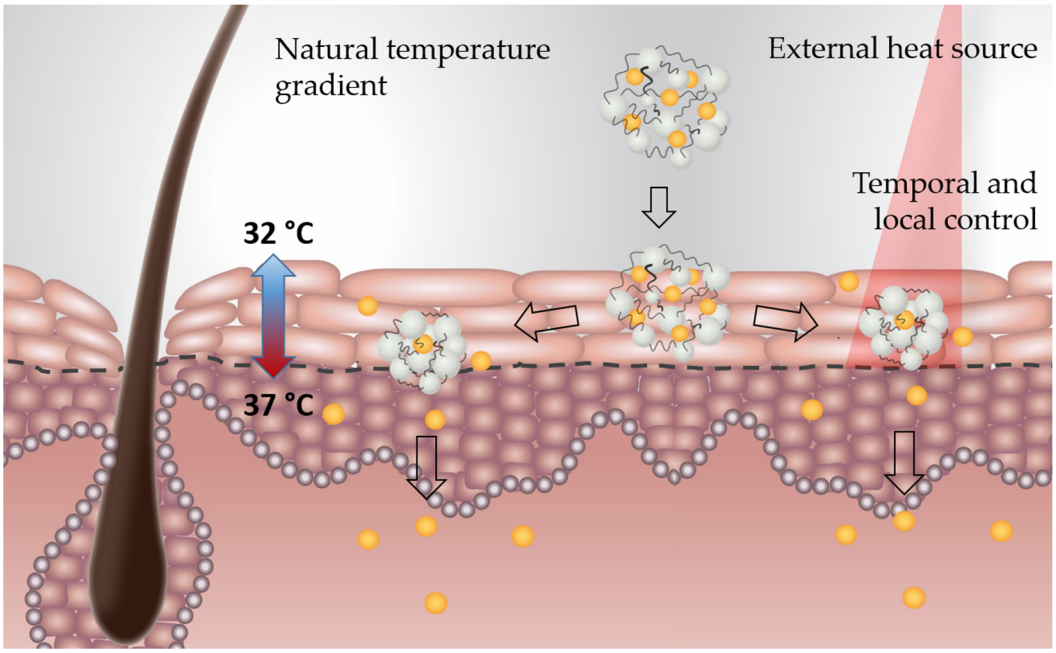

Figure 42. Schematic presentation of dermal delivery triggered by the thermal gradient in the skin or by an external heat source like an IR lamp allowing temporal and local control over the release.

In the temperature gradient setup, only NIPAM based nanogels show significant enhancement of the BSA penetration into viable skin layers (Figure 43A,B). Topical application of BSA solution as well as BSA encapsulated in Co(1:1)-dPG and PNIPMAM-dPG nanogels resulted in no significant BSA penetration into the viable epidermis (VE) (Figure 43B). These findings can be related to the fact that PNIPAM-dPG nanogels show a VPTT of 34 °C and are therefore the only nanogels in the tested setup, which VPTT is crossed. This shows that the release mechanism found in the *in vitro* studies could be successfully transferred to the intended application on skin.

In a second setup, we used a medical IR lamp to increase the temperature to maximally 41 °C for a short time period of 120 s. As anticipated, a significantly increased intradermal delivery of BSA to the VE was observed for both nanogels of which we cross the VPTT, PNIPAM-dPG and Co(1:1)-dPG, with PNIPAM-dPG showing superior penetration enhancement (Figure 43C,D). This is concordance with the *in vitro* release study, in which we observed a steeper release profile at 42 °C for PNIPAM-dPG than for the copolymeric nanogels (Figure 40). This could be attributed to the fact that, at temperature of 41 °C the copolymeric nanogels are still not completely collapsed (85% of total size change), whereas the transition of PNIPAM based nanogels is occurring already earlier. PNIPMAM-dPG nanogels at 41 °C are still in a swollen state and therefore do not release their loaded BSA into the VE resulting in MFI values non-significantly different to the free BSA control. Anyhow, application of the IR-irradiation results for all nanogels to an enhanced MFI in the SC in comparison to the free BSA solution as well as to the non-irradiated controls (Figure 43D). These results might indicate an increased penetration of the nanogels themselves upon IR irradiation similar to our findings for other thermo-responsive nanogels.[69]

Interestingly, the comparison between MFI values from the temperature gradient setup and the external triggered release reveals that for the PNIPAM-dPG nanogels the penetration to the VE is slightly higher using the IR lamp regardless of the relatively short exposure period. Furthermore, MFI of BSA delivered upon IR irradiation by copolymeric nanogels reaches similar values like achieved with PNIPAM-dPG in the temperature gradient setup. These results

highlight the effectiveness of an external trigger showing similar or even pronounced penetration enhancement despite only a single and relatively short exposure time. In addition, with the copolymeric nanogels an effective delivery system was generated that, besides the triggered delivery, allows for a local control of the release through a defined area of irradiation. Bringing the results from the two different setups together, we can conclude that the release of the BSA from the nanogels is following a temperature trigger, which is in concordance with *in vitro* data showing shrinkage/expulsion of water of the nanogels above their VPTT and temperature dependent release profiles. The comparison of external and internal trigger revealed that with the external trigger a similar or even increased penetration enhancement can be achieved. In addition, with a system showing a higher VPTT than 37 °C like the copolymeric nanogel, the delivery of encapsulated cargos can be local and temporal controlled through application of the external trigger.

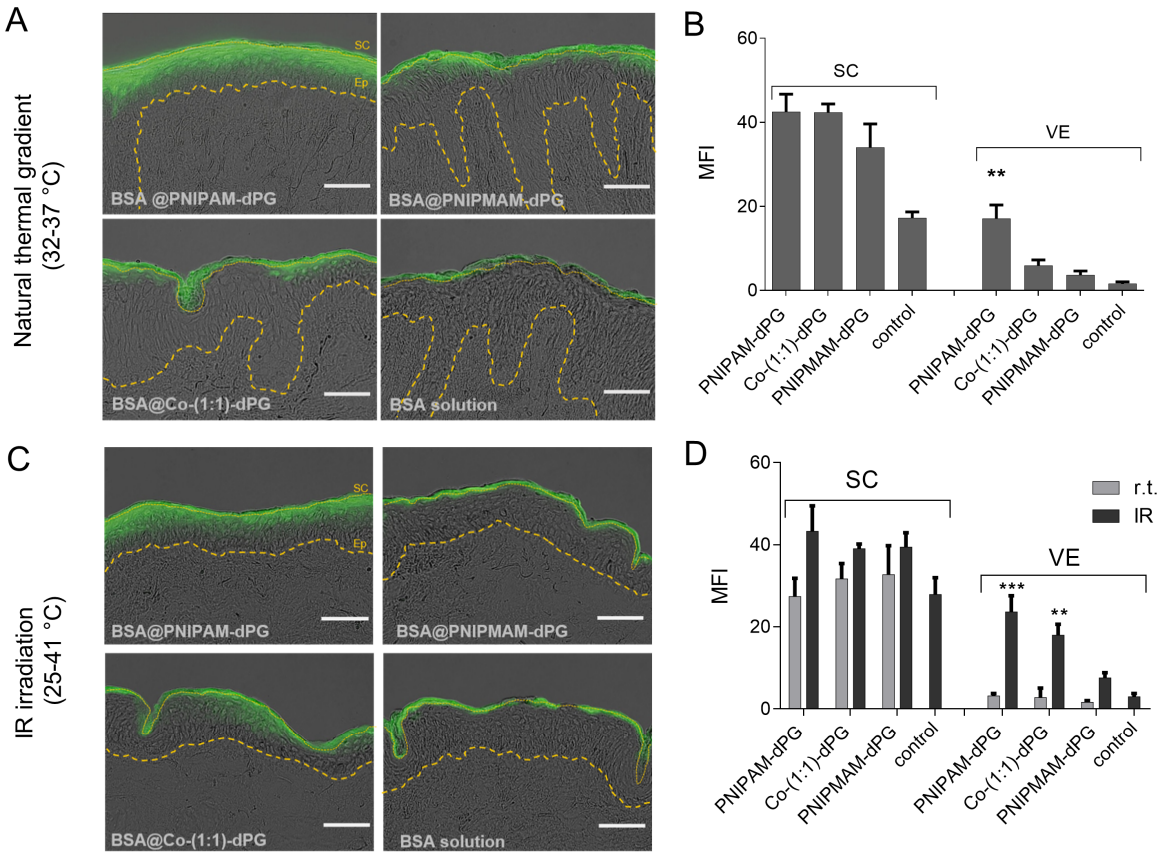

Figure 43. Intradermal delivery of BSA using the temperature gradient approach or IR-irradiation following topical application of PNIPAM-dPG, Co(1:1)-dPG and PNIPMAM-dPG. (A) Representative fluorescence images of skin explants following topical application of BSA-loaded nanogels for 6 h and by applying a temperature ramp from 32 to 37 °C. Images show fluorescence of the FITC-labeled BSA. Scale bars = 50 µm. (B) Analysis of mean fluorescence intensity (MFI) by area in stratum corneum (SC) and viable epidermis (VE) of skin punches from temperature gradient setup. N=3. Mean values were normalized to the untreated control (PBS, pH 7.4). (C) Representative fluorescence microscopy images of skin explants topically treated with BSA-loaded nanogels after 1 h incubation at r.t. in the dark, followed by IR-irradiation for 120 s and another hour incubation at r.t. Images show fluorescence intensity of the FITC-labeled BSA. Scale bars = 50 µm. (D) Mean fluorescence analysis of SC and VE of skin punches treated with FITC-BSA loaded nanogels following irradiation with an IR lamp for 120 s. N=3. Mean values were normalized to the untreated control (PBS, pH 7.4). Statistical significance for figures (B) and (D) was determined by one-way analysis of variance deploying Bonferroni's post-test to compare the differences between all values in VE and SC separately, with *P ≤ 0.05 as significant, **P ≤ 0.01 as very significant, and ***P ≤ 0.001 as highly significant. All depicted values are mean ± standard error of the mean (SEM).

4.2.2 REDOX-DEGRADABLE NANOGELS FOR SUBMUCOSAL DELIVERY OF ANTI-INFLAMMATORY DRUGS

Author Contributions: Encapsulation study of the ETN and analysis of its stability by CD were perfomed by me. Encapsulation of BUD was performed by me. The determination of the encapsulation efficiency of BUD by LC-MS/MS was performed by Fabian Schumacher. Activity of ETN by ELISA, cytotoxicity of the nanogels and cell uptake studies were performed by Rawan Charbaji.

For the evaluation as mucopenetrating drug carrier, we selected two anti-inflammatory drugs for the encapsulation in the degradable nanogels. The first, Budesonide (BUD), is a hydrophobic, small molecular weight drug (430 Da) while ETN is a large and hydrophilic protein (M_W 150 kDa). Due to the water insolubility of BUD, the encapsulation into PNIPAM-(S-S)-dPG was performed at elevated temperature, where the nanogels are in their collapsed and more hydrophobic state by dispersing BUD in the hot nanogel solution and following cooling to r.t. After separation of the non-encapsulated BUD, encapsulation efficiency was determined using LC-MS/MS. We could demonstrate that by encapsulation into the nanogels, we were able to increase the solubility of BUD by a factor of 5.2 from 28 μg/mL in water[205, 206] to a concentration of 147 μg/mL, corresponding a loading of 2.6 wt%. Similar values are obtained for the non-degradable PNIPMAM-dPG nanogels (Table 11).

Table 11. Drug loading of BUD and ETN in PNIPMAM-(S-S)-dPG and PNIPAM-dPG nanogels.

	BUD		ETN	
Nanogel	Loading Efficiency (%)	Loading (wt%)	Loading Efficiency (%)	Loading (wt%)
PNIPMAM-(S-S)-dPG	5.3 ± 0.2	2.6 ± 0.1	79.0 ± 3.8	7.9 ± 0.4
PNIPMAM-dPG	4.9 ± 0.2	2.5 ± 0.1	88.6 ± 2.5	8.9 ± 0.3

The encapsulation of ETN was achieved by swelling dry nanogels in a solution of the protein. Encapsulation efficiency was determined after purification by Bradford assay. Similar to the

encapsulation efficiencies found in thermo-responsive (non-degradable) nanogels for BSA (Chapter 4.2.1), ETN was found to be encapsulated with high efficiency of 79% (PNIPMAM-(S-S)-dPG) and 88% (PNIPMAM-dPG), respectively (Table 11). For both nanogels, the stability of the encapsulated and released ETN was assayed using CD measurements. No major changes in the CD spectra between free, encapsulated and released ETN were observed. The secondary structure of ETN seems to be unaffected by the presence of nanogels (Figure 44).

As the therapeutic activity of ETN relies on its ability to bind TNF-α und thus inhibit inflammatory processes, we evaluated its ability to bind TNF-α using ELISA (Figure 45). ETN in both nanogels shows high binding ability to TNF-α of over 80%. In comparison to the benchmark control, which was stored under same conditions than the loaded nanogels, they show slightly higher binding abilities indicating that the nanogels are able to protect the encapsulated ETN from degradation.

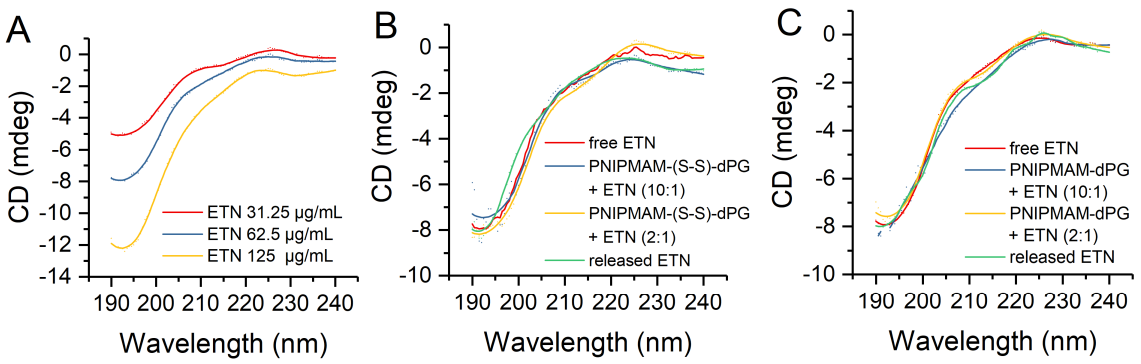

Figure 44. CD spectra of ETN (A) in solution (PB, pH 7.4) at different concentrations, (B) upon encapsulation and released from PNIPMAM-(S-S)-dPG and (C) PNIPMAM-dPG, respectively.

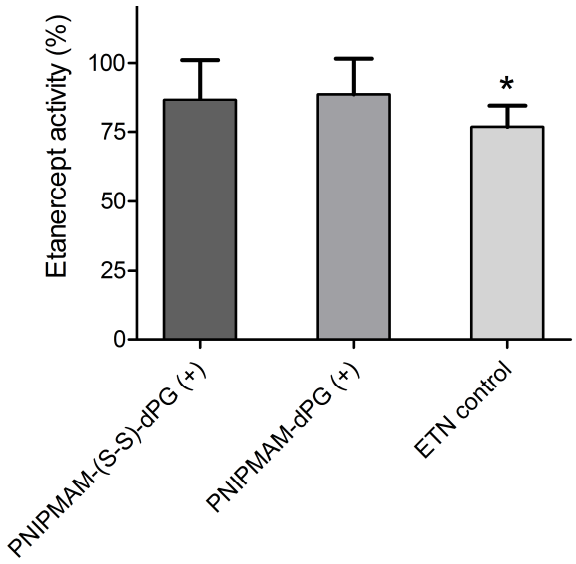

Figure 45. ETN activity quantified by ELISA determining the binding ability of ETN to TNF-α two weeks after loading into the nanogels and storage at 4 °C. ETN control stored at similar conditions. All data were normalized to ETN binding ability found for freshly thawed ETN solution. All values are expressed as mean ± SEM obtained from three independent experiments. *$p < 0.05$ (one-sample t test to hypothetical value of 100).

Cell viability and uptake

As we could successfully demonstrate the nanogels ability to efficiently penetrate the mucus and reach underlying cell layers *ex vivo*, we investigated potential cytotoxic effects of the nanogels on two submucosal epithelial cell lines: human ectocervix epithelial cell line Ect1/E6E7 and human vaginal epithelial VK2/E6E7. Additionally, we screened cytotoxic effects on human macrophages as cells of the immune system. The cell viability after treatment with PNIPMAM-(S-S)-dPG and PNIPMAM-dPG nanogels in differenent concentrations was determined using MTT assay. For both epithelial cell lines evaluated, no cytotoxic effects were observed after 24 h and 48 h incubation even for high concentrations (5 mg/mL) of the nanogels (Figure 46A,B). Compatibility of the nanogels with human macrophages was found to be very good with no major changes in the macrophage viability (Figure 46C). In addition, cellular uptake of the nanogels in the macrophages was assayed using fluorescence analysis post incubation with RhodB labeled nanogels at 4 °C and 37 °C (Figure 46D). At reduced temperature (4 °C) only energy independent diffusion processes may help the passage of materials into the cells. In

contrast, at 37 °C active internalization processes like endocytosis are functional. Hence, the comparison of both allows conclusions about the uptake mechanism. As can be seen in Figure 46D, increased fluorescence is found for both nanogels upon incubation at 37°C while at 4 °C no changes in the fluorescence in comparison to the PBS treated control are observed. This implies a fast and active uptake mechanism for both nanogels, which is even more pronounced for the disulfide containing nanogel.

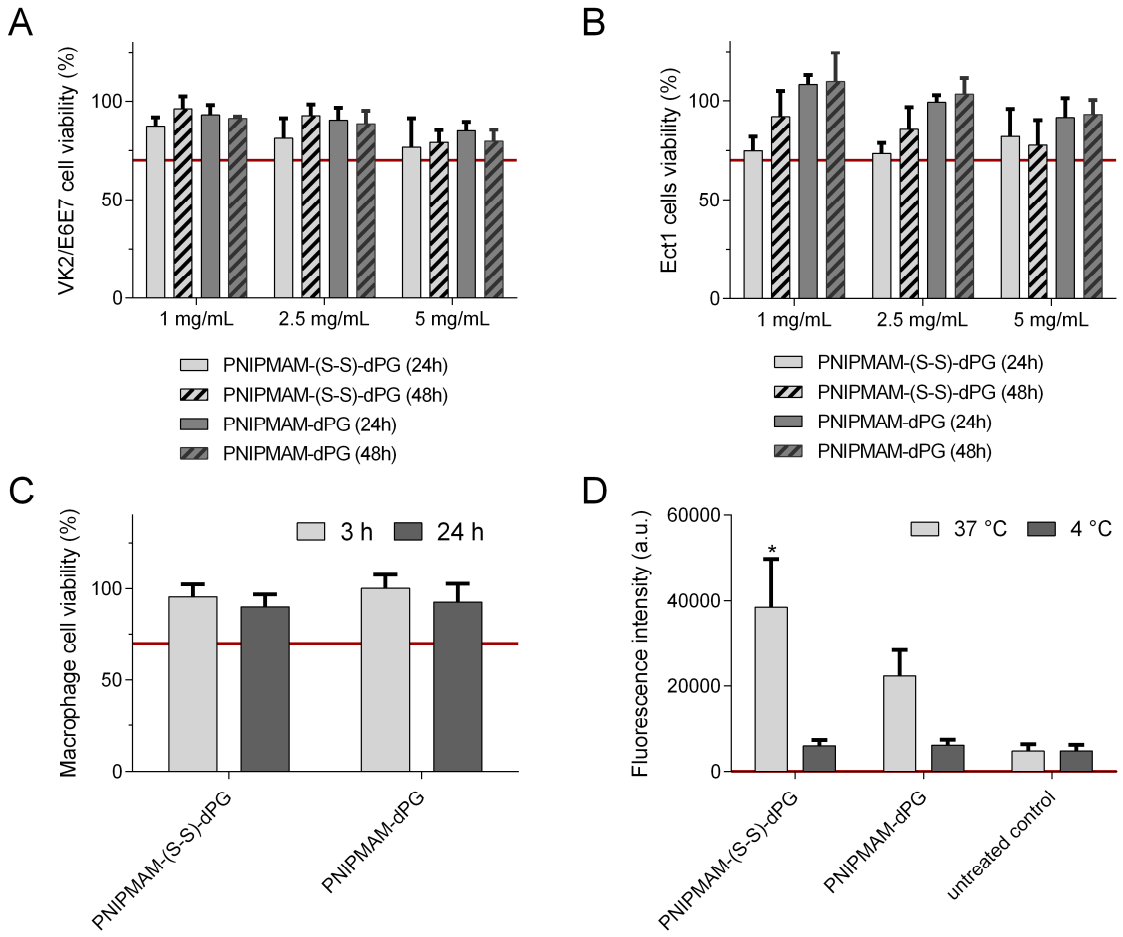

Figure 46. Viability assay on (A) human ectocervix epithelial cell line (Ect1/E6E7) and (B) human vaginal epithelial cell line (VK2/E6E7) after treatment with degradable PNIPMAM-(S-S)-dPG and non-degradable PNIPMAM-dPG nanogels in different concentrations (1, 2.5, and 5 mg/mL) over 24 h and 48 h. (C) Viability of macrophages after incubation with RhodB labeled nanogels (1 mg/mL) for 3 h and 24 h and (D) internalization of the nanogels at 37 °C and 4 °C in macrophages determined by fluorescence analysis. n = 3, mean ± SEM, *p ≤ 0.05.

4.2.3 THERMO-RESPONSIVE, SEMI-INTERPENETRATED NANOGELS AS COMBINATIONAL PHOTOTHERMAL THERAPY AND CHEMOTHERAPEUTIC DELIVERY AGENT

This chapter is based on the manuscript "NIR- and thermo-responsive semi-interpenetrated polypyrrole nanogels for imaging guided combinational photothermal and chemotherapy" (Appendix 7.3), which has been submitted to the Journal of Controlled Release. Author Contributions: Encapsulation and Release studies in vitro were performed by me. Cytotoxicity was evaluated by Stefanie Wedepohl. Photoacoustic imaging was done by Jens Buchmann, we discussed the results and I wrote the manuscript. Photothermal response and biodistribution method development was performed by me. All animal studies were performed by employees of the company EPO GmbH. Analysis of the resulting data was done by me.

Encapsulation and Release of MTX

Having shown that our nanogels act as photothermal transducing agents and that the produced heat can be used to trigger the nanogels temperature response (Chapter 4.1.3), we evaluated the performance of the nanogels as a drug delivery device. Therefore, we analysed the encapsulation and release properties using the anti-cancer drug methotrexate (MTX). The thermo-responsive nanogels have been proven to act as an excellent thermally triggered drug delivery device for proteins (Chapter 4.1.1).[170] For the small molecule drug MTX however, we found low encapsulation efficiencies and fast, temperature independent release profiles for all three nanogels when they are not semi-interpenetrated with a second polymer (Figure 47A,B). This is likely caused by a lack of beneficial interactions between the nanogels and MTX in combination with large mesh-sizes of the polymeric network, so that the small drug cannot be retained within the nanogels structure and its unhindered diffusion occurs. In contrast, we found about three fold higher encapsulation efficiencies for MTX in the semi-interpenetrated PPY nanogels up to 20wt% (Figure 47A). There are two factors which may cause these findings: first, upon interpenetration the nanogels' network is filled with PPY chains increasing the network density in each nanogel and thereby reducing their mesh size and restraining the free diffusion of the drug. Second, PPY is an electron-rich conjugated π-system which can interact

with MTX molecules through π-π- and hydrophobic interactions and, with that, offer a driving force to MTX molecules to stay associated with the nanogels.[161]

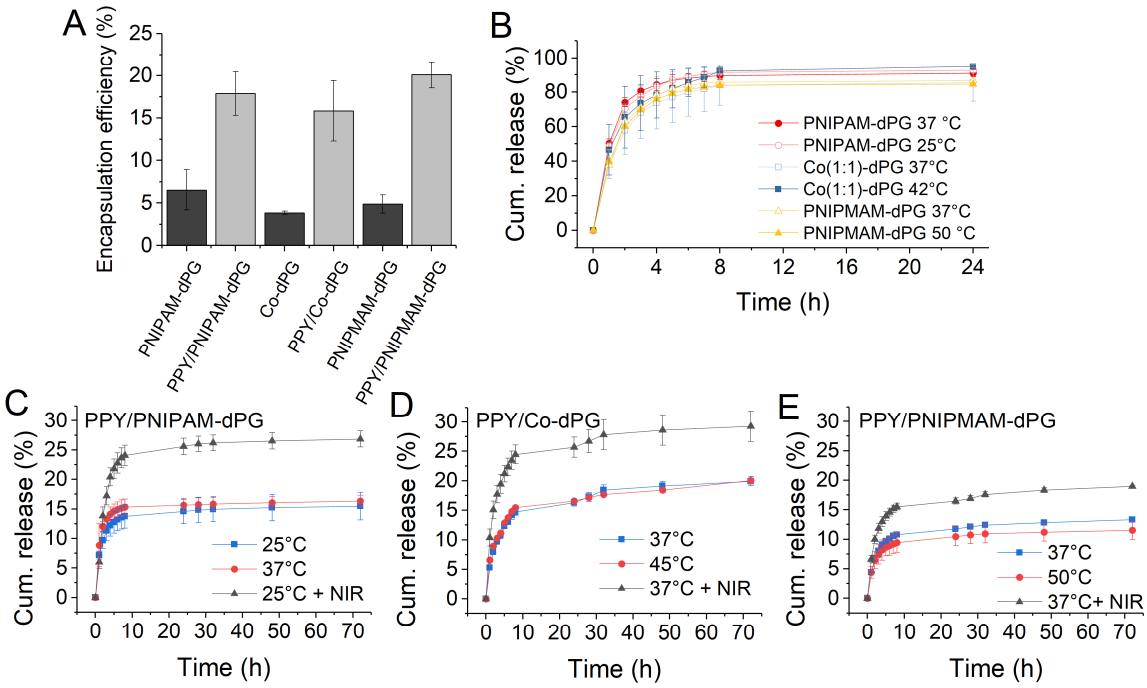

Figure 47. (A) Encapsulation efficiency of MTX in non-interpenetrated and corresponding PPY nanogels, (B) release profiles of MTX above and below VPTT of the non-interpenetrated thermo-responsive nanogels, release profiles of semi-interpenetrated PPY nanogels: (C) PPY/PNIPAM, (D) PPY/Co, and (E) PPY/PNIPMAM each below and above the corresponding VPTT and upon NIR-irradiation with a NIR laser (785 nm, 500 mW) for 5 min every 2 h within the first 8 h.

To test whether after semi-interpenetration the temperature-response of the nanogels has an impact on the release of the encapsulated MTX, release profiles of MTX from all PPY nanogels were assayed below and above their individual VPTT (Figure 47C-E). Similar to the non-interpenetrated nanogels, we found no major influence of the temperature on the release profiles but a cumulative release of a maximum of 10 – 15% only, supporting the assumption of a strong interaction between PPY and MTX which keeps the drug preferably associated with the nanogels network. Remarkably, with the application of a NIR trigger, the release rate could be significantly promoted for all three PPY nanogels. We think that the main reason for this is the

strong and local heating by the PPY chains able to loosen the interactions with the drug and in combination with the induced over-collapse of the nanogels network promoting its release.

Evaluation of cytotoxicity and therapeutic activity in vitro

Biocompatibility is a crucial factor for the application of new drug delivery materials. To obtain a first basis for an assessment, potential cytotoxic effects of all three semi-interpenetrated PPY nanogels was studied by MTT assay on A549 lung carcinoma cell line *in vitro*. For all three tested nanogels we found a very high tolerance of the cells for unloaded nanogels without reduction of cell viability up to concentrations of 1 mg/mL (Figure 48A). The therapeutic activity of the nanogels was investigated in terms of their photothermal effect, delivery of the chemotherapeutic agent MTX and combinational effects of both. For drug loaded nanogels (10wt% MTX), a reduction in cell viability is visible from nanogel concentrations of 15 µg/mL onwards indicating that the loaded drug was successfully delivered from the nanogels in its active form (Figure 48B).

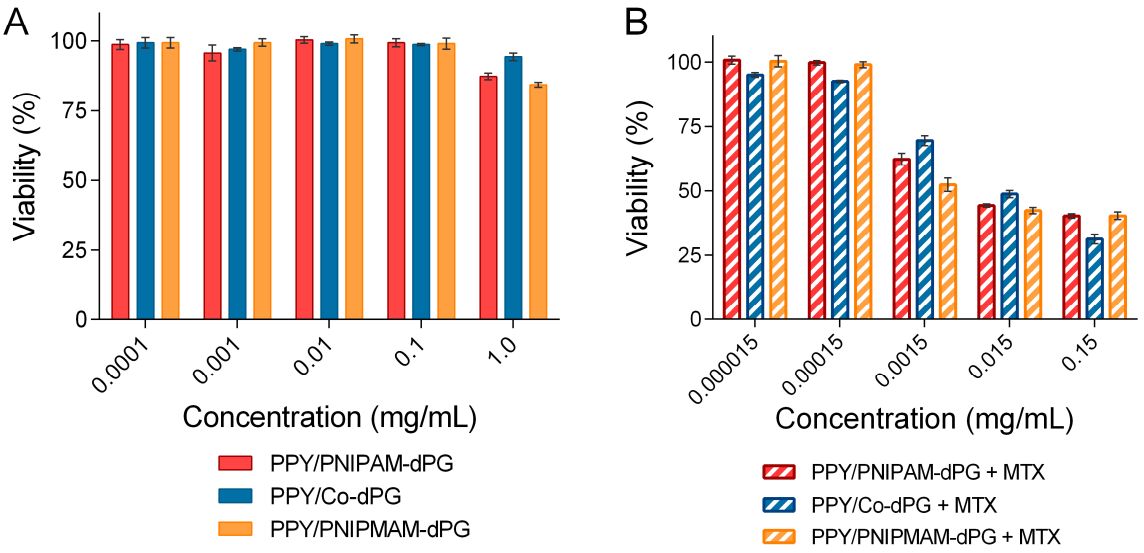

Figure 48. Cell viability of A549 lung carcinoma cell line determined by MTT assay incubated for 48 h with (A) PPY nanogels in different concentrations and (B) MTX loaded nanogels (10 wt%) in different concentrations. N=3. Mean ± SEM.

For evaluation of the photothermal activity and combination therapy with MTX, cells were incubated with the nanogels followed by irradiation for 7 min with a NIR laser. In order to gain comparability between the three nanogels systems, the applied nanogel concentrations were adjusted in order to have same absorbance properties at the wavelength of irradiation (785 nm). Indeed, for all three nanogels, we see a similar photo-thermally induced reduction in cell viability to about 75 – 80% after irradiation and no reduction in the non-irradiated controls (Figure 49). For the MTX loaded nanogels, a combinational effect between chemotherapeutic activity of loaded MTX and photothermal heating by the nanogels is visible, appearing as an additional reduction of the cell viability upon irradiation in comparison to the action of MTX alone as well as to the irradiated but non loaded nanogels. The NIR exposure of cells treated with only MTX did not cause this additional viability reduction proving that the increase in cell death is due to a combinational effect of MTX and the photothermal heating.

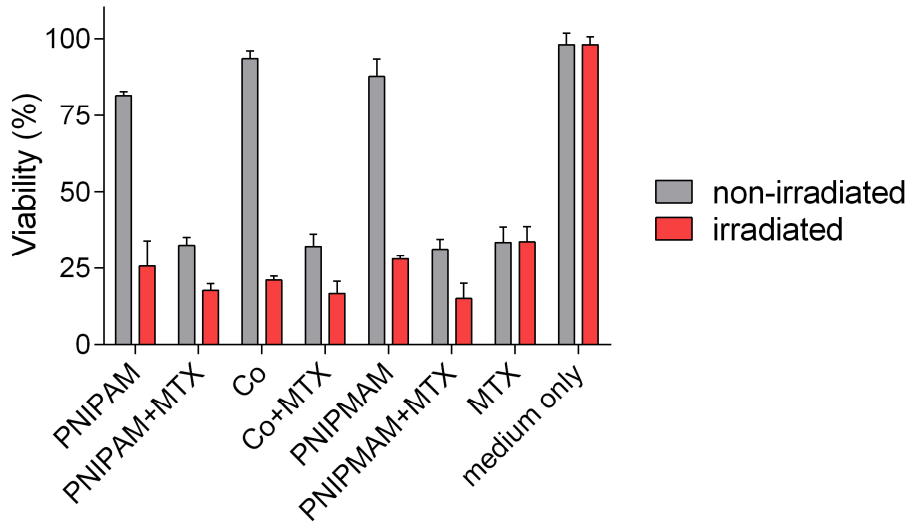

Figure 49. Photothermal and combinational therapy in vitro. Cell viability of A549 lung carcinoma cell line determined by MTT assay incubated for 48h with MTX loaded (10 wt%) and unloaded PPY nanogels with and without exposure to NIR laser (785 nm, 500 mW) for 7 min. All values are expressed as mean ± SEM.

Evaluation of toxicity in vivo

Our results of *in vitro* efficiency suggest that all three nanogels are feasible candidates for application in a combinational anti-cancer therapy. As for all three PPY nanogels the thermo-responsiveness did not have an influence on the drug delivery profile, the main difference of the nanogels in an *in vivo* setting would be their hydration state. At systemic body temperature of 37 °C, semi-interpenetrated PPY/PNIPAM-dPG nanogels would be in a collapsed state whereas PPY/Co-dPG and PPY/PNIPMAM-dPG are still hydrated. Recently, we could demonstrate that the hydration state of thermo-responsive nanogels plays an important role in the formation of a protein corona which is known to be a key parameter for nanoparticles biodistribution profiles.[104]

Therefore, we picked two out of the three nanogels of which one is in its collapsed state immediately upon administration (PPY/PNIPAM-dPG) and the other is still in a hydrated state, for evaluation in the mouse model. As hydrated nanogel we chose PPY/Co-dPG due to the higher MTX release rate under NIR exposure and slightly higher efficiency in the reduction of A549 cell viability by photothermal heating. First, tolerability of the nanogels in healthy mice was evaluated by following the body weight development after i.v. administration of first single injections with increasing doses (10 – 100 mg/kg) and then, five consecutive doses of the highest tolerated dose (100 mg/kg) over five days. For both tested nanogels, the body weight in the following two weeks was stable indicating no major toxicity effects (Figure 50). Afterwards, selected organs were collected for histopathological examination. Macroscopically, particle accumulation mainly in the liver and spleen was visible as a black discoloration in these organs (Figure 51). Apart from pigment storage seen in the spleen and liver, the histopathology revealed no specific inflammatory infiltrations or tissue damage (Figure 52).

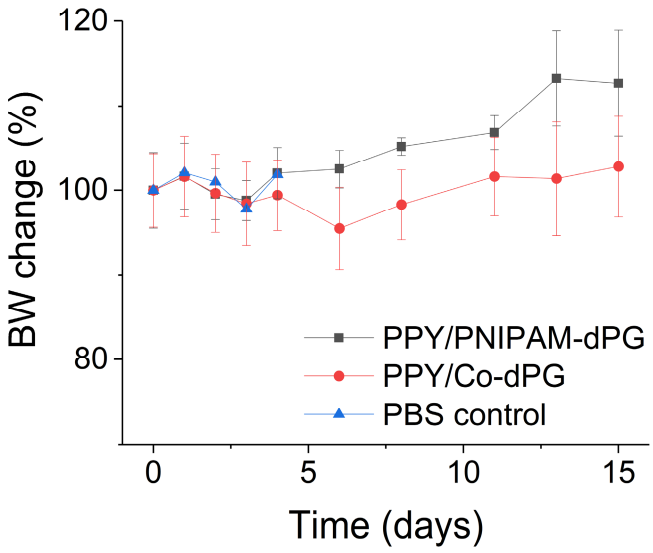

Figure 50. Body weight change of mice treated daily for 5 consecutive days with 100 mg/kg PPY nanogels (i.v.).

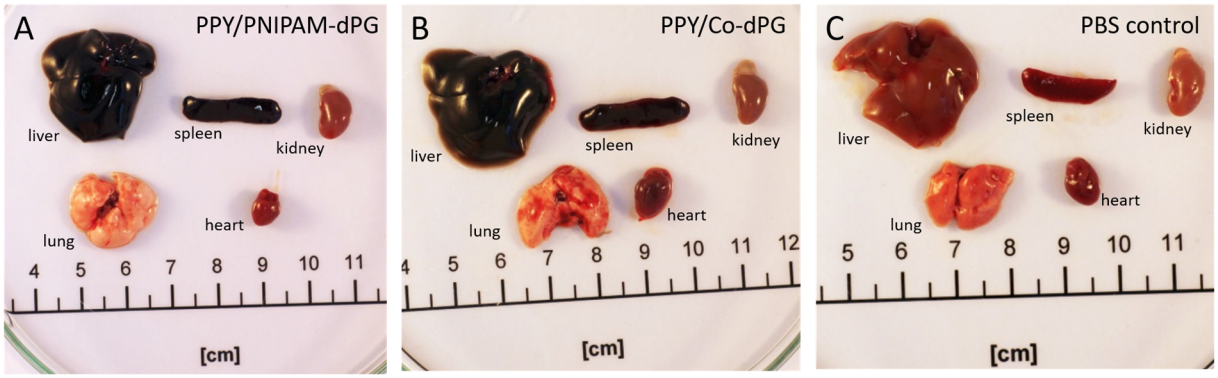

Figure 51. Images of representative organs from mice treated intravenously with (A) PPY/PNIPAM-dPG and (B) PPY/Co-dPG for 5 consecutive days (100mg/kg) and (C) untreated control (PBS, i.v.).

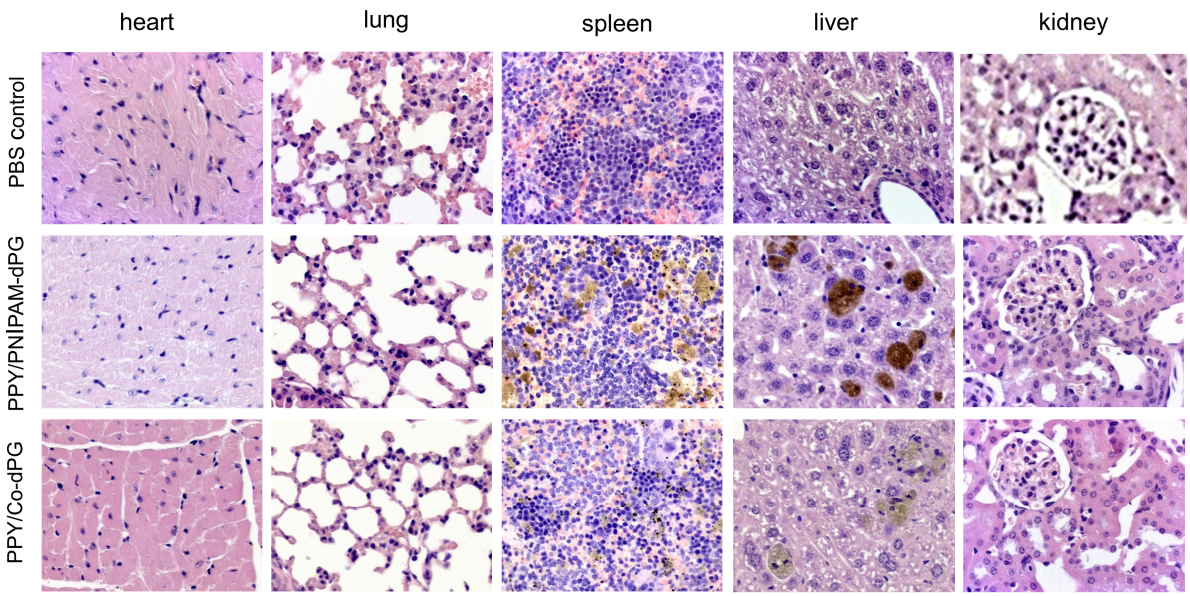

Figure 52. H&E stained sections of selected organs of mice treated with PPY/PNIPMAM-dPG and PPY/Co-dPG nanogels in comparison to PBS control.

Biodistribution

The biodistribution profile of therapeutic actives is an important parameter to determine suitable dosing and study the fate of the carrier after systemic application. In the case of triggered drug delivery systems, we also need to determine the best time point for the application of the trigger, which is ideally characterized by an optimum accumulation of the carrier at the target site. Usually, biodistribution profiles are determined using radioactive or fluorescent labels for the particles of interest. In the case of PPY nanogels, fluorescent labeling is not feasible due to the strong absorbance of PPY resulting in strong quenching of the fluorescence signals. Radiolabels complicate the way of handling and the synthesis of the particles due to safety regulations working with radioactive substances. Both approaches anyhow require chemical modifications of the particles, which could influence the particles behaviour after administration. However, due to the photothermal transducing properties of the nanogels, they are ideal candidates to be used as PA signal enhancers usable as PA theranostic devices.

Thus, we assessed the nanogels accumulation by *ex vivo* imaging of organs excised from mice treated with the nanogels (5d x 100 mg/kg i.v.). Mean intensity projections (MIPs) over the x-y-plane of 3D PA images of the acquired organs at 800 nm are shown in Figure 53A. The average image intensities (and standard deviations thereof) are shown in Figure 53B. The strongest increase in PA image intensity compared to the control group (note the different scale bars in Figure 53A) is observed for spleen and liver, which is in good agreement with the findings from macroscopic images that both nanogel systems mainly accumulate here (Figure 51). Image intensity increases, albeit less pronounced, can also be seen in the kidney. By contrast, the PA image intensity measured in the heart and the lungs showed only minor changes indicating low to negligible particle accumulation.

Since the increase PA image intensity is based on the photothermal transducing ability of the nanogels, the *ex vivo* PA measurements were confirmed by measurements of the nanogel photothermal response. The organ samples imaged using PA tomography were illuminated with the output of a NIR lamp and the resultant temperature increase was measured with an IR-camera. We found that the pattern of measured temperature increases agreed with the PA image intensity values, i.e. the highest values were found for both nanogels in the liver, closely followed by the spleen, and only slightly increased temperatures for the kidney and the lung (Figure 53C).

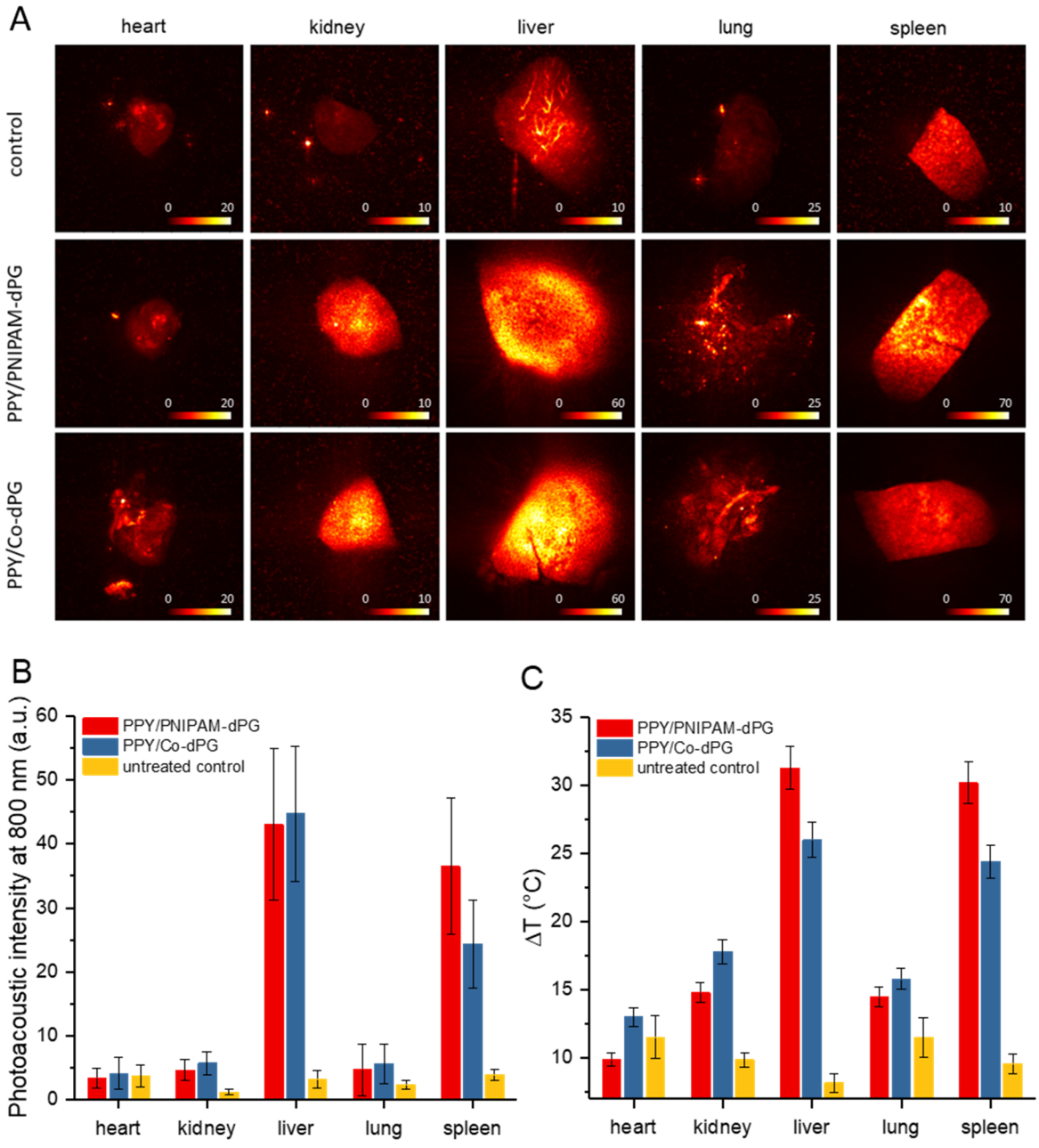

Figure 53. (A) x-y MIPs of PA images of excised organs at 800 nm. Note that scale bars for intensity within organ groups are kept the same except for liver and spleen where the scale bar of the control organs were set much lower for better contrast. (B) Mean PA image intensity of excised, formalin fixed organs of a female nude mouse (NMRI, nu/nu) treated over five consecutive days with 100 mg/kg of PPY nanogels. (C) Photothermal response (max. ΔT after 5 min) of the same samples after irradiation with the output of a NIR lamp.

These results motivated us to develop a setup for quantitative evaluation of the biodistribution profiles of our nanogels based on their photothermal response. In order to do so, results we needed to fulfil two requirements: first, a maximized uniform distribution of particles in the investigated tissue to be able to compare reached temperature differences and second, a setup allowing to produce a calibration curve. We therefore decided to homogenize the organs and dilute them – either with PBS or with a nanogels containing solution for calibration purposes. With the established calibrations curves, weight prior and the volume after homogenisation, and the applied dilution factor, we were able to calculate quantitative biodistribution profiles with accuracy down to 50 µg/mL using a NIR lamp and even lower to values of 12.5 µg/mL using a NIR laser (Figure 54). The resulting profiles for both nanogels directly after the last treatment or at the end of the study are shown in Figure 55. These profiles were meant for method validation and interpretation of the results can only serve as first indication due to the low number of mice evaluated (n=1 for d6 and n=2 for d21).

In accordance with the photoacoustic measurement, main particle accumulation is detected in liver and spleen. Interestingly, emphasis of the organ weight, reflecting particle density in the organ sample, slightly higher values are observed in the spleen than in the liver. In addition, it seems that the particles segregate from the liver over time, showing much lower values at d21 than directly after treatment.

In general, for polymeric nanocarriers such biodistribution pattern, exhibiting the majority of particles accumulated in the liver and the spleen, is quite common. This is due to the particles clearance by the reticuloendothelial system (RES). Induced by the binding of opsonins to the nanoparticles surface, phagocytes such as macrophages can recognise the nanoparticles, internalize them and start to secret enzymes and other oxidative-reactive chemical factors to break down the particles. However, most polymeric nanoparticles cannot be degraded significantly by this process. . This results in particular for high molecular weight particles in a storage in the organs of the RES; the liver and the spleen.[25, 207]

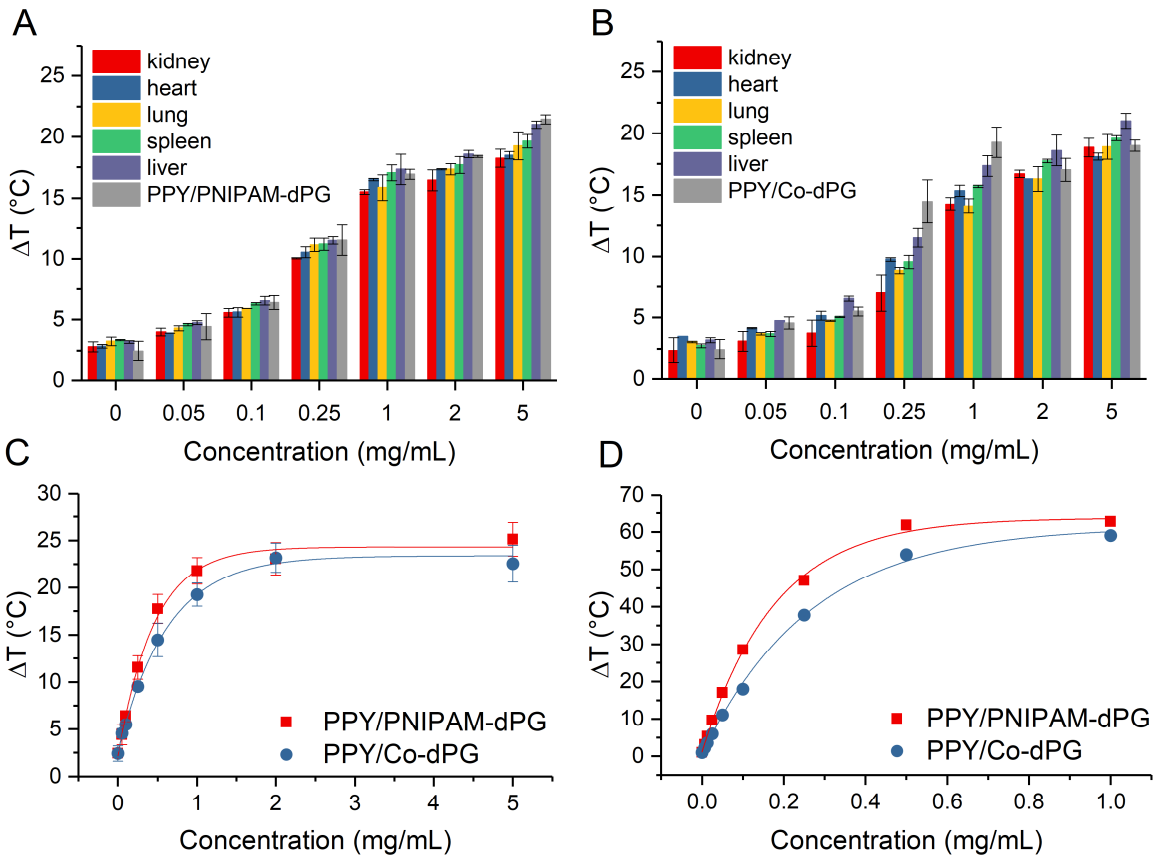

Figure 54. Photothermal response of semi-interpenetrated PPY nanogels in organ samples. (A) PPY/PNIPAM-dPG and (B) PPY/Co-dPG, pure and mixed with homogenized organ samples from untreated mice in different concentrations and fitted calibration curves for both nanogels for (C) NIR lamp and (D) NIR laser. The comparison of calibration curves of pure nanogel solutions and organs mixed with nanogels did not show major differences, allowing the use pure nanogels as a calibration standard.

In order to achieve that polymeric carriers reach their target and deliver their cargos prior to the recognition by the RES, several factors are commonly addressed. Foremost, the reduction of the opsonisation of the particles is tackled through impairment of stealth properties to the surface of the nanoparticles preventing the absorption of proteins. Here, most commonly a surface functionalization with PEG is performed. The reduction of protein binding to PEGylated particles delays the particle recognition by the RES and increases their blood circulation time. This allows sufficient accumulation of particles at the target site, e.g. using the EPR effect.[159, 208] Beside the surface stealth properties, additionally the size of the nanoparticles and their

hydrophilic-hydrophobic character are known to influence the opsonisation process.[25, 209] Independent of stealth properties, it was found that particles with sizes below 200 nm have greater circulations times and are more slowly cleared from the body. In addition, the opsonisation of hydrophobic particles, as compared to hydrophilic particles, has been shown to occur more quickly.[25, 207, 210]

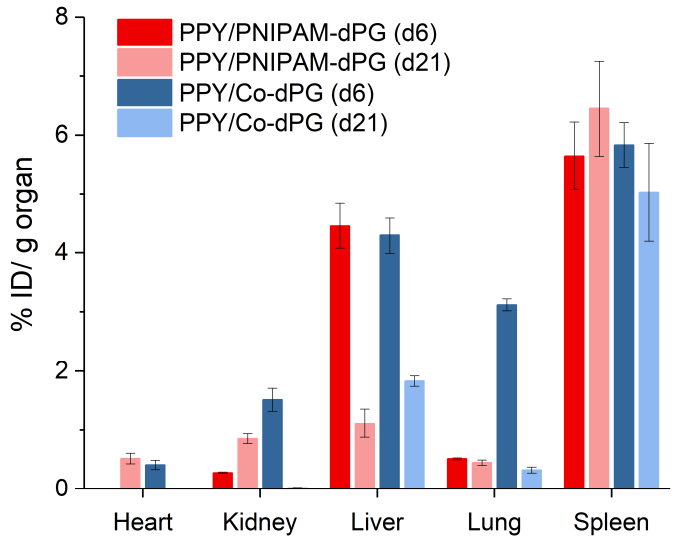

Figure 55. Biodistribution profiles of PPY nanogels in healthy female nude (NMRI, nu/nu) mice immediately after last dose (d6, n=1) and 15 days after treatment (d21, n=2) determined by photothermal response of selected organs.

With the new method in hand, we thus aimed to investigate the ability of our nanogels to accumulate at the tumor side and prolong the circulation in the blood. The effect of the hydration state on the biodistribution additionally can be investigated with the two nanogels PPY/PNIPAM-dPG and PPY/Co-dPG being in different hydration state upon administration.

Therefore, biodistribution profiles after single i.v. dosage (100 mg/kg) in tumor bearing mice (A549/NMRI: nu/nu (f)) were employed 2 h, 12 h, and 48 h after the injection. As can be seen from Figure 56, for both nanogels the majority of the particles can be found in the liver whereas particle density was found to be similar with 50-80 %ID/g in the liver and spleen (Figure 57A).

Both nanogels show an increase in particle density in the liver from 2 h to 12 h and then start to segregate slowly, whereas highest particle density in the spleen is already reached after 2 h with a continuous decrease afterwards. Interestingly, in the other organs (heart, kidney, lung and, tumor) major differences between the two nanogel systems are visible. PPY/Co-dPG nanogels are found in heart, lung and kidney in relatively high concentrations after 2 h, with decreasing concentrations in all organs over time, indicating that the particles are still circulating in the bloodstream in the first hours after injection. In contrast, PPY/PNIPAM-dPG nanogels show only notable presence in the lung 2 h post injection and are already almost completely cleared therefrom after 12 h.

To our surprise, we could detect only the PPY/Co-dPG nanogels, not however the PPY/PNIPAM-dPG nanogels in the tumor site with highest accumulation 48 h after treatment (Figure 57B). We assume this could be due to the different hydration state of the nanogels. PPY/PNIPAM-dPG nanogels are in their collapsed state at systemic temperatures of 37 °C immediately after injection whereas PYY/Co-dPG nanogels are still hydrated. The collapse of the nanogels induce three major changes which may be responsible for the different behaviour upon administration: first, the hydrophilic-hydrophobic balance is shifted to a more hydrophobic state with a pronounced polymer-polymer interaction and less hydration; second, upon the collapse of the thermo-responsive network a higher ratio of semi-interpenetrating polymer PPY will be located outside or on the nanogels surface and reduce the presence of dPG acting as stabilizing agent; and third the size of the nanogels drops significantly down from 200 nm to 120 nm. All three factors are known to be important as the nanogels surface properties prevent opsonisation in the blood and are important to reduce recognition by the RES leading to prolonged blood circulation time which is a major factor for passive targeting of tumor tissue.[20, 24, 25, 211, 212] PPY/Co-dPG nanogels reach an accumulation of 5% ID/g which corresponds to a particle concentration of 70 μg/cm^3 tumor volume equivalent to a temperature increase up to 41 – 42 °C under NIR irradiation with the NIR laser. This temperature may be feasible for hyperthermia applications where increased temperature exposure is kept for several hours,[126] but are still too low for tumor ablation with short application of the external NIR irradiation.

Alltogether, we can conclude that PPY/PNIPAM-dPG nanogels are only feasible candidates for i.t. applications and PPY/Co nanogels need higher dosed or several times administered in order to increase the concentration at the tumor site for photothermal ablation.

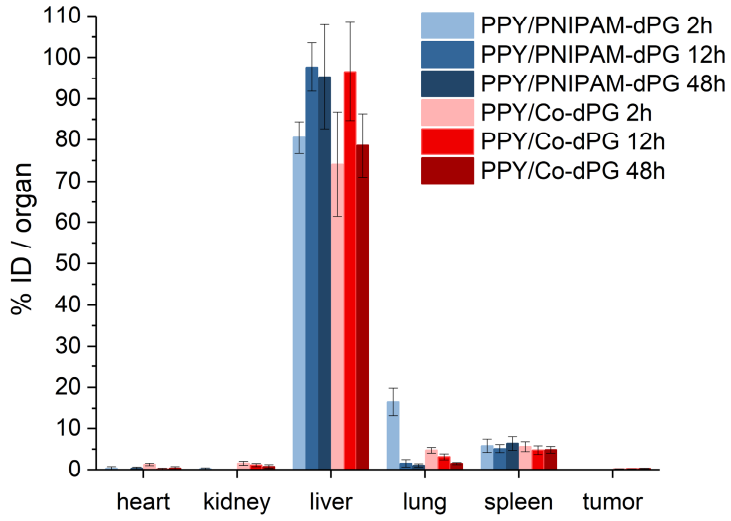

Figure 56. Biodistribution profile of PPY/PNIPAM-dPG and PPY/Co-dPG nanogels in tumor bearing mice (A549/female nu/nu) shown as percent of injected dose (%ID) per organ.

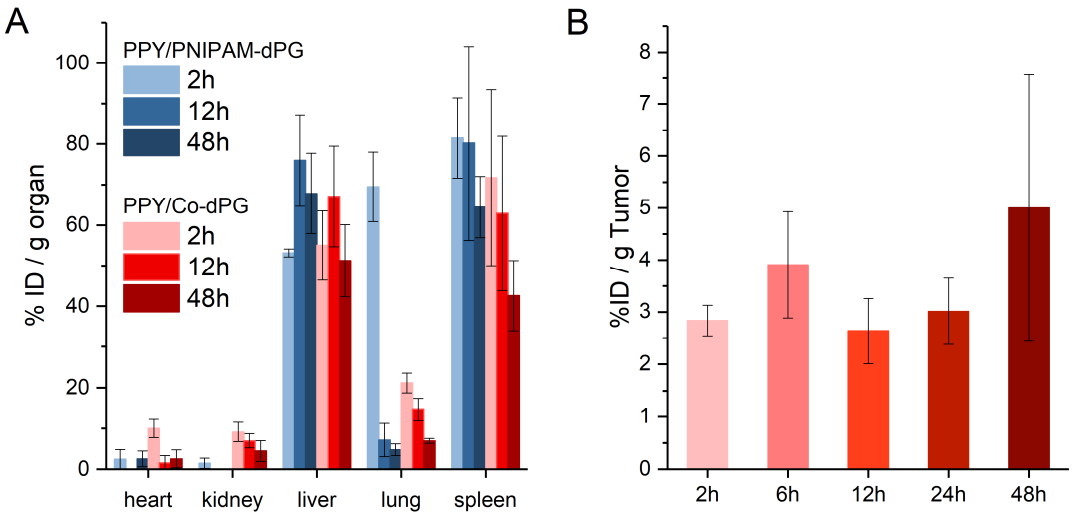

Figure 57. (A) Biodistribution profile of PPY/PNIPAM-dPG and PPY/Co-dPG nanogels shown as percent of injected dose (%ID) per g organ after 2 h, 12 h, 48 h post injection and (B) accumulation of PPY/Co-dPG nanogels in the tumor site at 2 h, 6 h, 12 h, 24 h, and 48 h after i.v. injection.

Therapeutic activity in vivo

We evaluated the antitumoral activity of the PPY nanogels in several manners. First, the nanogels were administered i.t. in order to study the photothermal effect of a known concentration at the tumor site and combinational effect with the loaded drug (Figure 58). Therefore, A549 xenograft tumor bearing mice were treated i.t. with 300 µg of each nanogel and irradiated with the NIR laser for 5 min.

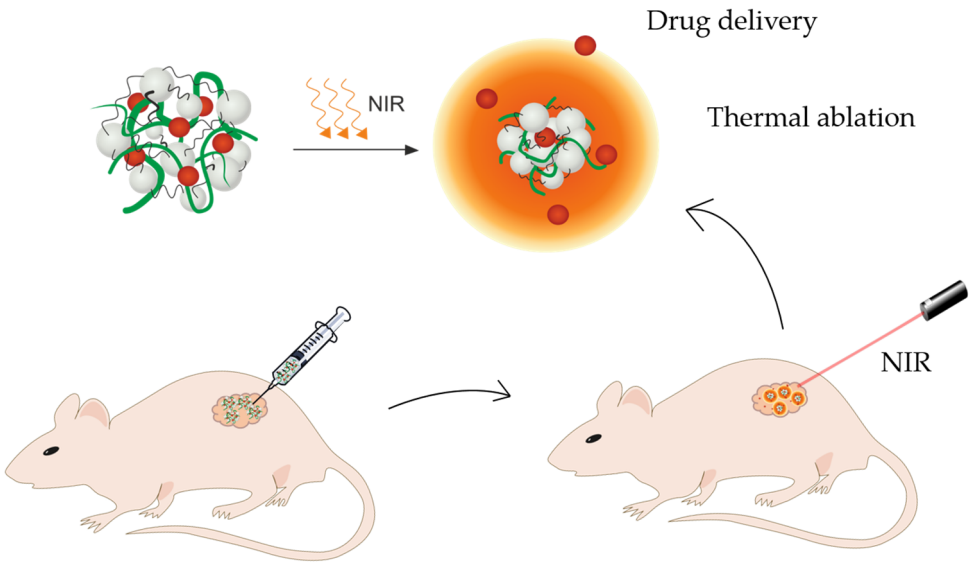

Figure 58. Schematic representation of combinational tumor treatment with semi-interpenetrated PPY nanogels delivering a chemotherapeutic drug and inducing photothermal ablation of the tumor tissue under exposure to NIR light.

The temperature increase during irradiation was monitored using an IR camera (Figure 60A) proving that the temperature increase is very local only at the tumor site with temperature of the surrounding tissue of 36 – 37 °C. For both nanogels, strong heating of the tumor site upon NIR exposure was recorded reaching temperatures >50 °C. These high temperatures caused skin burns in the mice after the treatment which however healed over the following 10 days (Figure 59). In addition, we assessed the particle distribution within the tumors after the treatment by taking photoacoustic images (*ex vivo*, one tumor per group). In comparison to the

untreated control (Figure 60B) PA intensities are increased within the whole tumor indicating a distribution of particles, but highest values are found close to the puncture site reflecting higher concentration of nanogels here (Figure 60C).

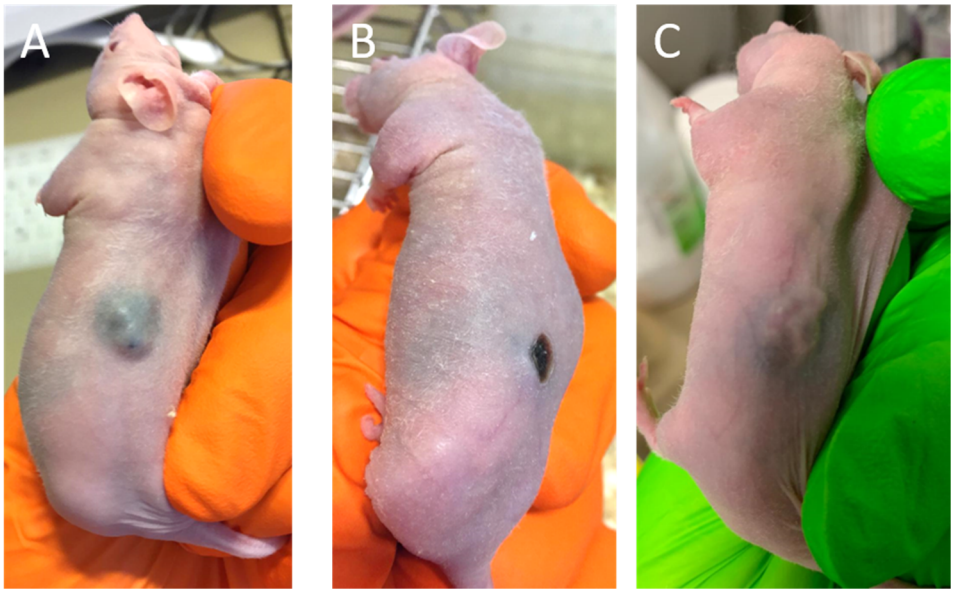

Figure 59. Representative images of mice (A) immediately after i.t. injection of the PPY/Co-dPG nanogels, (B) after NIR treatment (5min) and 10 days after treatment.

All assayed treatment modalities were found to be well tolerated reflected in no major BW changes over the whole period of the study (Figure 61). For both nanogels, PTT significantly inhibited the tumor growth, whereas non-irradiated controls did not show any effect on the tumor size (Figure 60D,E). In good agreement with the results obtained *in vitro,* the drug loaded nanogels slowed down tumor progression in a similar manner to the free drug demonstrating the ability of nanogels to deliver MTX. The combination of PTT and chemotherapeutic action of MTX result in reduced tumor regrowth, even though it has to be mentioned that the high efficiency of the PTT alone impede measurements of significant differences.

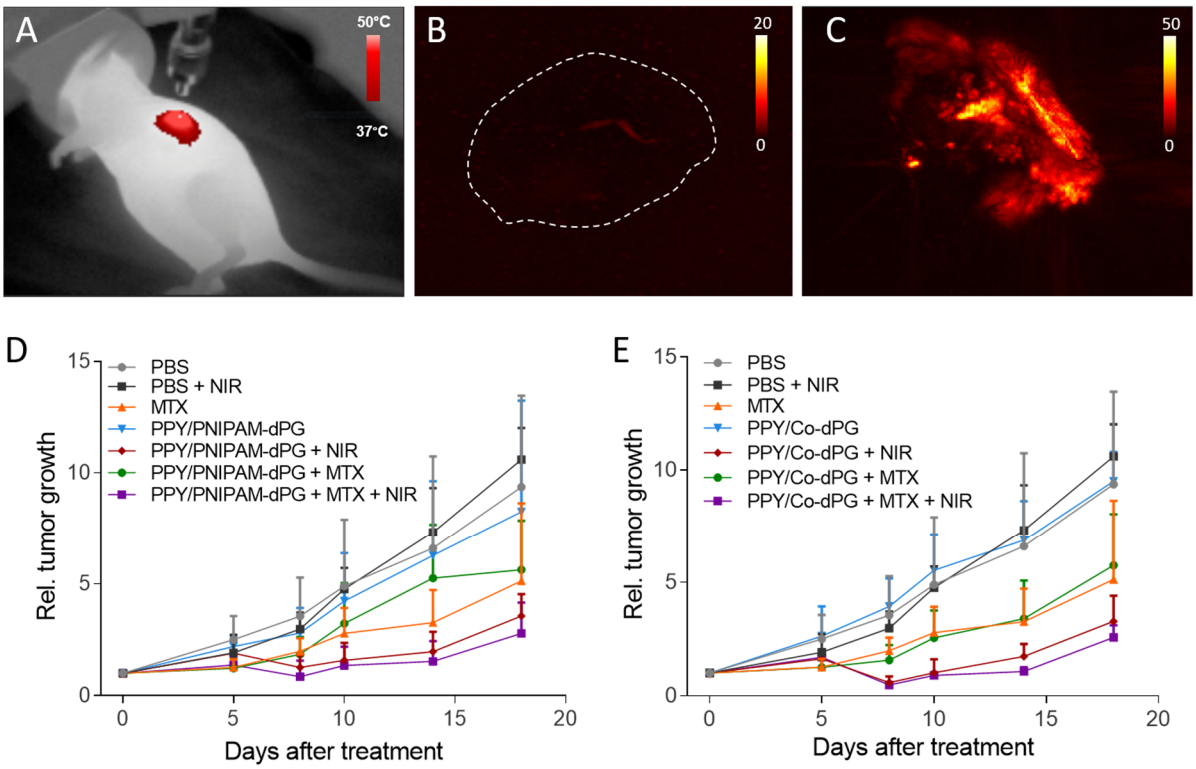

Figure 60. (A) IR image of a mice under NIR irradiation with i.t. injected nanogels, (B) MIP of photoacoustic image of an untreated control tumor *ex vivo* and (C) MIP of photoacoustic image of a tumor after injection of nanogels and 5 min NIR irradiation (30 µL, 10 mg/mL) *ex vivo*. (D-E) Rel. tumor growth over time of mice treated i.t. with MTX loaded and bare PPY nanogels (D) PPY/PNIPAM-dPG and (E) PPY/Co-dPG with and without exposure to NIR for 5 min. PBS treated mice with and without NIR exposure and MTX treated mice served as control.

We therefore performed tumor inhibition studies limiting the temperature at the tumor site upon NIR exposure to 45 °C by reduction of the laser power, but found that neither 5 min nor a prolonged irradiation time of 15 min had a significant influence on tumor growth (Figure 62A). Similar findings where observed by Liu et al.[161] with only minimal growth inhibition of tumors of a breast cancer cell line 4T1 implanted on mice with local temperature increases to 44 °C. By the same authors, efficient tumor reduction by PTT was only achieved with temperature increases of the tumor to 47 – 48 °C.

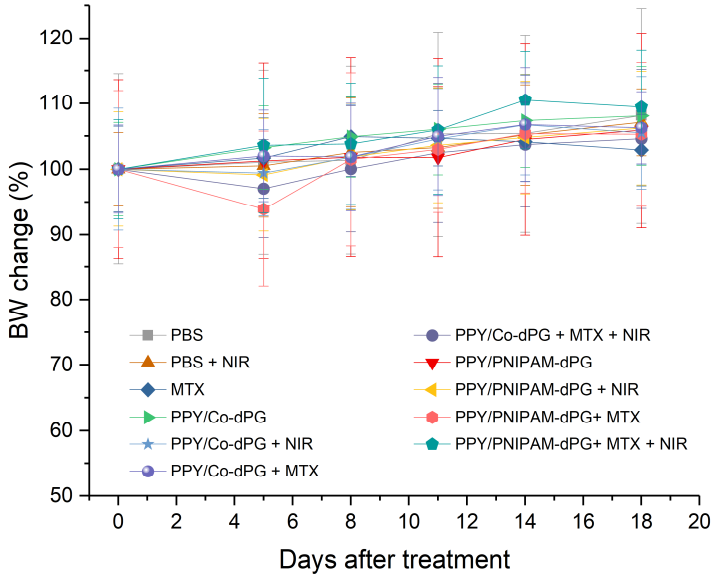

Figure 61. BW change of mice post treatment with MTX loaded and pure semi-interpenetrated nanogels PPY/Co-dPG and PPY/PNIPAM-dPG (i.t) with and without NIR exposure. PBS and MTX treated mice served as control.

As biodistribution profiles revealed that only PPY/Co-dPG nanogels are feasible candidates for i.v. administration and knowing that high temperatures are required for photothermal ablation of cancer cells, we decided to try to increase the intratumoral concentration of the PPY/Co-dPG nanogels by applying several i.v. doses in a consecutive manner. In addition, we were interested if several NIR irradiations will increase the efficiency of the treatment. Indeed, the development of the tumor volume with a single or two expositions to NIR revealed that both treatments are able to slow down tumor growth with slightly higher effectiveness of the inhibition upon several NIR expositions (Figure 62B). Together with the result from i.t. administration, we would expect better performance of tumor inhibition with drug loaded nanogels, nevertheless for future work additional active targeting moieties or combination with EPR augmenting agents need to be considered.

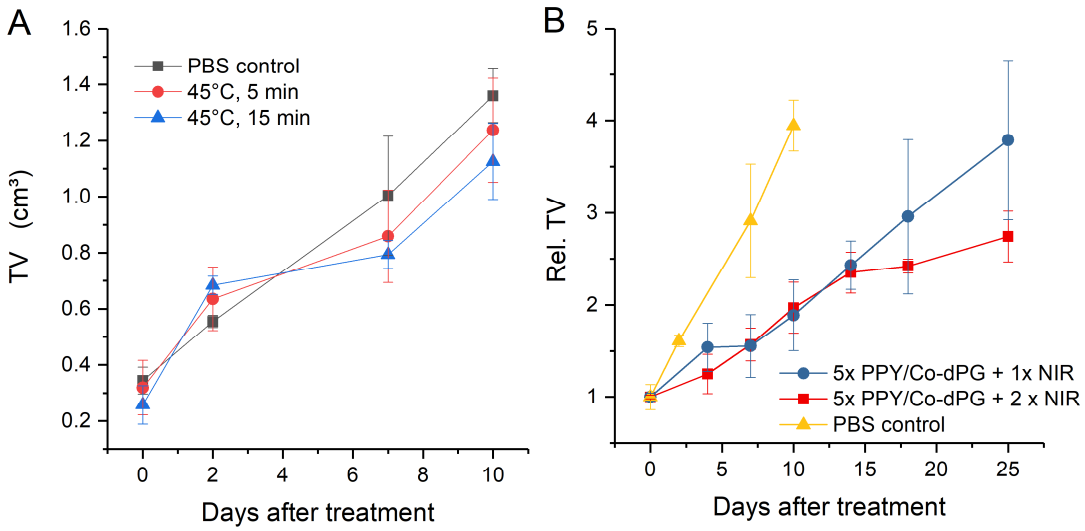

Figure 62. Tumor growth over time of (A) mice treated i.t. with PPY/Co-dPG nanogels and 5 min, respectively 15 min NIR exposure after injections and (B) after i.v. administration of 5 consecutive doses (100 mg/kg) of PPY/Co-dPG and exposure to NIR (5 min) 48h after last injection and with additional irradiation after the third injection.

.

5 CONCLUSION AND OUTLOOK

Fuelled by the promise to increase the treatment efficiency through improved pharmacokinetic profiles and targeted delivery of therapeutic actives, the development of nano-sized smart drug carriers attained intense scientific interest. However, the individual properties of therapeutic actives and the complexity of occurring diseases require rational adjustment of the carriers to disease- and drug-specific requirements. The main goal of this thesis is the development of adaption concepts and the identification of key parameters to control the properties and structure of responsive nanogels to broaden the range of cargo therapeutics and applications.

The common basis for the carrier systems employed in this thesis are thermo-responsive nanogels. Properties such as network density, hydrophilic/hydrophobic character, charge, and size govern efficient delivery of proteins in dermal applications. In the frame of the first project, fundamental investigations to gain control over these parameters should be carried out. Tuning of the nanogels' temperature-response should allow the use of external-triggers for temporal and local control of the release. The results of these assessments should then be incorporated in the design of multi-functional nanogels tuned for mucosal and systemic delivery applications.

In chapter 4.1.1, thermo-responsive nanogels were synthesized with poly-N-isopropyl methacrylamide (PNIPMAM) and poly-N-isopropyl acrylamide (PNIPAM) as thermo-responsive polymers, and acrylated dendritic polyglycerol (dPG) as macromolecular cross-linker. Investigation of the influence of the monomers and the hydrophilic and macromolecular nature of the cross-linker on nanogel formation and architecture yielded critical synthetic parameters controlling the desired features. The hydrophilic character of dPG allowed it to stabilize the growing particles during polymerization. It thereby has, together with the monomer reaction rates, a strong impact on the final particle size. In addition, the multi-functionality of dPG caused a "trapping" effect of cross-linking points inferred from the change

in the swelling ability during the formation of the nanogels. The final nanogels' network density and swelling ability modulation was achieved through tuning the crosslinker feed, and, albeit with less effect, the functionalization degree of dPG. The co-polymerization of NIPAM and NIPMAM allowed fine-tuning of the volume phase transition temperature (VPTT) of the resulting nanogels in the range of 34 – 47 °C.

Optimized candidates were chosen for evaluating the encapsulation and temperature-dependent release of the model protein bovine serum albumin (BSA) *in vitro* and *ex vivo* (chapter 4.2.1). All tested nanogels show high encapsulation efficiencies and temperature-triggered release profiles. Evaluation of the delivery of encapsulated BSA to the skin revealed, that nanogels with VPTTs below 37 °C are capable dermal delivery systems: they promote the penetration of encapsulated cargos using the skin's natural temperature gradient. For nanogels with higher VPTTs, applying an external heat source induced efficient dermal penetration even for short exposure times of 2 min. These nanogels thus offer precise local and temporal control over therapeutic protein delivery into the skin.

Within the frame of the second project, the assessed thermo-responsive nanogels should be adapted for delivering anti-inflammatory drugs to submucosal cells. The incorporation of a disulfide moiety should enable the nanogels to interact with mucus and thus overcome the mucosal clearance mechanism and deliver their cargo to submucosal cell layers.

In chapter 4.1.2, a bi-functional disulfide-containing linker design was employed for conjugating to dPG via copper-catalysed cycloaddition. Bearing a methacrylate group on one end, the linker conjugation translates dPG into a cross-linker. It allows the nanogel synthesis in analogy to bare thermo-responsive nanogels using the monomers NIPAM, NIPMAM and mixtures of both. Using the reductive cleavage of disulfides into thiols, the presence of disulfides could be investigated by monitoring nanogel degradation in reductive environments. It was found, that the presence of NIPAM during the polymerization induced premature cleavage of the disulfides yielding non-degradable nanogels. Fully degradable nanogels could only be generated using PNIPMAM. The copolymerization of NIPAM and NIPMAM confirmed, that the presence of NIPAM is likely to be responsible for the premature cleavage of disulfides, yielding partly

degradable nanogels. With decreasing PNIPAM content in copolymeric nanogels, the degradability was found to be higher.

It was hypothesized that the presence of disulfides endows the nanogels with the ability for submucosal delivery based on interactions with mucus. Thus, interactions of the nanogels with mucus were assayed *ex vivo*, revealing a time-dependent degradation of the nanogels upon incubation with mucus. The application of nanogels on freshly excised mucus showed, that the nanogels are able to penetrate the mucus layer and reach underlying epithelial cells. The comparison with non-degradable nanogels confirmed, that the presence of disulfides is the cause of the ability to overcome the mucosal self-clearance mechanism.

In chapter 4.2.2, the adapted nanogels are evaluated for encapsulation of two anti-inflammatory drugs, namely small molecular hydrophobic Budesonide (BUD) and the large, hydrophilic protein Etanercept (ETN). The nanogels were found to be suitable for both drugs, with increased aqueous solubilisation of BUD by the factor of 5 and high encapsulation efficiency of 80% for ETN. The protein structure of ETN and its activity was largely unaffected by encapsulation and release, demonstrating the excellent suitability of the nanogels to transport and protect sensitive biomacromolecules. The evaluation of the delivery and anti-inflammatory therapeutic efficiency are currently under investigation. Yet, the present results already show the promise of using disulfide-containing materials for mucosal applications. They also encourage further exploration of such materials and studies on the underlying interaction mechanisms. The gluthathione (GSH) induced cleavage of the nanogels additionally could be used to trigger the release of the encapsulated drugs upon internalization to cells. This might help to overcome drug resistance. For future research, in order to generate PNIPAM-based nanogels containing disulfides, a different linker design or other synthetic strategies might help to overcome the premature disulfide cleavage.

The last project aimed at generating new hybrid nanogels applicable in combinational therapy approaches of cancer. Improvements of therapeutic efficiency should be gained through controlled delivery of a chemotherapeutic drug in combination with photothermal therapy (PTT). As adaption tool for thermo-responsive nanogels, semi-interpenetration was employed

to introduce the NIR-transducing polymer polypyrrole (PPY). The physical entanglement of linear PPY in the nanogel network offers the advantage of complementing properties of both without affecting each other. As a result, the semi-interpenetrated nanogels still exhibit the same VPTT as their thermo-responsive non-interpenetrated analogues but act as excellent photothermal transducer with high photostability (chapter 4.1.3). The hydrophilic thermo-responsive network can stabilize water-insoluble PPY and prevent its aggregation over long time. The photothermal transducing abilities of PPY could be used to trigger the shrinkage of the nanogels, even to a higher extent than the application of elevated temperature could induce.

In addition, the PPY nanogels could be used for photoacoustic (PA) signal enhancement, which allowed tracking of the nanogels after administration. A new method for determination of *ex vivo* biodistribution was developed using the photothermal response of the nanogels. The method allowed label free detection of the particles with an accuracy down to concentrations of 12.5 µg/mL and was validated using *ex vivo* PA images.

The integration of PPY into the nanogels should endow the nanogels with a dual-functionality with potential increased therapeutic efficiency through the combination of chemotherapeutic drug delivery and photothermal tumor ablation. This was evaluated in chapter 4.2.3 *in vitro* and *in vivo.* Studies on the encapsulation and release of the anticancer drug Methotrexate (MTX) revealed that the presence of PPY assists the loading of this small molecular weight drug and allows for an NIR-triggered release. Evaluation of the PPY nanogels for PTT and as chemotherapeutic delivery agent, performed individually and in combination, showed combinational effects of both with additional decrease in cell viability *in vitro* and almost complete tumor elimination upon intratumorally (i.t.) administration *in vivo*. The hydration state of the thermo-responsive nanogels turned out to be an important factor for the tumor accumulation behaviour. Due to the collapse of PNIPAM-based nanogels at body temperature of 37 °C, these nanogels were only feasible for i.t. administration. In contrast, PPY/Co-dPG nanogels, which are in their hydrated state at 37 °C, accumulate sufficiently at the tumor site with several intravenous (i.v.) injections. In combination with NIR exposure, they were able to slow down tumor growth.

In order to improve the tumor accumulation of the nanogels, several options could be employed. For instance, to achieve increased passive targeting, (macro)molecules augmenting the enhanced permeation and retention (EPR) effect could be encapsulated into the nanogels. Typical vascular mediators to do so are nitric oxide, the vascular endothelial growth factor (VEGF/VPF) and the enzyme Bradykinin.[29] In addition, active targeting strategies could be employed taking advantage of the overexpression of specific receptors on the surface of tumor cells. Through the conjugation of suitable receptor ligands to the nanogels surface, e.g. Transferrin or the amino acid sequence RGD, the nanogels' accumulation at the tumor site could be increased. Moreover, the temperature-trigger for the release of molecules of larger size is working for the thermo-responsive nanogels. This knowledge opens the way for the investigation of the semi-interpenetrated nanogels to deliver therapeutic proteins or nanoparticle-conjugated drugs of larger size as well.

Altogether, this thesis demonstrates, that thermo-responsive nanogels are an excellent and variable platform for delivering a range of therapeutic actives, in particular for large molecules like proteins. Cross-linker modification and semi-interpenetration with a functional polymer were proven to be efficient tools for adding useful functionalities to the nanogels. It could be shown, that by adjusting the nanogels, the field of possible applications can be broadened from dermal to mucosal and systemic administration.

6 REFERENCES

[1] Gogotsi, Y. (2014) What Nano Can Do for Energy Storage, *ACS Nano 8*, 5369-5371.

[2] Chen, Q., De Marco, N., Yang, Y., Song, T.-B., Chen, C.-C., Zhao, H., Hong, Z., Zhou, H., and Yang, Y. (2015) Under the spotlight: The organic–inorganic hybrid halide perovskite for optoelectronic applications, *Nano Today 10*, 355-396.

[3] Parisi, C., Vigani, M., and Rodríguez-Cerezo, E. (2015) Agricultural Nanotechnologies: What are the current possibilities?, *Nano Today 10*, 124-127.

[4] He, X., and Hwang, H.-M. (2016) Nanotechnology in food science: Functionality, applicability, and safety assessment, *J. Food Drug Anal. 24*, 671-681.

[5] Duhan, J. S., Kumar, R., Kumar, N., Kaur, P., Nehra, K., and Duhan, S. (2017) Nanotechnology: The new perspective in precision agriculture, *Biotechnol Rep 15*, 11-23.

[6] Yetisen, A. K., Qu, H., Manbachi, A., Butt, H., Dokmeci, M. R., Hinestroza, J. P., Skorobogatiy, M., Khademhosseini, A., and Yun, S. H. (2016) Nanotechnology in Textiles, *ACS Nano 10*, 3042-3068.

[7] Wagner, V., Dullaart, A., Bock, A.-K., and Zweck, A. (2006) The emerging nanomedicine landscape, *Nat Biotech 24*, 1211-1217.

[8] Min, Y., Caster, J. M., Eblan, M. J., and Wang, A. Z. (2015) Clinical Translation of Nanomedicine, *Chem. Rev. 115*, 11147-11190.

[9] Etheridge, M. L., Campbell, S. A., Erdman, A. G., Haynes, C. L., Wolf, S. M., and McCullough, J. (2013) The big picture on nanomedicine: the state of investigational and approved nanomedicine products, *Nanomed. Nanotechnol. Biol. Med. 9*, 1-14.

[10] Raj, S., Jose, S., Sumod, U., and Sabitha, M. (2012) Nanotechnology in cosmetics: Opportunities and challenges, *4*, 186-193.

[11] Hoferichter, A. "Sand in Sonnenmilch" *Süddeutsche Zeitung* 12.06.2014, 07.02.2019, [https://www.sueddeutsche.de/wissen/umstrittene-nanopartikel-sand-in-der-sonnenmilch-1.1994845].

[12] Behrens, C. "Sonnencreme belastet Meere " *Süddeutsche Zeitung*, 25.08.2014, 07.02.2019, [https://www.sueddeutsche.de/wissen/nanopartikel-sonnencreme-belastet-meere-1.2099472].

[13] Stuart, C. "Why sunscreens are in the nanotechnology safety spotlight" *The Guardian*, 12.12.2011, 08.02.2019, [https://www.theguardian.com/nanotechnology-world/sunscreens-in-the-nanotechnology-safety-spotlight].

[14] Umwelt Bundesamt, "Was sind Nanoteilchen (Nanomaterialien) und wofür werden sie technisch eingesetzt? Wie kommt der Mensch mit ihnen in Kontakt und kennen wir besondere Risiken für die menschliche Gesundheit?" (07.11.2017) 07.02.2019

[https://www.umweltbundesamt.de/themen/gesundheit/umwelteinfluesse-auf-den-menschen/nanomaterial].

[15] Bundesamt für Risikobewertung, "Gesundheitliche Bewertung von Nanomaterialien" 08.02.2019 [https://www.bfr.bund.de/de/gesundheitliche_bewertung_von_nanomaterialien-30413.html].

[16] Mirza, A. Z., and Siddiqui, F. A. (2014) Nanomedicine and drug delivery: a mini review, *Int Nano Lett 4*, 94.

[17] Duncan, R., and Gaspar, R. (2011) Nanomedicine(s) under the Microscope, *Mol. Pharm. 8*, 2101-2141.

[18] Conti, M., Tazzari, V., Baccini, C., Pertici, G., Serino, L. P., and De Giorgi, U. (2006) Anticancer Drug Delivery with Nanoparticles, *In Vivo 20*, 697-701.

[19] Mura, S., Nicolas, J., and Couvreur, P. (2013) Stimuli-responsive nanocarriers for drug delivery, *Nat Mater 12*, 991-1003.

[20] Khandare, J., Calderon, M., Dagia, N. M., and Haag, R. (2012) Multifunctional dendritic polymers in nanomedicine: opportunities and challenges, *Chem. Soc. Rev. 41*, 2824-2848.

[21] Ringsdorf, H. (1975) Structure and properties of pharmacologically active polymers, *Journal of Polymer Science: Polymer Symposia 51*, 135-153.

[22] Duncan, R. (2003) The dawning era of polymer therapeutics, *Nat Rev Drug Discov 2*, 347.

[23] Nel, A. E., Madler, L., Velegol, D., Xia, T., Hoek, E. M. V., Somasundaran, P., Klaessig, F., Castranova, V., and Thompson, M. (2009) Understanding biophysicochemical interactions at the nano-bio interface, *Nat Mater 8*, 543-557.

[24] Li, S.-D., and Huang, L. (2008) Pharmacokinetics and Biodistribution of Nanoparticles, *Mol. Pharm. 5*, 496-504.

[25] Owens, D. E., and Peppas, N. A. (2006) Opsonization, biodistribution, and pharmacokinetics of polymeric nanoparticles, *Int. J. Pharm. 307*, 93-102.

[26] Peer, D., Karp, J. M., Hong, S., Farokhzad, O. C., Margalit, R., and Langer, R. (2007) Nanocarriers as an emerging platform for cancer therapy, *Nat Nanotechnol 2*, 751-760.

[27] Matsumura, Y., and Maeda, H. (1986) A New Concept for Macromolecular Therapeutics in Cancer Chemotherapy: Mechanism of Tumoritropic Accumulation of Proteins and the Antitumor Agent Smancs, *Cancer Res. 46*, 6387-6392.

[28] Maeda, H., Bharate, G. Y., and Daruwalla, J. (2009) Polymeric drugs for efficient tumor-targeted drug delivery based on EPR-effect, *Eur J Pharm Biopharm 71*, 409-419.

[29] Maeda, H., Tsukigawa, K., and Fang, J. (2016) A Retrospective 30 Years After Discovery of the Enhanced Permeability and Retention Effect of Solid Tumors: Next‐Generation Chemotherapeutics and Photodynamic Therapy—Problems, Solutions, and Prospects, *Microcirculation 23*, 173-182.

[30] Soni, K. S., Desale, S. S., and Bronich, T. K. (2016) Nanogels: An overview of properties, biomedical applications and obstacles to clinical translation, *J. Control Release 240*, 109-126.

[31] Sivaram, A. J., Rajitha, P., Maya, S., Jayakumar, R., and Sabitha, M. (2015) Nanogels for delivery, imaging and therapy, *WIREs Nanomed Nanobiotechnol 7*, 509-533.

[32] Kabanov, A. V., and Vinogradov, S. V. (2009) Nanogels as pharmaceutical carriers: finite networks of infinite capabilities, *Angew. Chem. Int. Ed. Engl. 48*, 5418-5429.

[33] Molina, M., Asadian-Birjand, M., Balach, J., Bergueiro, J., Miceli, E., and Calderon, M. (2015) Stimuli-responsive nanogel composites and their application in nanomedicine, *Chem. Soc. Rev. 44*, 6161-6186.

[34] Wu, W., Mitra, N., Yan, E. C., and Zhou, S. (2010) Multifunctional hybrid nanogel for integration of optical glucose sensing and self-regulated insulin release at physiological pH, *ACS Nano 4*, 4831-4839.

[35] Ghimire, A., Zore, O., Thilakarathne, V., Briand, V., Lenehan, P., Lei, Y., Kasi, R., and Kumar, C. (2015) "Stable-on-the-Table" Biosensors: Hemoglobin-Poly (Acrylic Acid) Nanogel BioElectrodes with High Thermal Stability and Enhanced Electroactivity, *Sensors 15*, 23868-23885.

[36] Hoare, T., and Pelton, R. (2008) Charge-Switching, Amphoteric Glucose-Responsive Microgels with Physiological Swelling Activity, *Biomacromolecules 9*, 733-740.

[37] Soleimani, A., Martinez, F., Economopoulos, V., Foster, P. J., Scholl, T. J., and Gillies, E. R. (2013) Polymer cross-linking: a nanogel approach to enhancing the relaxivity of MRI contrast agents, *J. Mater. Chem. B 1*, 1027-1034.

[38] Wang, H., Ke, F., Mararenko, A., Wei, Z., Banerjee, P., and Zhou, S. (2014) Responsive polymer-fluorescent carbon nanoparticle hybrid nanogels for optical temperature sensing, near-infrared light-responsive drug release, and tumor cell imaging, *Nanoscale 6*, 7443-7452.

[39] Qian, X., Li, J., and Nie, S. (2009) Stimuli-Responsive SERS Nanoparticles: Conformational Control of Plasmonic Coupling and Surface Raman Enhancement, *J. Am. Chem. Soc. 131*, 7540-7541.

[40] Cuggino, J. C., Molina, M., Wedepohl, S., Igarzabal, C. I. A., Calderón, M., and Gugliotta, L. M. (2016) Responsive nanogels for application as smart carriers in endocytic pH-triggered drug delivery systems, *Eur. Polym. J. 78*, 14-24.

[41] Sultana, F., Manirujjaman, Imran-Ul-Haque, M., Arafat, M., and Sharmin, S. (2013) An Overview of Nanogel Drug Delivery System, *J. Appl. Pharm. Sci. 3*, 95-105.

[42] Kar, M., Fechner, L., Nagel, G., Glitscher, E., Noe Rimondino, G., and Calderón, M. (2018) Chapter 12 Responsive Nanogels for Anti-cancer Therapy, In *Nanogels for Biomedical Applications*, pp 210-260, The Royal Society of Chemistry.

[43] Fleige, E., Quadir, M. A., and Haag, R. (2012) Stimuli-responsive polymeric nanocarriers for the controlled transport of active compounds: Concepts and applications, *Adv. Drug Delivery Rev. 64*, 866-884.

[44] Wu, H.-Q., and Wang, C.-C. (2016) Biodegradable Smart Nanogels: A New Platform for Targeting Drug Delivery and Biomedical Diagnostics, *Langmuir 32*, 6211-6225.

[45] Danhier, F., Feron, O., and Préat, V. (2010) To exploit the tumor microenvironment: Passive and active tumor targeting of nanocarriers for anti-cancer drug delivery, *J. Control Release 148*, 135-146.

[46] Song, C. W., Park, H., and Ross, B. D. (1999) Intra- and Extracellular pH in Solid Tumors, In *Antiangiogenic Agents in Cancer Therapy* (Teicher, B. A., Ed.), pp 51-64, Humana Press, Totowa, NJ.

[47] Zha, L., Banik, B., and Alexis, F. (2011) Stimulus responsive nanogels for drug delivery, *Soft Matter 7*, 5908-5916.

[48] Xue, Y., Xia, X., Yu, B., Luo, X., Cai, N., Long, S., and Yu, F. (2015) A green and facile method for the preparation of a pH-responsive alginate nanogel for subcellular delivery of doxorubicin, *RSC Advances 5*, 73416-73423.

[49] Hoffman, A. S. (1995) "Intelligent" Polymers in Medicine and Biotechnology, *Artif. Organs 19*, 458-467.

[50] Gandhi, A., Paul, A., Sen, S. O., and Sen, K. K. (2015) Studies on thermoresponsive polymers: Phase behaviour, drug delivery and biomedical applications, *Asian Journal of Pharmaceutical Sciences 10*, 99-107.

[51] Teotia, A. K., Sami, H., and Kumar, A. (2015) Thermo-responsive polymers: structure and design of smart materials, In *Switchable and Responsive Surfaces and Materials for Biomedical Applications* (Zhang, Z., Ed.), pp 3-43, Woodhead Publishing, Oxford.

[52] Schmaljohann, D. (2006) Thermo- and pH-responsive polymers in drug delivery, *Adv. Drug Delivery Rev. 58*, 1655-1670.

[53] Schild, H. G., and Tirrell, D. A. (1990) Microcalorimetric detection of lower critical solution temperatures in aqueous polymer solutions, *J. Phys. Chem. 94*, 4352-4356.

[54] Shibayama, M., Suetoh, Y., and Nomura, S. (1996) Structure Relaxation of Hydrophobically Aggregated Poly(N-isopropylacrylamide) in Water, *Macromolecules 29*, 6966-6968.

[55] Lin, S.-Y., Chen, K.-S., and Liang, R.-C. (1999) Thermal micro ATR/FT-IR spectroscopic system for quantitative study of the molecular structure of poly(N-isopropylacrylamide) in water, *Polymer 40*, 2619-2624.

[56] Pelton, R. (2010) Poly(N-isopropylacrylamide) (PNIPAM) is never hydrophobic, *J. Colloid Interface Sci. 348*, 673-674.

[57] Meeussen, F., Nies, E., Berghmans, H., Verbrugghe, S., Goethals, E., and Du Prez, F. (2000) Phase behaviour of poly(N-vinyl caprolactam) in water, *Polymer 41*, 8597-8602.

[58] Weber, C., Hoogenboom, R., and Schubert, U. S. (2012) Temperature responsive bio-compatible polymers based on poly(ethylene oxide) and poly(2-oxazoline)s, *Prog. Polym. Sci. 37*, 686-714.

[59] Asadian-Birjand, M., Bergueiro, J., Rancan, F., Cuggino, J. C., Mutihac, R. C., Achazi, K., Dernedde, J., Blume-Peytayi, U., Vogt, A., and Calderon, M. (2015) Engineering thermoresponsive polyether-based nanogels for temperature dependent skin penetration, *Polym. Chem. 6*, 5827-5831.

[60] Giulbudagian, M., Asadian-Birjand, M., Steinhilber, D., Achazi, K., Molina, M., and Calderon, M. (2014) Fabrication of thermoresponsive nanogels by thermo-nanoprecipitation and in situ encapsulation of bioactives, *Polym. Chem. 5*, 6909-6913.

[61] Pelton, R. H., and Chibante, P. (1986) Preparation of aqueous latices with N-isopropylacrylamide, *Colloids Surf. 20*, 247-256.

[62] Cuggino, J. C., Alvarez I, C. I., Strumia, M. C., Welker, P., Licha, K., Steinhilber, D., Mutihac, R.-C., and Calderon, M. (2011) Thermosensitive nanogels based on dendritic

polyglycerol and N-isopropylacrylamide for biomedical applications, *Soft Matter 7*, 11259-11266.

[63] Singka, G. S., Samah, N. A., Zulfakar, M. H., Yurdasiper, A., and Heard, C. M. (2010) Enhanced topical delivery and anti-inflammatory activity of methotrexate from an activated nanogel, *Eur J Pharm Biopharm 76*, 275-281.

[64] Tian, Y., Bian, S., and Yang, W. (2016) A redox-labile poly(oligo(ethylene glycol)methacrylate)-based nanogel with tunable thermosensitivity for drug delivery, *Polym. Chem. 7*, 1913-1921.

[65] Melle, A., Balaceanu, A., Kather, M., Wu, Y., Gau, E., Sun, W., Huang, X., Shi, X., Karperien, M., and Pich, A. (2016) Stimuli-responsive poly(N-vinylcaprolactam-co-2-methoxyethyl acrylate) core–shell microgels: facile synthesis, modulation of surface properties and controlled internalisation into cells, *J. Mater. Chem. B 4*, 5127-5137.

[66] Madhusudana Rao, K., Mallikarjuna, B., Krishna Rao, K. S. V., Siraj, S., Chowdoji Rao, K., and Subha, M. C. S. (2013) Novel thermo/pH sensitive nanogels composed from poly(N-vinylcaprolactam) for controlled release of an anticancer drug, *Colloids Surf., B 102*, 891-897.

[67] Benedict, F. G., Miles, W. R., and Johnson, A. (1919) The Temperature of the Human Skin, *PNAS 5*, 218-222.

[68] Aizawa, S., and Cabanac, M. (2000) Temperature gradient across the skin's layers has no influence on local skin vasomotor responses, *J. Therm. Biol. 25*, 313-316.

[69] Rancan, F., Giulbudagian, M., Jurisch, J., Blume-Peytavi, U., Calderón, M., and Vogt, A. (2017) Drug delivery across intact and disrupted skin barrier: Identification of cell populations interacting with penetrated thermoresponsive nanogels, *Eur. J. Pharm. Biopharm. 116*, 4-11.

[70] Giulbudagian M, Y. G., Hönzke S, Edlich A, Geisendörfer B, Kleuser B, Hedtrich S, Calderón M. (2018) Breaking the Barrier - Potent Anti-Inflammatory Activity following Efficient Topical Delivery of Etanercept using Thermoresponsive Nanogels., *Theranostics 8*, 450-463.

[71] Giulbudagian, M., Honzke, S., Bergueiro, J., Isk, D., Schumacher, F., Saeidpour, S., Lohan, S. B., Meinke, M. C., Teutloff, C., Schafer-Korting, M., Yealland, G., Kleuser, B., Hedtrich, S., and Calderon, M. (2018) Enhanced topical delivery of dexamethasone by [small beta]-cyclodextrin decorated thermoresponsive nanogels, *Nanoscale 10*, 469-479.

[72] Witting, M., Molina, M., Obst, K., Plank, R., Eckl, K. M., Hennies, H. C., Calderón, M., Frieß, W., and Hedtrich, S. (2015) Thermosensitive dendritic polyglycerol-based nanogels for cutaneous delivery of biomacromolecules, *Nanomed. Nanotechnol. Biol. Med. 11*, 1179-1187.

[73] Zavgorodnya, O., Carmona-Moran, C. A., Kozlovskaya, V., Liu, F., Wick, T. M., and Kharlampieva, E. (2017) Temperature-responsive nanogel multilayers of poly(N-vinylcaprolactam) for topical drug delivery, *J. Colloid Interface Sci. 506*, 589-602.

[74] Chanmugam, A., Langemo, D., Thomason, K., Haan, J., Altenburger, E. A., Tippett, A., Henderson, L., and Zortman, T. A. (2017) Relative Temperature Maximum in Wound Infection and Inflammation as Compared with a Control Subject Using Long-Wave Infrared Thermography, *Adv Skin Wound Care 30*, 406-414.

[75] Wu, X., Pelton, R. H., Hamielec, A. E., Woods, D. R., and McPhee, W. (1994) The kinetics of poly(N-isopropylacrylamide) microgel latex formation, *Colloid. Polym. Sci. 272*, 467-477.

[76] Fujishige, S., Kubota, K., and Ando, I. (1989) Phase transition of aqueous solutions of poly(N-isopropylacrylamide) and poly(N-isopropylmethacrylamide), *J. Phys. Chem. 93*, 3311-3313.

[77] Hu, X., Tong, Z., and Lyon, L. A. (2011) Control of Poly(N-isopropylacrylamide) Microgel Network Structure by Precipitation Polymerization near the Lower Critical Solution Temperature, *Langmuir 27*, 4142-4148.

[78] von Nessen, K., Karg, M., and Hellweg, T. (2013) Thermoresponsive poly-(N-isopropylmethacrylamide) microgels: Tailoring particle size by interfacial tension control, *Polymer 54*, 5499-5510.

[79] Ramos, J., Imaz, A., and Forcada, J. (2012) Temperature-sensitive nanogels: poly(N-vinylcaprolactam) versus poly(N-isopropylacrylamide), *Polym. Chem. 3*, 852-856.

[80] Meyer, S., and Richtering, W. (2005) Influence of Polymerization Conditions on the Structure of Temperature-Sensitive Poly(N-isopropylacrylamide) Microgels, *Macromolecules 38*, 1517-1519.

[81] Yang, H., Wang, Q., Huang, S., Xiao, A., Li, F., Gan, L., and Yang, X. (2016) Smart pH/Redox Dual-Responsive Nanogels for On-Demand Intracellular Anticancer Drug Release, *ACS Appl Mater Interfaces 8*, 7729-7738.

[82] Rimondino, G. N., Miceli, E., Molina, M., Wedepohl, S., Thierbach, S., Rühl, E., Strumia, M., Martinelli, M., and Calderón, M. (2017) Rational design of dendritic thermoresponsive nanogels that undergo phase transition under endolysosomal conditions, *J. Mater. Chem. B 5*, 866-874.

[83] Debord, J. D., and Lyon, L. A. (2003) Synthesis and Characterization of pH-Responsive Copolymer Microgels with Tunable Volume Phase Transition Temperatures, *Langmuir 19*, 7662-7664.

[84] Hoare, T., and Pelton, R. (2006) Titrametric Characterization of pH-Induced Phase Transitions in Functionalized Microgels, *Langmuir 22*, 7342-7350.

[85] Hoare, T., and Pelton, R. (2004) Highly pH and Temperature Responsive Microgels Functionalized with Vinylacetic Acid, *Macromolecules 37*, 2544-2550.

[86] Karg, M., Pastoriza-Santos, I., Rodriguez-González, B., von Klitzing, R., Wellert, S., and Hellweg, T. (2008) Temperature, pH, and Ionic Strength Induced Changes of the Swelling Behavior of PNIPAM−Poly(allylacetic acid) Copolymer Microgels, *Langmuir 24*, 6300-6306.

[87] Feng, L., Li, K., Shi, X., Gao, M., Liu, J., and Liu, Z. (2014) Smart pH-Responsive Nanocarriers Based on Nano-Graphene Oxide for Combined Chemo- and Photothermal Therapy Overcoming Drug Resistance, *Advanced Healthcare Materials 3*, 1261-1271.

[88] Lundqvist, M., Stigler, J., Elia, G., Lynch, I., Cedervall, T., and Dawson, K. A. (2008) Nanoparticle size and surface properties determine the protein corona with possible implications for biological impacts, *PNAS 105*, 14265-14270.

[89] Lazarovits, J., Chen, Y. Y., Sykes, E. A., and Chan, W. C. W. (2015) Nanoparticle-blood interactions: the implications on solid tumour targeting, *Chem. Commun. 51*, 2756-2767.

[90] Berndt, I., Pedersen, J. S., and Richtering, W. (2005) Structure of Multiresponsive "Intelligent" Core–Shell Microgels, *J. Am. Chem. Soc. 127*, 9372-9373.

[91] Dubbert, J., Nothdurft, K., Karg, M., and Richtering, W. (2015) Core-shell-shell and hollow double-shell microgels with advanced temperature responsiveness, *Macromol. Rapid Commun. 36*, 159-164.

[92] Hu, X., Tong, Z., and Lyon, L. A. (2011) One-pot synthesis of microcapsules with nanoscale inclusions, *Macromol. Rapid Commun. 32*, 1461-1466.

[93] Hou, L., and Wu, P. (2015) Comparison of LCST-transitions of homopolymer mixture, diblock and statistical copolymers of NIPAM and VCL in water, *Soft Matter 11*, 2771-2781.

[94] Dybal, J., Trchová, M., and Schmidt, P. (2009) The role of water in structural changes of poly(N-isopropylacrylamide) and poly(N-isopropylmethacrylamide) studied by FTIR, Raman spectroscopy and quantum chemical calculations, *Vib. Spectrosc 51*, 44-51.

[95] Djokpé, E., and Vogt, W. (2001) N-Isopropylacrylamide and N-Isopropylmethacrylamide: Cloud Points of Mixtures and Copolymers, *Macromol. Chem. Phys. 202*, 750-757.

[96] Wedel, B., Hertle, Y., Wrede, O., Bookhold, J., and Hellweg, T. (2016) Smart Homopolymer Microgels: Influence of the Monomer Structure on the Particle Properties, *Polymers 8*.

[97] Keerl, M., Pedersen, J. S., and Richtering, W. (2009) Temperature Sensitive Copolymer Microgels with Nanophase Separated Structure, *J. Am. Chem. Soc. 131*, 3093-3097.

[98] Bouwstra, J. A., and Ponec, M. (2006) The skin barrier in healthy and diseased state, *Biochim. Biophys. Acta 1758*, 2080-2095.

[99] Alvarez-Román, R., Naik, A., Kalia, Y. N., Guy, R. H., and Fessi, H. (2004) Skin penetration and distribution of polymeric nanoparticles, *J. Control Release 99*, 53-62.

[100] Cevc, G. (2012) Rational design of new product candidates: The next generation of highly deformable bilayer vesicles for noninvasive, targeted therapy, *J. Control Release 160*, 135-146.

[101] Cevc, G., and Blume, G. (2001) New, highly efficient formulation of diclofenac for the topical, transdermal administration in ultradeformable drug carriers, Transfersomes, *Biochim. Biophys. Acta 1514*, 191-205.

[102] Abbina, S., Vappala, S., Kumar, P., Siren, E. M. J., La, C. C., Abbasi, U., Brooks, D. E., and Kizhakkedathu, J. N. (2017) Hyperbranched polyglycerols: recent advances in synthesis, biocompatibility and biomedical applications, *J. Mater. Chem. B 5*, 9249-9277.

[103] Steinhilber, D., Witting, M., Zhang, X., Staegemann, M., Paulus, F., Friess, W., Küchler, S., and Haag, R. (2013) Surfactant free preparation of biodegradable dendritic polyglycerol nanogels by inverse nanoprecipitation for encapsulation and release of pharmaceutical biomacromolecules, *J. Control Release 169*, 289-295.

[104] Miceli, E., Kuropka, B., Rosenauer, C., Blanco, E. R. O., Theune, L. E., Kar, M., Weise, C., Morsbach, S., Freund, C., and Calderón, M. (2018) Understanding the elusive protein corona of thermoresponsive nanogels, *Nanomedicine 13*, 2657-2668.

[105] Hatahet, F., Nguyen, V. D., Salo, K. E., and Ruddock, L. W. (2010) Disruption of reducing pathways is not essential for efficient disulfide bond formation in the cytoplasm of E. coli, *Microb Cell Fact 9*, 67.

[106] Singh, S., Topuz, F., Hahn, K., Albrecht, K., and Groll, J. (2013) Embedding of Active Proteins and Living Cells in Redox-Sensitive Hydrogels and Nanogels through Enzymatic Cross-Linking, *Angew. Chem. Int. Ed. 52*, 3000-3003.

[107] Meister, A., and Anderson, M. E. (1983) GLUTATHIONE, *Annu. Rev. Biochem 52*, 711-760.

[108] Li, S., Zhang, J., Deng, C., Meng, F., Yu, L., and Zhong, Z. (2016) Redox-Sensitive and Intrinsically Fluorescent Photoclick Hyaluronic Acid Nanogels for Traceable and Targeted Delivery of Cytochrome c to Breast Tumor in Mice, *ACS Applied Materials & Interfaces*.

[109] Tian, Y., Wang, Y., Shen, S., Jiang, X., Wang, Y., and Yang, W. (2015) Temperature and Redox Dual-Responsive Biodegradable Nanogels for Optimizing Antitumor Drug Delivery, *Part. Part. Syst. Charact. 32*, 1092-1101.

[110] Netsomboon, K., and Bernkop-Schnürch, A. (2016) Mucoadhesive vs. mucopenetrating particulate drug delivery, *Eur. J. Pharm. Biopharm. 98*, 76-89.

[111] Murgia, X., Loretz, B., Hartwig, O., Hittinger, M., and Lehr, C.-M. (2018) The role of mucus on drug transport and its potential to affect therapeutic outcomes, *Adv. Drug Delivery Rev. 124*, 82-97.

[112] Chater, P. I., Wilcox, M. D., and Pearson, J. P. (2018) Efficacy and safety concerns over the use of mucus modulating agents for drug delivery using nanoscale systems, *Adv. Drug Delivery Rev. 124*, 184-192.

[113] Tabachnik, N. F., Blackburn, P., and Cerami, A. (1981) Biochemical and rheological characterization of sputum mucins from a patient with cystic fibrosis, *J. Biol. Chem. 256*, 7161-7165.

[114] Dünnhaupt, S., Barthelmes, J., Hombach, J., Sakloetsakun, D., Arkhipova, V., and Bernkop-Schnürch, A. (2011) Distribution of thiolated mucoadhesive nanoparticles on intestinal mucosa, *Int. J. Pharm. 408*, 191-199.

[115] Bernkop-Schnürch, A., Egger, C., Elhassan Imam, M., and Krauland, A. H. (2003) Preparation and in vitro characterization of poly(acrylic acid)–cysteine microparticles, *J. Control Release 93*, 29-38.

[116] Rahmat, D., Müller, C., Barthelmes, J., Shahnaz, G., Martien, R., and Bernkop-Schnürch, A. (2013) Thiolated hydroxyethyl cellulose: Design and in vitro evaluation of mucoadhesive and permeation enhancing nanoparticles, *Eur. J. Pharm. Biopharm. 83*, 149-155.

[117] Sharma, R., Ahuja, M., and Kaur, H. (2012) Thiolated pectin nanoparticles: Preparation, characterization and ex vivo corneal permeation study, *Carbohydr. Polym. 87*, 1606-1610.

[118] Iqbal, J., Shahnaz, G., Perera, G., Hintzen, F., Sarti, F., and Bernkop-Schnürch, A. (2012) Thiolated chitosan: Development and in vivo evaluation of an oral delivery system for leuprolide, *Eur. J. Pharm. Biopharm. 80*, 95-102.

[119] Shahnaz, G., Vetter, A., Barthelmes, J., Rahmat, D., Laffleur, F., Iqbal, J., Perera, G., Schlocker, W., Dünnhaput, S., Augustijns, P., and Bernkop-Schnürch, A. (2012) Thiolated chitosan nanoparticles for the nasal administration of leuprolide: Bioavailability and pharmacokinetic characterization, *Int. J. Pharm. 428*, 164-170.

[120] Arshady, R. (1992) Suspension, emulsion, and dispersion polymerization: A methodological survey, *Colloid. Polym. Sci. 270*, 717-732.

[121] Schork, F. J., Luo, Y., Smulders, W., Russum, J. P., Butté, A., and Fontenot, K. (2005) Miniemulsion Polymerization, In *Polymer Particles: -/-* (Okubo, M., Ed.), pp 129-255, Springer Berlin Heidelberg, Berlin, Heidelberg.

[122] Yong, C. P., and Gan, L. M. (2005) Microemulsion Polymerizations and Reactions, In *Polymer Particles: -/-* (Okubo, M., Ed.), pp 257-298, Springer Berlin Heidelberg, Berlin, Heidelberg.

[123] Landfester, K. (2006) Synthesis of colloidal particles in miniemulsions, *Annu. Rev. Mater. Res. 36*, 231-279.

[124] Greco, F., and Vicent, M. J. (2009) Combination therapy: Opportunities and challenges for polymer–drug conjugates as anticancer nanomedicines, *Adv. Drug Delivery Rev. 61*, 1203-1213.

[125] Heo, C. Y., and Kwon, Y. J. (2016) Killing two birds or more with one stone, *Adv. Drug Delivery Rev. 98*, 1-2.

[126] Jaque, D., Martinez Maestro, L., del Rosal, B., Haro-Gonzalez, P., Benayas, A., Plaza, J. L., Martin Rodriguez, E., and Garcia Sole, J. (2014) Nanoparticles for photothermal therapies, *Nanoscale 6*, 9494-9530.

[127] Rao, W., Deng, Z. S., and Liu, J. (2010) A review of hyperthermia combined with radiotherapy/chemotherapy on malignant tumors, *Crit. Rev. Biomed. Eng. 38*, 101-116.

[128] Hildebrandt, B., Wust, P., Ahlers, O., Dieing, A., Sreenivasa, G., Kerner, T., Felix, R., and Riess, H. (2002) The cellular and molecular basis of hyperthermia, *Crit. Rev. Oncol./Hematol. 43*, 33-56.

[129] Liu, Y., Bhattarai, P., Dai, Z., and Chen, X. (2018) Photothermal therapy and photoacoustic imaging via nanotheranostics in fighting cancer, *Chem. Soc. Rev.*

[130] Wang, M. (2016) Emerging Multifunctional NIR Photothermal Therapy Systems Based on Polypyrrole Nanoparticles, *Polymers 8*, 373.

[131] Li, Z., Huang, H., Tang, S., Li, Y., Yu, X.-F., Wang, H., Li, P., Sun, Z., Zhang, H., Liu, C., and Chu, P. K. (2016) Small gold nanorods laden macrophages for enhanced tumor coverage in photothermal therapy, *Biomaterials 74*, 144-154.

[132] Kim, J., Park, S., Lee, J. E., Jin, S. M., Lee, J. H., Lee, I. S., Yang, I., Kim, J.-S., Kim, S. K., Cho, M.-H., and Hyeon, T. (2006) Designed Fabrication of Multifunctional Magnetic Gold Nanoshells and Their Application to Magnetic Resonance Imaging and Photothermal Therapy, *Angew. Chem. 118*, 7918-7922.

[133] Liang, C., Diao, S., Wang, C., Gong, H., Liu, T., Hong, G., Shi, X., Dai, H., and Liu, Z. (2014) Tumor Metastasis Inhibition by Imaging-Guided Photothermal Therapy with Single-Walled Carbon Nanotubes, *Adv. Mater. 26*, 5646-5652.

[134] Chen, D., Wang, C., Nie, X., Li, S., Li, R., Guan, M., Liu, Z., Chen, C., Wang, C., Shu, C., and Wan, L. (2014) Photoacoustic Imaging Guided Near-Infrared Photothermal Therapy Using Highly Water-Dispersible Single-Walled Carbon Nanohorns as Theranostic Agents, *Adv. Funct. Mater. 24*, 6621-6628.

[135] Yu, J., Javier, D., Yaseen, M. A., Nitin, N., Richards-Kortum, R., Anvari, B., and Wong, M. S. (2010) Self-Assembly Synthesis, Tumor Cell Targeting, and Photothermal Capabilities of Antibody-Coated Indocyanine Green Nanocapsules, *J. Am. Chem. Soc. 132*, 1929-1938.

[136] Zheng, X., Xing, D., Zhou, F., Wu, B., and Chen, W. R. (2011) Indocyanine Green-Containing Nanostructure as Near Infrared Dual-Functional Targeting Probes for Optical Imaging and Photothermal Therapy, *Mol. Pharm. 8*, 447-456.

[137] Shanmugam, V., Selvakumar, S., and Yeh, C. S. (2014) Near-infrared light-responsive nanomaterials in cancer therapeutics, *Chem. Soc. Rev. 43*, 6254-6287.

[138] Zhao, X.-q., Wang, T.-x., Liu, W., Wang, C.-d., Wang, D., Shang, T., Shen, L.-h., and Ren, L. (2011) Multifunctional Au@IPN-pNIPAAm nanogels for cancer cell imaging and combined chemo-photothermal treatment, *J. Mater. Chem. 21*, 7240.

[139] Wu, W., Shen, J., Banerjee, P., and Zhou, S. (2011) Water-dispersible multifunctional hybrid nanogels for combined curcumin and photothermal therapy, *Biomaterials 32*, 598-609.

[140] Wu, W., Shen, J., Banerjee, P., and Zhou, S. (2010) Core–shell hybrid nanogels for integration of optical temperature-sensing, targeted tumor cell imaging, and combined chemo-photothermal treatment, *Biomaterials 31*, 7555-7566.

[141] Yang, J., Choi, J., Bang, D., Kim, E., Lim, E.-K., Park, H., Suh, J.-S., Lee, K., Yoo, K.-H., Kim, E.-K., Huh, Y.-M., and Haam, S. (2011) Convertible Organic Nanoparticles for Near-Infrared Photothermal Ablation of Cancer Cells, *Angew. Chem. Int. Ed. 50*, 441-444.

[142] Yang, J., Choi, J., Bang, D., Kim, E., Lim, E. K., Park, H., Suh, J. S., Lee, K., Yoo, K. H., Kim, E. K., Huh, Y. M., and Haam, S. (2011) Convertible organic nanoparticles for near-infrared photothermal ablation of cancer cells, *Angew. Chem. Int. Ed. 50*, 441-444.

[143] Yslas, E. I., Ibarra, L. E., Molina, M. A., Rivarola, C., Barbero, C. A., Bertuzzi, M. L., and Rivarola, V. A. (2015) Polyaniline nanoparticles for near-infrared photothermal destruction of cancer cells, *J. Nanopart. Res. 17*, 389.

[144] Molina, M., Wedepohl, S., and Calderón, M. (2016) Polymeric near-infrared absorbing dendritic nanogels for efficient in vivo photothermal cancer therapy, *Nanoscale 8*, 5852-5856.

[145] Zhou, Y., Hu, Y., Sun, W., Zhou, B., Zhu, J., Peng, C., Shen, M., and Shi, X. (2017) Polyaniline-loaded γ-polyglutamic acid nanogels as a platform for photoacoustic imaging-guided tumor photothermal therapy, *Nanoscale 9*, 12746-12754.

[146] Zha, Z., Yue, X., Ren, Q., and Dai, Z. (2013) Uniform Polypyrrole Nanoparticles with High Photothermal Conversion Efficiency for Photothermal Ablation of Cancer Cells, *Adv. Mater. 25*, 777-782.

[147] Yang, K., Xu, H., Cheng, L., Sun, C., Wang, J., and Liu, Z. (2012) In Vitro and In Vivo Near-Infrared Photothermal Therapy of Cancer Using Polypyrrole Organic Nanoparticles, *Adv. Mater. 24*, 5586-5592.

[148] Chen, M., Fang, X., Tang, S., and Zheng, N. (2012) Polypyrrole nanoparticles for high-performance in vivo near-infrared photothermal cancer therapy, *Chem. Commun. 48*, 8934-8936.

[149] Tian, Y., Zhang, J., Tang, S., Zhou, L., and Yang, W. (2016) Polypyrrole Composite Nanoparticles with Morphology‐Dependent Photothermal Effect and Immunological Responses, *Small 12*, 721-726.

[150] Gong, H., Cheng, L., Xiang, J., Xu, H., Feng, L., Shi, X., and Liu, Z. (2013) Near-Infrared Absorbing Polymeric Nanoparticles as a Versatile Drug Carrier for Cancer Combination Therapy, *Adv. Funct. Mater. 23*, 6059-6067.

[151] Cheng, L., Yang, K., Chen, Q., and Liu, Z. (2012) Organic Stealth Nanoparticles for Highly Effective in Vivo Near-Infrared Photothermal Therapy of Cancer, *ACS Nano 6*, 5605-5613.

[152] Aoki, T., Tanino, M., Sanui, K., Ogata, N., and Kumakura, K. (1996) Secretory function of adrenal chromaffin cells cultured on polypyrrole films, *Biomaterials 17*, 1971-1974.

[153] Ghasemi-Mobarakeh, L., Prabhakaran, M. P., Morshed, M., Nasr-Esfahani, M. H., Baharvand, H., Kiani, S., Al-Deyab, S. S., and Ramakrishna, S. (2011) Application of conductive polymers, scaffolds and electrical stimulation for nerve tissue engineering, *Journal of Tissue Engineering and Regenerative Medicine 5*, e17-e35.

[154] Balint, R., Cassidy, N. J., and Cartmell, S. H. (2014) Conductive polymers: Towards a smart biomaterial for tissue engineering, *Acta Biomater. 10*, 2341-2353.

[155] George, P. M., Lyckman, A. W., LaVan, D. A., Hegde, A., Leung, Y., Avasare, R., Testa, C., Alexander, P. M., Langer, R., and Sur, M. (2005) Fabrication and biocompatibility of polypyrrole implants suitable for neural prosthetics, *Biomaterials 26*, 3511-3519.

[156] Fahlgren, A., Bratengeier, C., Gelmi, A., Semeins, C. M., Klein-Nulend, J., Jager, E. W. H., and Bakker, A. D. (2015) Biocompatibility of Polypyrrole with Human Primary Osteoblasts and the Effect of Dopants, *PLOS ONE 10*, e0134023.

[157] Ateh, D. D., Navsaria, H. A., and Vadgama, P. (2006) Polypyrrole-based conducting polymers and interactions with biological tissues, *J R Soc Interface 3*, 741-752.

[158] Chen, M., Fang, X., Tang, S., and Zheng, N. (2012) Polypyrrole nanoparticles for high-performance in vivo near-infrared photothermal cancer therapy., *Chem. Commun. 48*, 8934-8936.

[159] Liang, X., Li, Y., Li, X., Jing, L., Deng, Z., Yue, X., Li, C., and Dai, Z. (2015) PEGylated Polypyrrole Nanoparticles Conjugating Gadolinium Chelates for Dual-Modal MRI/Photoacoustic Imaging Guided Photothermal Therapy of Cancer, *Adv. Funct. Mater. 25*, 1451-1462.

[160] Zhou, Y., Hu, Y., Sun, W., Lu, S., Cai, C., Peng, C., Yu, J., Popovtzer, R., Shen, M., and Shi, X. (2018) Radiotherapy-Sensitized Tumor Photothermal Ablation Using γ-Polyglutamic Acid Nanogels Loaded with Polypyrrole, *Biomacromolecules 19*, 2034-2042.

[161] Wang, C., Xu, H., Liang, C., Liu, Y., Li, Z., Yang, G., Cheng, L., Li, Y., and Liu, Z. (2013) Iron Oxide @ Polypyrrole Nanoparticles as a Multifunctional Drug Carrier for

Remotely Controlled Cancer Therapy with Synergistic Antitumor Effect, *ACS Nano 7*, 6782-6795.

[162] Wang, Y., Xiao, Y., and Tang, R. (2014) Spindle-Like Polypyrrole Hollow Nanocapsules as Multifunctional Platforms for Highly Effective Chemo–Photothermal Combination Therapy of Cancer Cells in Vivo, *Chemistry – A European Journal 20*, 11826-11834.

[163] Lohani, A., Singh, G., Bhattacharya, S. S., and Verma, A. (2014) Interpenetrating polymer networks as innovative drug delivery systems, *Journal of drug delivery 2014*, 583612.

[164] Liu, X., Guo, H., and Zha, L. (2012) Study of pH/temperature dual stimuli-responsive nanogels with interpenetrating polymer network structure, *Polym. Int. 61*, 1144-1150.

[165] Meng, Z., Chen, X., Liu, Z., Chen, S., Yu, N., Wei, P., Chen, Z., and Zhu, M. (2016) NIR-laser-triggered smart full-polymer nanogels for synergic photothermal-/chemo-therapy of tumors, *RSC Advances 6*, 90111-90119.

[166] Zha, Z., Deng, Z., Li, Y., Li, C., Wang, J., Wang, S., Qu, E., and Dai, Z. (2013) Biocompatible polypyrrole nanoparticles as a novel organic photoacoustic contrast agent for deep tissue imaging, *Nanoscale 5*, 4462-4467.

[167] Suga, Y., Sunayama, H., Ooya, T., and Takeuchi, T. (2013) Molecularly imprinted polymers prepared using protein-conjugated cleavable monomers followed by site-specific post-imprinting introduction of fluorescent reporter molecules, *Chem. Commun. 49*, 8450-8452.

[168] Roller, S., Zhou, H., and Haag, R. (2005) High-loading polyglycerol supported reagents for Mitsunobu- and acylation-reactions and other useful polyglycerol derivatives, *Mol. Divers. 9*, 305-316.

[169] Kar, M., Tiwari, N., Tiwari, M., Lahiri, M., and Gupta, S. S. (2013) Poly-L-Arginine Grafted Silica Mesoporous Nanoparticles for Enhanced Cellular Uptake and their Application in DNA Delivery and Controlled Drug Release, *Part. Part. Syst. Charact. 30*, 166-179.

[170] Theune, L. E., Charbaji, R., Kar, M., Wedepohl, S., Hedtrich, S., and Calderón, M. (2019) Critical parameters for the controlled synthesis of nanogels suitable for temperature-triggered protein delivery, *Materials Science and Engineering: C 100*, 141-151.

[171] Schindelin, J., Arganda-Carreras, I., Frise, E., Kaynig, V., Longair, M., Pietzsch, T., Preibisch, S., Rueden, C., Saalfeld, S., Schmid, B., Tinevez, J.-Y., White, D. J., Hartenstein, V., Eliceiri, K., Tomancak, P., and Cardona, A. (2012) Fiji: an open-source platform for biological-image analysis, *Nat. Methods 9*, 676.

[172] Rueden, C. T., Schindelin, J., Hiner, M. C., DeZonia, B. E., Walter, A. E., Arena, E. T., and Eliceiri, K. W. (2017) ImageJ2: ImageJ for the next generation of scientific image data, *BMC Bioinformatics 18*, 529.

[173] Rohrer, J., Partenhauser, A., Hauptstein, S., Gallati, C. M., Matuszczak, B., Abdulkarim, M., Gumbleton, M., and Bernkop-Schnürch, A. (2016) Mucus permeating thiolated self-emulsifying drug delivery systems, *Eur. J. Pharm. Biopharm. 98*, 90-97.

[174] Dezani, A. B., Pereira, T. M., Caffaro, A. M., Reis, J. M., and Serra, C. H. d. R. (2013) Determination of lamivudine and zidovudine permeability using a different ex vivo method in Franz cells, *J. Pharmacol. Toxicol. Methods 67*, 194-202.

[175] Fichorova, R. N., Rheinwald, J. G., and Anderson, D. J. (1997) Generation of papillomavirus-immortalized cell lines from normal human ectocervical, endocervical, and vaginal epithelium that maintain expression of tissue-specific differentiation proteins, *Biology of reproduction 57*, 847-855.

[176] Mosmann, T. (1983) Rapid colorimetric assay for cellular growth and survival: Application to proliferation and cytotoxicity assays, *J. Immunol. Methods 65*, 55-63.

[177] Bradford, M. M. (1976) A rapid and sensitive method for the quantitation of microgram quantities of protein utilizing the principle of protein-dye binding, *Anal. Biochem. 72*, 248-254.

[178] Zhang, E., Laufer, J., and Beard, P. (2008) Backward-mode multiwavelength photoacoustic scanner using a planar Fabry-Perot polymer film ultrasound sensor for high-resolution three-dimensional imaging of biological tissues, *Appl. Opt. 47*, 561-577.

[179] Buchmann, J., Guggenheim, J., Zhang, E., Scharfenorth, C., Spannekrebs, B., Villringer, C., and Laufer, J. (2017) Characterization and modeling of Fabry–Perot ultrasound sensors with hard dielectric mirrors for photoacoustic imaging, *Appl. Opt. 56*, 5039-5046.

[180] Treeby, B. E., and Cox, B. T. (2010) *k-Wave: MATLAB toolbox for the simulation and reconstruction of photoacoustic wave fields*, Vol. 15, SPIE.

[181] Treeby, B. E., Jaros, J., and Cox, B. T. (2016) *Advanced photoacoustic image reconstruction using the k-Wave toolbox*, Vol. 9708, SPIE.

[182] Feng, X. D., Guo, X. Q., and Qiu, K. Y. (1988) Study of the initiation mechanism of the vinyl polymerization with the system persulfate/N,N,N′,N′-tetramethylethylenediamine, *Die Makromolekulare Chemie 189*, 77-83.

[183] Duracher, D., Elaïssari, A., and Pichot, C. (1999) Preparation of poly(N-isopropylmethacrylamide) latexes kinetic studies and characterization, *J. Polym. Sci., Part A: Polym. Chem. 37*, 1823-1837.

[184] Smith, M. H., Herman, E. S., and Lyon, L. A. (2011) Network deconstruction reveals network structure in responsive microgels, *J. Phys. Chem. B 115*, 3761-3764.

[185] Virtanen, O. L. J., Brugnoni, M., Kather, M., Pich, A., and Richtering, W. (2016) The next step in precipitation polymerization of N-isopropylacrylamide: particle number density control by monochain globule surface charge modulation, *Polym. Chem. 7*, 5123-5131.

[186] McPhee, W., Tam, K. C., and Pelton, R. (1993) Poly(N-isopropylacrylamide) Latices Prepared with Sodium Dodecyl Sulfate, *J. Colloid Interface Sci. 156*, 24-30.

[187] Kabanov, A. V., and Vinogradov, S. V. (2009) Nanogels as Pharmaceutical Carriers: Finite Networks of Infinite Capabilities, *Angew. Chem. Int. Ed. 48*, 5418-5429.

[188] Montero, D., Tachibana, C., Rahr Winther, J., and Appenzeller-Herzog, C. (2013) Intracellular glutathione pools are heterogeneously concentrated, *Redox biology 1*, 508-513.

[189] Go, Y.-M., and Jones, D. P. (2008) Redox compartmentalization in eukaryotic cells, *Biochim. Biophys. Acta 1780*, 1273-1290.

[190] Kar, M., Vernon Shih, Y.-R., Velez, D. O., Cabrales, P., and Varghese, S. (2016) Poly(ethylene glycol) hydrogels with cell cleavable groups for autonomous cell delivery, *Biomaterials 77*, 186-197.

[191] Gouyer, V., Dubuquoy, L., Robbe-Masselot, C., Neut, C., Singer, E., Plet, S., Geboes, K., Desreumaux, P., Gottrand, F., and Desseyn, J.-L. (2015) Delivery of a mucin domain enriched in cysteine residues strengthens the intestinal mucous barrier, *Sci Rep. 5*, 9577-9577.

[192] Molina, M., Wedepohl, S., Miceli, E., and Calderón, M. (2017) Overcoming drug resistance with on-demand charged thermoresponsive dendritic nanogels, *Nanomedicine 12*, 117-129.

[193] Lopez-Cabarcos, E., Mecerreyes, D., Sierra-Martin, B., Romero-Cano, M. S., Strunz, P., and Fernandez-Barbero, A. (2004) Structural study of poly (N-isopropylacrylamide) microgels interpenetrated with polypyrrole, *PCCP 6*, 1396-1400.

[194] Nguyen, S. C., Zhang, Q., Manthiram, K., Ye, X., Lomont, J. P., Harris, C. B., Weller, H., and Alivisatos, A. P. (2016) Study of Heat Transfer Dynamics from Gold Nanorods to the Environment via Time-Resolved Infrared Spectroscopy, *ACS Nano 10*, 2144-2151.

[195] Rafiei Miandashti, A., Khosravi Khorashad, L., Govorov, A. O., Kordesch, M. E., and Richardson, H. H. (2019) Time-Resolved Temperature-Jump Measurements and Theoretical Simulations of Nanoscale Heat Transfer Using NaYF4:Yb3+:Er3+ Upconverting Nanoparticles, *J Phys Chem C Nanomater Interfaces 123*, 3770-3780.

[196] Michnik, A., Michalik, K., and Drzazga, Z. (2005) Stability of bovine serum albumin at different pH, *J. Therm. Anal. Calorim. 80*, 399-406.

[197] Michnik, A. (2003) Thermal stability of bovine serum albumin DSC study, *J. Therm. Anal. Calorim. 71*, 509-519.

[198] Giancola, C., De Sena, C., Fessas, D., Graziano, G., and Barone, G. (1997) DSC studies on bovine serum albumin denaturation Effects of ionic strength and SDS concentration, *Int. J. Biol. Macromol. 20*, 193-204.

[199] Leader, B., Baca, Q. J., and Golan, D. E. (2008) Protein therapeutics: a summary and pharmacological classification, *Nat Rev Drug Discov 7*, 21.

[200] Mease, P. J., Goffe, B. S., Metz, J., VanderStoep, A., Finck, B., and Burge, D. J. (2000) Etanercept in the treatment of psoriatic arthritis and psoriasis: a randomised trial, *The Lancet 356*, 385-390.

[201] Moreland, L. W., Schiff, M. H., Baumgartner, S. W., Tindall, E. A., Fleischmann, R. M., Bulpitt, K. J., Weaver, A. L., Keystone, E. C., Furst, D. E., Mease, P. J., Ruderman, E. M., Horwitz, D. A., Arkfeld, D. G., Garrison, L., Burge, D. J., Blosch, C. M., Lange, M. L. M., McDonnell, N. D., and Weinblatt, M. E. (1999) Etanercept Therapy in Rheumatoid Arthritis: A Randomized, Controlled Trial, *Annals of Internal Medicine 130*, 478-486.

[202] Geborek, P., Crnkic, M., Petersson, I. F., Saxne, T., and South Swedish Arthritis Treatment, G. (2002) Etanercept, infliximab, and leflunomide in established

rheumatoid arthritis: clinical experience using a structured follow up programme in southern Sweden, *Ann. Rheum. Dis. 61*, 793-798.

[203] Enbrel 25mg/50mg Injektionslösung im Fertigpen, July 2018 ed., p https://www.pfizermed.de/fileadmin/produktdatenbank/pdf/011927_freigabe.pdf, Pfizer.

[204] Plank, R., Yealland, G., Miceli, E., Lima Cunha, D., Graff, P., Thomforde, S., Gruber, R., Moosbrugger-Martinz, V., Eckl, K., Calderón, M., Hennies, H. C., and Hedtrich, S. (2018) Transglutaminase 1 Replacement Therapy Successfully Mitigates the Autosomal Recessive Congenital Ichthyosis Phenotype in Full-Thickness Skin Disease Equivalents, *J Invest Dermatol*.

[205] Bhatt, H., Naik, B., and Dharamsi, A. (2014) Solubility Enhancement of Budesonide and Statistical Optimization of Coating Variables for Targeted Drug Delivery, *J Pharm 2014*, 13.

[206] Ali, H. S. M., York, P., Blagden, N., Soltanpour, S., Acree, W. E., and Jouyban, A. (2010) Solubility of Budesonide, Hydrocortisone, and Prednisolone in Ethanol + Water Mixtures at 298.2 K, *Journal of Chemical & Engineering Data 55*, 578-582.

[207] Ernsting, M. J., Murakami, M., Roy, A., and Li, S.-D. (2013) Factors controlling the pharmacokinetics, biodistribution and intratumoral penetration of nanoparticles, *J. Control Release 172*, 782-794.

[208] Almeida, J. P. M., Chen, A. L., Foster, A., and Drezek, R. (2011) In vivo biodistribution of nanoparticles, *Nanomedicine 6*, 815-835.

[209] Raza, K., Kumar, P., Kumar, N., and Malik, R. (2017) 9 - Pharmacokinetics and biodistribution of the nanoparticles, In *Advances in Nanomedicine for the Delivery of Therapeutic Nucleic Acids* (Nimesh, S., Chandra, R., and Gupta, N., Eds.), pp 165-186, Woodhead Publishing.

[210] Neagu, M., Piperigkou, Z., Karamanou, K., Engin, A. B., Docea, A. O., Constantin, C., Negrei, C., Nikitovic, D., and Tsatsakis, A. (2017) Protein bio-corona: critical issue in immune nanotoxicology, *Arch. Toxicol. 91*, 1031-1048.

[211] Gao, H., Xiong, J., Cheng, T., Liu, J., Chu, L., Liu, J., Ma, R., and Shi, L. (2013) In Vivo Biodistribution of Mixed Shell Micelles with Tunable Hydrophilic/Hydrophobic Surface, *Biomacromolecules 14*, 460-467.

[212] Mitragotri, S., and Lahann, J. (2009) Physical approaches to biomaterial design, *Nat Mater 8*, 15.

7 APPENDIX

7.1 RESPONSIVE NANOGELS FOR ANTI-CANCER THERAPY

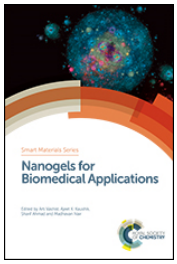

Responsive Nanogels for Anti-cancer Therapy

Mrityunjoy Kar, **Loryn Fechner**, Gregor Nagel, Emanuel Glitscher, Guido Noe Rimondino and Marcelo Calderón

Chapter 12 in *Nanogels for Biomedical Applications*, 2018, pages 210-260
The Royal Society of Chemicals, Book Series: Smart Materials
Editors: Arti Vashist, Ajeet K Kaushik, Sharif Ahmad, Madhavan Nair
https://doi.org/10.1039/9781788010481-00210

Abstract:
Nanogels (or nano-sized hydrogels) have been extensively investigated as an effective drug delivery system due to their various advantageous properties. Among them, stimuli responsive 'smart' nanogels, which have the ability to respond to various external stimuli, such as pH, redox, temperature, enzymes, and light, are the most attractive in the area of controlled anti-cancer drug delivery. In this book chapter, we review and discuss recent progress in the synthesis and applications of polymer-based stimuli-responsive nanogels for anti-cancer therapy and their future prospects.

7.2 CRITICAL PARAMETERS FOR THE CONTROLLED SYNTHESIS OF NANOGELS SUITABLE FOR TEMPERATURE-TRIGGERED PROTEIN DELIVERY

Critical parameters for the controlled synthesis of nanogels suitable for temperature-triggered protein delivery

Loryn E. Theune[a], Rawan Charbaji[b], Mrityunjoy Kar[a], Stefanie Wedepohl[a], Sarah Hedtrich[b,c] and Marcelo Calderón[a]

[a] Freie Universität Berlin, Institute of Chemistry and Biochemistry, Takustr. 3, 14195 Berlin, Germany
[b] Freie Universität Berlin, Institute for Pharmacy (Pharmacology and Toxicology), Königin-Luise-Str. 2+4, 14195 Berlin, Germany
[c] University of British Columbia, Faculty of Pharmaceutical Sciences, 2405 Wesbrook Mall, V6T 1Z3, Vancouver, Canada

Materials Science and Engineering: C, Volume 100, 2019, pages 141-151, Elsevier
https://doi.org/10.1016/j.msec.2019.02.089

Abstract: Macromolecular bioactives, like proteins and peptides, emerged as highly efficient therapeutics. The main limitation for their clinical application is their instability and potential immunogenicity. Thus, controlled delivery systems able protect the proteins prior release are highly on demand. In the present study, we developed hydrophilic thermo-responsive nanogels with tunable volume phase transition temperatures (VPTTs) and suitable features for controlled protein delivery by the use of multifunctional, dendritic polyglycerol (dPG) as macromolecular cross-linker and temperature-sensitive polymers poly(N-isopropylacrylamide) (NIPAM) and poly(N-isopropylacrylmethacrylate) as linear counterpart. We comprehensively studied the impact of the initiator, monomers and cross-linker on the nanogel structure during the synthesis. Careful analysis of the polymerization process revealed importance of balanced reactions kinetics to form particles with diameters in the range 100–200 nm and low polydispersity. We can control the cross-linking density of the nanogels mainly by the dPG feed and its degree of acrylation. In addition, our screenings revealed that the hydrophilic character of dPG enables it to stabilize the growing particles during the polymerization and thereby reduces final particle size. Co-polymerization of NIPAM and NIPMAM allows precise tuning of the VPTT of the nanogels in the desired range of 34–47 °C. Our nanogels showed outstanding high protein encapsulation efficiency and triggered cargo release upon a temperature change. The delivery efficiency of these nanogels was investigated on excised human skin demonstrating efficient dermal penetration of encapsulated proteins dependent on a temperature triggered release mechanism.

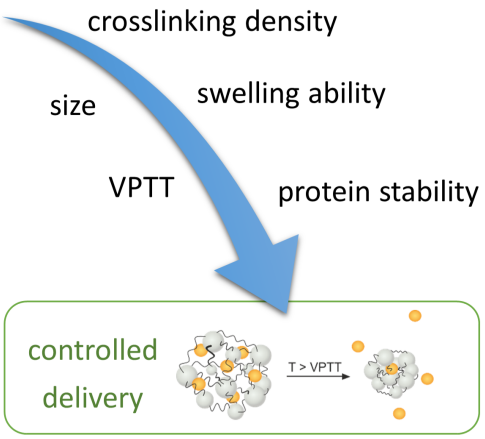

7.3 NIR- AND THERMO-RESPONSIVE SEMI-INTERPENETRATED POLYPYRROLE NANOGELS FOR IMAGING GUIDED COMBINATIONAL PHOTOTHERMAL AND CHEMOTHERAPY

NIR- and thermo-responsive semi-interpenetrated polypyrrole nanogels for imaging guided combinational photothermal and chemotherapy

Loryn E. Theune[a], Jens Buchmann[b], Stefanie Wedepohl[a], Maria Molina[a], Jan Laufer[b] and Marcelo Calderón[acd]

[a] Freie Universität Berlin, Institute of Chemistry and Biochemistry, Takustr. 3, 14195 Berlin, Germany
[b] Institut für Physik, Martin-Luther-Universität Halle-Wittenberg, Von-Danckelmann-Platz 3, 06120 Halle (Saale), Germany
[c] POLYMAT and Applied Chemistry Department, Faculty of Chemistry, University of the Basque Country UPV/EHU, Paseo Manuel de Lardizabal 3, 20018 Donostia-San Sebastián, Spain
[d] IKERBASQUE, Basque Foundation for Science, 48013 Bilbao, Spain

submitted to the Journal of Controlled Release

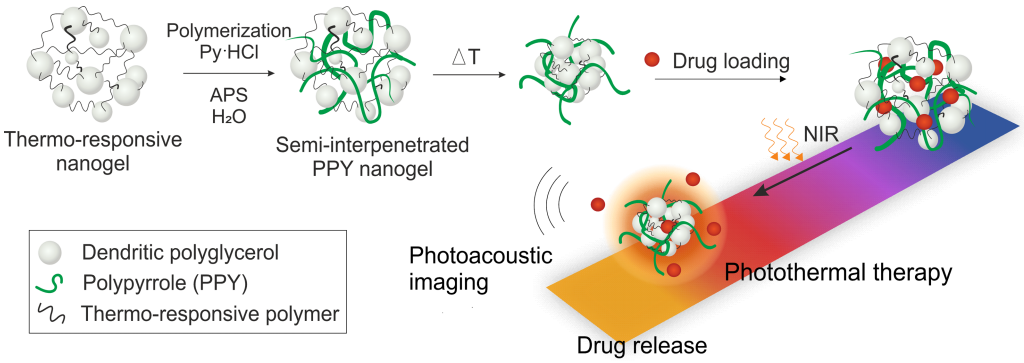

Abstract: Versatile, multifunctional nanomaterials for theranostic approaches in cancer treatment are highly on demand in order to increase therapeutic outcomes. Here, we developed thermo-responsive nanogels equipped with the efficient near-infrared (NIR) transducing polymer polypyrrole (PPY) for combinational photothermal and chemotherapeutic therapy along with photoacoustic imaging ability. Long-term stability and water-dispersibility of PPY was achieved using semi-interpenetration method for ***in situ*** polymerization of PPY into hydrophilic thermo-responsive nanogels. The semi-interpenetrated nanogels of spherical shape and with hydrodynamic sizes of around 200 nm retained the temperature response behaviour and exhibit excellent photothermal transducing abilities in the NIR region. The PPY nanogels

served as photoacoustic contrast agents, which allowed determination of biodistribution profiles ***ex vivo***. In addition, we developed a new method for biodistribution determination based on the photothermal response of the nanogels with an accuracy down to 12.5 μg/mL. We examined the ability of the nanogels as photothermal agents and drug delivery systems ***in vitro*** and ***in vivo.*** We showed that they efficiently inhibit tumor growth with combinational effects of chemotherapeutics and photothermal treatment. Our work encourages further exploration of nanogels as functional stabilizing matrix for photothermal transducers and their application as drug delivery devices in combination with photothermal therapy and imaging.

7.4 PUBLICATIONS AND CONFERENCE CONTRIBUTIONS

Publications

1. **Loryn E. Theune**, Jens Buchmann, Stefanie Wedepohl, Maria Molina, Jan Laufer, Marcelo Calderón (2019), "NIR- and thermo-responsive semi-interpenetrated polypyrrole nanogels for imaging guided combinational photothermal and chemotherapy", *submitted to the Journal of Controlled Release*
2. **Loryn E. Theune**, Rawan Charbaji, Mrityunjoy Kar, Stefanie Wedepohl, Sarah Hedtrich, Marcelo Calderón (2019), "Critical parameters for the controlled synthesis of nanogels suitable for temperature-triggered protein delivery", *Materials Science and Engineering C,* https://doi.org/10.1016/j.msec.2019.02.089
3. Enrico Miceli, Benno Kuropka, Christine Rosenauer, Ernesto R Osorio Blanco, **Loryn E. Theune**, Mrityunjoy Kar, Christoph Weise, Svenja Morsbach, Christian Freund, and Marcelo Calderón (2018) "Understanding the elusive protein corona of thermoresponsive nanogels" *Nanomedicine,* https://doi.org/10.2217/nnm-2018-0217
4. Gianpaolo Dagrada, Katia Rupel, Serena Zacchigna, Elena Tamborini, Silvana Pilotti, Adalberto Cavalleri, **Loryn E. Fechner**, Erik Laurini, David K. Smith, Silvia Brich, and Sabrina Pricl, "Self-Assembled Nanomicelles as Curcumin Drug Delivery Vehicles: Impact on Solitary Fibrous Tumor Cell Protein Expression and Viability" *Molecular Pharmaceutics,* https://doi.org/10.1021/acs.molpharmaceut.8b00655
5. M. Kar, **L. E. Fechner**, G. Nagel, E. Glitscher, G.N. Rimondino, M. Calderón (2017) Responsive nanogels for anticancer therapy, *RSC Book*, Smart Material Series 'Nanogels for Biomedical Applications, https://doi.org/10.1039/9781788010481-00210
6. **L. E. Fechner**, B. Albanyan, V. M. P. Vieira, E. Laurini, P. Posocco, S. Pricl, D. K. Smith, (2016) "Electrostatic Binding of Polyanions using Self-Assembled Multivalent (SAMul) Ligand Displays – Structure-Activity Effects on DNA/Heparin Binding", *Chemical Science,* https://doi.org/10.1039/C5SC04801J

Conference Contributions and Summerschools

1. **Loryn E. Fechner**, Rawan Charbaji, Mritjunjoy Kar, Stefanie Wedepohl, Sarah Hedtrich, Marcelo Calderón, Tunable Thermo-responsive Nanogels As Versatile Drug Delivery System. *15th European Symposium Controlled Drug Delivery (ESCDD)*, Egmond aan Zee, Netherlands, 2018.

2. E. A. Glitscher, **L. E. Fechner**, J. Bergueiro, S. Wedepohl, M. Calderón, Biomedical Application of Thermo-responsive Nanogels with Near Infra-red Transducers for the Controlled Transport and Release of Therapeutic Molecules, *Wissenschaftsforum - Chemie bewegt*, Berlin, Germany, 2017.

3. **Loryn E. Fechner**, Mrityunjoy Kar, Maria Molina, Stefanie Wedepohl, Marcelo Calderón, Thermoresponsive Near-Infrared Absorbing Nanogels for Combinational Chemo- and Photothermal therapy of Cancer. *6th International Colloids Conference*, Berlin, Germany, 2016.

4. **Loryn E. Fechn**er, Mrityunjoy Kar, Maria Molina, Stefanie Wedepohl, Marcelo Calderón, Semi-interpenetrated polymeric near-infrared absorbing nanogels for efficient photothermal therapy of cancer. *11th Int. Symp. Polymer Therapeutic*, Valencia, Spain, 2016.

5. **Loryn E. Fechner**, Emanuel A. Glitscher, Mrityunjoy Kar, Stefanie Wedepohl, Marcelo Calderón, ThermoNanogele: Neuartige thermoresponsive Nanogele für den zielgerichteten Wirkstofftransport und die kontrollierte Freisetzung von Zytostatika und/oder fluoreszierenden Substanzen. *MedTech Summit 2016*, Nürnberg, Germany, 2016.

7.5 CURRICULUM VITAE

The curriculum Vitae is not published in the online version for reason of data protection.